

OmniOpt: Taxonomy, Geometry, and Benchmarking of Modern Optimizers

Siyuan Li^{*1,3}, Jiabao Pan^{*1,2}, Yumou Liu^{*1,4}, Zhuoli Ouyang^{*7}, Xin Jin^{*3}, Xinglong Xu⁵, Jingxuan Wei⁵, Shengye Pang^{†2}, Jintao Chen⁶, Xuanhe Zhou⁴, Conghui He¹, Cheng Tan^{†1}

¹Shanghai Artificial Intelligence Laboratory, ²Shanghai University, ³Westlake University, ⁴Shanghai Jiao Tong University, ⁵UCAS, ⁶Zhejiang University, ⁷Southern University of Science and Technology

Optimizer selection for large-scale model training has become a system-level design decision constrained jointly by compute, memory, tuning budget, and task diversity, yet the landscape of over one hundred methods remains fragmented. We therefore present **OmniOpt**, a unified survey and benchmark cookbook of optimizers for the research community. OmniOpt rests on four coupled components. First, we treat every optimizer update as a structured transformation through a five-stage meta-pipeline, and show that most methods engage only one or two of these stages. Second, we use norm-constrained linear minimization oracles (LMOs) to unify different optimizers. Third, these two views ground a dual-dimension taxonomy, one dimension assigning each method to a mechanism family and the other recording the measurable training objectives it aims to improve. Fourth, and at the core of this paper, we instantiate the full taxonomy in a unified cross-domain benchmark spanning representative optimizers, model scales, and training regimes from language model pretraining to image classification, systematically analyzing each method family across multiple effect objectives and laying out their trade-offs. OmniOpt thus supplies the research community with an operational coordinate system for selecting optimizers under explicit mechanism and objective assumptions, and charts a direction for the future development of the optimizer community.

 [Code](#)  [Website](#)  [Hugging Face](#)

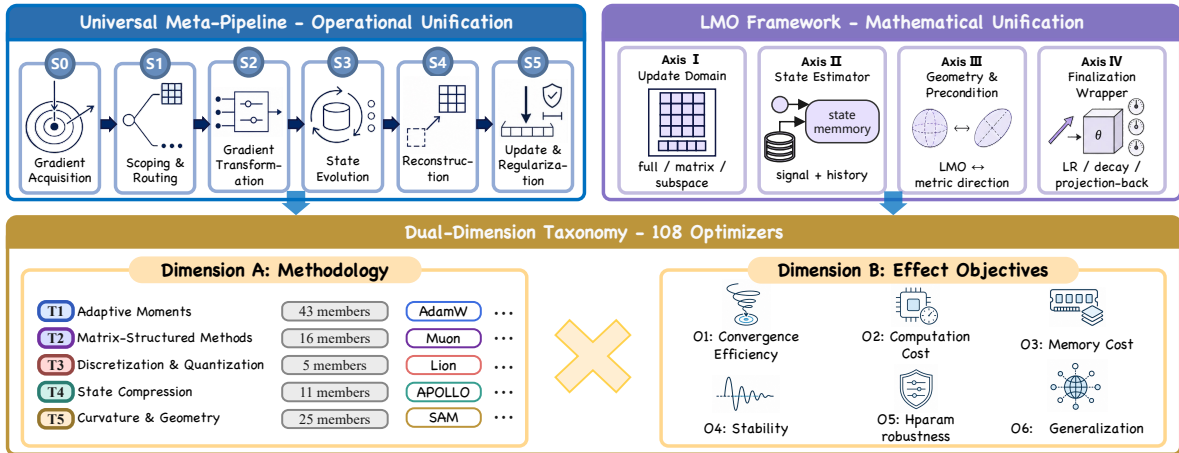


Figure 1: Overview of the proposed survey and benchmark framework for a wild range of optimizers. The paper first introduces a universal meta-pipeline, then develops an LMO-driven four-axis decomposition, builds a process-aligned methodological taxonomy and an effect-objective taxonomy, and finally connects both taxonomies to a large-scale benchmark study.

*Equal contribution. †Corresponding authors.

Contents

1	Introduction	4
1.1	Background and Motivation	4
1.2	Contributions and Paper Organization	5
1.3	Positioning Against Existing Surveys and Benchmarks	6
1.3.1	Prior Literature Strands and Survey-Theory Baselines	6
1.3.2	Benchmark Evidence and Taxonomy Mapping	7
1.3.3	Position of This Paper and Roadmap	8
2	Preliminaries	8
2.1	Problem Formulation	8
2.2	Classical Optimization Background	9
3	Unified Theoretical Framework for Optimizers	11
3.1	Universal Meta-Pipeline	11
3.1.1	Operational Steps	11
3.1.2	Identity Mapping and Representative Instantiations	14
3.2	A Mathematical Unification of Optimizer Updates	16
3.2.1	LMO Foundations and Norm-Induced Directions	17
3.2.2	A Four-Axis Decomposition of Optimizer Updates	18
3.2.3	Instantiations	20
4	Dual-Dimension Taxonomy	22
4.1	Taxonomy Design Principles	22
4.2	Methodological Taxonomy	23
4.3	Objective-Oriented Taxonomy	24
4.4	Cross-Dimension Analysis	26
5	Optimizer Method Families	27
5.1	T1: Element-Wise Adaptive Moment and Scalar Control	27
5.1.1	Family Overview and Meta-Pipeline Position	27
5.1.2	LMO-Driven Four-Axis Interpretation	29
5.1.3	Representative Methods	29
5.2	T2: Matrix-Level Structural Methods	33
5.2.1	Family Overview and Meta-Pipeline Position	33
5.2.2	LMO-Driven Four-Axis Interpretation	35
5.2.3	Representative Methods	36
5.2.4	Effect-Target Assessment	38
5.3	T3: Discretization and Directional Quantization	39
5.3.1	Family Overview and Meta-Pipeline Position	39
5.3.2	LMO-Driven Four-Axis Interpretation	40
5.3.3	Representative Methods	41
5.3.4	Effect-Target Assessment	42
5.4	T4: State Compression and Structural Aggregation	43
5.4.1	Family Overview and Meta-Pipeline Position	43
5.4.2	LMO-Driven Four-Axis Interpretation	45
5.4.3	Representative Methods	46
5.4.4	Effect-Target Assessment	48
5.5	T5: Curvature-Aware and Geometric Regularization	49
5.5.1	Family Overview and Meta-Pipeline Position	49
5.5.2	LMO-Driven Four-Axis Interpretation	51

5.5.3	Representative Methods	52
5.5.4	Effect-Target Assessment	54
6	Benchmark Study	55
6.1	Experimental Setup	55
6.2	Results and Analysis	56
6.2.1	Stage 1: Broad Screening on C4	56
6.2.2	Stage 1 Pareto Analysis over PPL, Runtime, and Memory	58
6.2.3	Stage 2: Generalization across Data, Context Length, and Architectures	60
6.2.4	Scenario Sensitivity of Memory-Efficient Optimizers	62
6.2.5	Optimizer Robustness Across Vision Backbones	63
6.2.6	Auxiliary Stability Analysis from Gradient-Norm Dynamics	64
6.2.7	Auxiliary Learning-Rate Perturbation Robustness	66
6.2.8	Family-Level Objective Summary	67
6.2.9	Tiered Optimizer Summary	68
6.3	Mechanistic Ablation of Muon	70
6.3.1	Single-scene decomposition on C4-350M	70
6.3.2	Cross-scale and cross-architecture validation	71
7	Discussion	72
7.1	Limitations	72
7.2	Technique-Level Lessons	73
7.3	Open Problems and Future Directions	75
8	Conclusion	76
A	Additional Experimental Hyperparameter Configurations	86
A.1	Stage-1 C4-LLaMA Short-Context Screening	86
A.2	Stage-2 FineWeb-Edu 32k Long-Context Experiments	86
B	Detailed Stage-2 Commonsense Reasoning Results	86

1 Introduction

1.1 Background and Motivation

Optimizers have become a system-level design choice in model training. Whether a modern training run succeeds depends on whether a stochastic update can reduce the empirical loss, and equally on a fixed budget of accelerators, optimizer-state memory, communication bandwidth, batch size, data scale, tuning effort, and downstream evaluation cost. Adam and AdamW established the dominant element-wise adaptive-moment template for deep learning [54, 70]. Recent LLM-oriented optimizers, however, no longer fit cleanly into this single template. Sign-based methods change the direction map [19], matrix-level methods exploit structured curvature or orthogonalized directions [38], low-rank methods reduce state in projected subspaces [138], and sharpness-aware methods regularize the geometry of the final update [32]. Optimizer selection has therefore become an empirical, mathematical, and engineering problem at the same time.

This rapidly expanding literature is difficult to navigate for three reasons. First, optimizer papers are usually organized around a local mechanism, such as a new moment estimator, preconditioner, projection, quantizer, or post-update correction. Such naming is useful for implementation, but it does not reveal whether two optimizers intervene at the same stage of the update process, whether their components are orthogonal, or whether they are compositionally compatible. Second, empirical claims are highly protocol-sensitive. Recent LLM optimizer studies show that conclusions can change with model scale, batch size, training duration, data-to-model ratio, learning-rate schedule, warmup, weight decay, and hyperparameter tuning budget [139, 97, 113]. A method that improves pretraining loss may increase memory, wall-clock time, or tuning burden. Conversely, a memory-saving method may change both the update direction and the state representation. Third, the mathematical accounts of modern optimizers remain fragmented. Element-wise adaptive methods, matrix preconditioners, sign optimizers, low-rank projections, and geometry-aware regularizers are often analyzed with different notation and different assumptions.

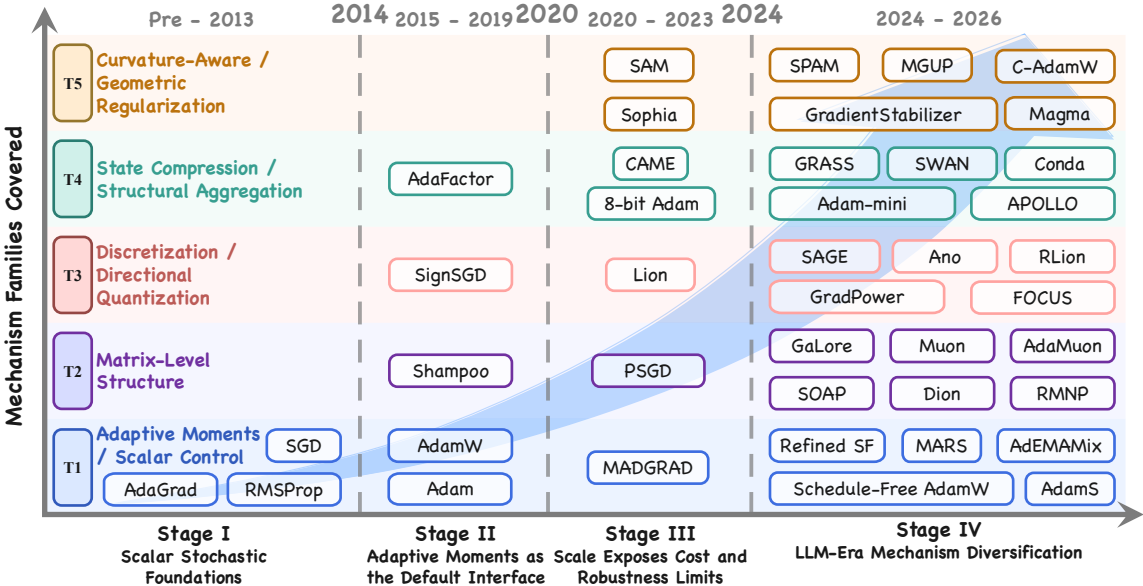


Figure 2: Evolution of optimizer design for deep learning and LLM training. The expanding coverage of T1–T5 mechanism lanes and the diagonal trend arrow indicate increasing method count and mechanism diversity, not a performance ranking or exact method counts.

This paper addresses these gaps by treating an optimizer as a structured transformation from a stochastic training signal to a parameter update. The central premise is that most modern optimizers are sparse modifications of a shared meta-pipeline: they route parameters, transform the gradient signal, evolve internal state, reconstruct an update, and finally apply scaling or regularization. This operational view induces a process-aligned methodological taxonomy in which each optimizer family is grouped by the stage where its primary non-identity operation occurs. On top of this view, we use linear minimization oracles (LMOs) as a geometric primitive for explaining norm-induced update directions, including sign directions, orthogonal matrix directions, and preconditioned directions [10, 87]. The resulting four-axis decomposition extends idealized LMO direction selection to practical optimizer updates by adding curvature estimation, gradient-estimation quality, and state-compression choices. A second, effect-oriented taxonomy then records which training objectives each method is designed or expected to improve, such as convergence efficiency, per-step cost, memory consumption, stability, hyperparameter robustness, and generalization. Together, these views form a mechanism-aware framework for answering three linked questions: where an optimizer acts, why its update has a particular mathematical form, and what practical training objective it is meant to improve.

1.2 Contributions and Paper Organization

This paper is a survey and benchmark study of optimizers for LLM training that aims to provide a mechanism-aware map for comparing, combining, and evaluating optimizers under explicit assumptions. Which optimizer is best depends on the specific training constraints. The four components below are intentionally coupled: the meta-pipeline defines non-overlapping operation sites, the methodological taxonomy is derived from those sites, the LMO-driven analysis explains the mathematical direction selected by each family, and the objective taxonomy turns optimizer claims into measurable evaluation axes. The main contributions are as follows.

1. **A universal meta-pipeline for optimizers.** We formulate a five-step operational pipeline that aligns modern optimizers under a common update process, namely parameter scoping and routing, gradient transformation, state evolution, update reconstruction, and update finalization. This view exposes an identity-mapping principle, that most optimizers perform nontrivial work in only one or two stages while leaving the remaining stages as defaults.
2. **An LMO-driven four-axis decomposition.** We use norm-constrained LMOs to unify direction selection and extend this view to a four-axis description of practical optimizer updates, whose axes specify the update domain, the state estimator, the geometry-and-precondition operator, and the finalization wrapper. Under this view, the update directions selected by different optimizers are unified by a single geometric language.
3. **A dual-dimension taxonomy for more than one hundred optimizers.** We organize optimizer methods along two complementary dimensions. The methodological dimension assigns each optimizer to a non-overlapping primary mechanism family, and the objective-oriented dimension records the measurable training objectives each method is intended to improve.
4. **A mechanism-aligned benchmark study.** This is the core of the paper. The empirical part instantiates the full taxonomy in a unified cross-domain benchmark, spanning language model pretraining from 60M to 1B parameters, across four architectures, and at context lengths from 256 to 32k tokens, together with image classification on CIFAR100 [55]. The evaluation is carried out at the family and axis level, systematically comparing representative optimizers across six effect objectives (convergence, cost, memory, stability, hyperparameter robustness, and generalization) and laying out their trade-offs one by one. We further perform a mechanistic ablation of the matrix-structured optimizer Muon [48] to examine how its sub-operations compose across scale and architecture. The benchmark yields several findings that recur throughout the paper. No single optimizer dominates this multi-objective frontier. Aggressive state compression excels under short context but degrades sharply as input complexity grows. Structured-matrix methods transfer most stably across architec-

Table 1: Relation to optimizer surveys and unifying-theory work.

Work	Type	Scope		Mathematical lens		Evidence and taxonomy	
		Primary object	LLM optimizer coverage	Optimizer update formulas	Geometric unification lens	Benchmark included	Update stage taxonomy
Survey and benchmark papers							
Evolution Methods [134]	Survey+bench.	Broad optimizers	✓	✓	△	✓	×
DL Optimizers [3]	Survey	DL optimizer history	△	✓	×	×	×
LLM Valley [91]	Survey	LLM optimizers	✓	△	×	△	×
Mem.-Eff. PT [36]	Survey+bench.	Memory-efficient LLM	✓	△	×	✓	×
Unifying mathematical theory							
Old Optimizer, New Norm [10]	Theory	Norm geometry	△	✓	✓	×	×
Norm-Constrained LMOs [87]	Theory+Algo.	LMO training	×	✓	✓	△	×
Lions/Muons [98]	Theory	Lion/Muon geometry	△	✓	✓	×	×
Ours	Survey+bench.	100+ LLM optimizers	✓	✓	✓	✓	✓

Note. ✓ indicates that the criterion is central to the work; △ indicates partial or secondary coverage; × indicates that the criterion is not central to the work. Bench., Algo., DL, and PT abbreviate benchmark, algorithm, deep learning, and pretraining.

tures and tasks but at substantial per-step cost. Optimizer rankings exhibit systematic crossings with scale, context length, and domain.

Figure 1 summarizes the planned organization of the paper. The key design is that the meta-pipeline, LMO-driven decomposition, methodological taxonomy, objective taxonomy, and benchmark study are mutually aligned and reinforce one another as an integrated whole.

1.3 Positioning Against Existing Surveys and Benchmarks

1.3.1 Prior Literature Strands and Survey-Theory Baselines

The closest prior work falls into three interlocking lines: optimizer surveys, unifying mathematical theory, and large-language-model optimizer benchmarks. General optimizer surveys describe the historical progression from stochastic gradient descent and momentum to adaptive, second-order, memory-efficient, and matrix-aware methods. Theoretical work supplies a complementary explanation of why some updates can be viewed as norm-induced steepest descent, stochastic Frank–Wolfe steps, or directions produced by a linear minimization oracle. Empirical benchmarks then show how these mechanisms behave under realistic pretraining or fine-tuning protocols. Taken separately, however, these lines do not identify where a method intervenes in the optimizer update pipeline, which mechanisms are compatible with one another, or how a taxonomy should determine the axes of a benchmark.

Table 1 places representative surveys and unifying-theory papers along three groups of criteria. The scope columns ask what object each work primarily studies and whether large-language-model optimizers are central to its scope. The mathematical-lens columns distinguish formula-level treatment of optimizer updates from geometric interpretations through norms, linear minimization oracles, or Frank–Wolfe geometry. The final columns record whether a work includes benchmark evidence and whether it organizes optimizers by the stage at which they intervene in an update. In Tables 1 and 2, ✓, △, and × indicate primary coverage, partial or secondary coverage, and a non-central topic, respectively.

The broad surveys by Zhang et al. [134] and Altinel and Ozcan [3] are useful references for update rules, optimizer families, and the historical development of deep-learning optimization, but their organization is mainly driven by gradient-information order, chronology, or application setting.

Table 2: Relation to large-language-model optimizer benchmarks and mechanistic empirical studies.

Work	Training setting	Method coverage					Evaluation focus				
		Adaptive moment	Matrix methods	Direction discretization	State compression	Geometry regularization	Tune	Protocol	Cost	Down-stream	Mechanism
Deconstructing Optimizers [139]	PT	✓	×	✓	✓	✓	✓	✓	△	×	✓
Benchmarking LLM Opt. [97]	PT	✓	✓	✓	×	✓	✓	✓	△	×	✓
Fantastic PT Opt. [113]	PT	✓	✓	✓	✓	✓	✓	✓	✓	×	△
Budgeted LLM PT [96]	Budget PT	✓	×	✓	×	✓	△	△	✓	✓	△
ZO FT Benchmark [135]	ZO FT	△	×	△	×	×	△	△	✓	✓	△
Muon Fine-tuning Study [89]	FT	✓	✓	×	×	×	△	△	×	✓	✓
Muon Spectral Study [100]	Mech.	△	✓	×	×	×	×	×	×	×	✓
Ours	PT	✓	✓	✓	✓	✓	✓	✓	✓	✓	✓

Note. ✓ indicates explicit coverage of the family; △ indicates analogue, boundary, or baseline-only coverage; × indicates no coverage under these labels. Opt., PT, ZO, FT, and Mech. abbreviate optimizers, pretraining, zeroth-order, fine-tuning, and mechanistic, respectively; Budget PT denotes budgeted pretraining.

Ranganath et al. [91] move closer to the setting of this paper by covering adaptive, sign-based, memory-efficient, low-rank, and matrix-based optimizers for large language models. Glentis et al. [36] focus more narrowly on parameter- and memory-efficient pretraining, which is especially relevant to optimizer-state memory and low-rank training. The unifying-theory papers play a different role. Bernstein et al. [10] connect several optimizers to architecture-dependent norms, Pethick et al. [87] develop training algorithms based on norm-constrained linear minimization oracles, and Sfyraiki et al. [98] relate Lion and Muon to stochastic Frank–Wolfe. These works supply the geometric language used later in this paper, but they do not provide a survey-scale taxonomy that maps optimizer mechanisms to update stages and then connects those stages to benchmark objectives.

1.3.2 Benchmark Evidence and Taxonomy Mapping

The second group consists of large-language-model optimizer benchmarks and mechanistic empirical studies. Their common message is that optimizer comparison is not a stable global ranking problem. Adam-like methods, sign methods, matrix-aware methods, curvature-aware methods, and memory-efficient variants can exchange relative positions when the tuning budget, model size, batch size, training duration, data regime, or evaluation endpoint changes. This makes it necessary to report effect-specific trade-offs, including convergence, wall-clock cost, optimizer-state memory, robustness to hyperparameters, and downstream generalization.

Table 2 summarizes this empirical literature by training setting, method coverage, and evaluation focus. The method-coverage columns use the Dimension-A families introduced in Section 4: T1 element-wise adaptive moment and scalar control, T2 matrix-level structural methods, T3 discretization and directional quantization, T4 state compression and structural aggregation, and T5 curvature-aware and geometric regularization. Coverage is assigned by mapping the optimizers actually benchmarked in each work to their primary mechanism labels according to what each optimizer actually does. Thus Lion and Signum count as T3 rather than T4 even when discussed as memory-saving methods, whereas AdaFactor and Adam-mini count as T4 because they change optimizer-state representation. Zeroth-order fine-tuning is treated as a boundary case: the signal-acquisition mechanism is outside the main T1–T5 taxonomy, but ZO-Adam and ZO-SGD-Sign can still be recorded as T1-like and T3-like update analogues. The evaluation columns distinguish hyperparameter tuning, protocol variation, cost accounting, downstream evaluation, and mechanistic analysis. Here *protocol variation* includes model size, batch size, training length, data-to-model ratio, architecture, training stage, and task setting, while *cost accounting* includes compute, memory, runtime, and query cost. The row for this paper describes its benchmark design, and the actual experimental results appear in the main text.

1.3.3 Position of This Paper and Roadmap

Zhao et al. [139] and Semenov et al. [97] are the closest pretraining benchmarks to our setting. Both compare Adam-like baselines with sign, curvature-aware, or memory-efficient variants, and both show that conclusions depend on hyperparameter sweeps and protocol choices. Wen et al. [113] sharpen this point by revisiting claimed optimizer speedups under stricter hyperparameter search, end-of-training evaluation, hyperparameter transfer, and scaling conditions. Schlotthauer et al. [96] focus on resource-limited pretraining, where the optimizer affects not only loss but also graphics-processing-unit hours and downstream quality. Zhang et al. [135] study zeroth-order fine-tuning, which marks a boundary case for our taxonomy, since its central innovation is how the training signal is acquired, whereas our main taxonomy begins after a signal enters the optimizer update. The Muon studies [89, 100] expose a different boundary by showing that matrix-structured directions interact with pretraining-versus-fine-tuning stage, low-rank adaptation subspaces, spectral exponents, and local descent geometry. Together, these studies motivate benchmark reporting by method family and by objective rather than by a single aggregate rank.

This paper connects these three lines through a mechanism-aware organization. The universal meta-pipeline specifies where an optimizer changes a training update. The LMO-driven four-axis decomposition specifies how the update direction, curvature estimate, gradient signal, and state representation are formed. The dual-dimension taxonomy specifies how optimizers should be grouped and which training effects should be measured. The benchmark component is therefore not an isolated leaderboard but an empirical test of whether the taxonomy separates mechanisms that lead to distinct convergence, cost, memory, stability, tuning, and generalization behavior.

The remainder of the paper follows the same progression from foundations to evaluation. Section 2 introduces the LLM training problem, classical adaptive optimization, and notation. Section 3 presents the unified theoretical framework of this work. Subsection 3.1 introduces the universal meta-pipeline, its five operational stages, and representative instantiations organized around the identity-mapping principle, while Subsection 3.2 develops the LMO-driven four-axis decomposition as a mathematical explanation of practical optimizer updates. Section 4 introduces the dual-dimension taxonomy and explains how the method dimension is aligned with pipeline operations while the objective dimension captures effect targets. Section 5 consolidates the major optimizer families, with Subsections 5.1–5.5 surveying T1–T5 through the meta-pipeline, LMO-driven coordinates, and objective-oriented assessments. Section 6 reports the benchmark study. Sections 7 and 8 discuss limitations, open problems, and conclusions.

2 Preliminaries

This section lays the groundwork for the rest of the paper and fixes the optimization framework, model-structural conventions, and mathematical notation used in the analysis that follows. Section 2.1 first formalizes large-language-model training as a stochastic optimization problem and clarifies its characteristic parameter topology. Building on this, Section 2.2 reviews the core mechanisms of classical optimization methods, ranging from SGD and momentum to adaptive moment estimation. It also introduces the preconditioning perspective behind the Newton method, the natural gradient, and Fisher or Hessian curvature, so that the later sections have the background they need to develop the unified theoretical framework.

2.1 Problem Formulation

Training objective and stochastic gradients. Let $\mathcal{D} = \{(\mathbf{x}_i, \mathbf{y}_i)\}_{i=1}^N$ denote a training corpus and let $\theta \in \mathbb{R}^d$ collect all trainable parameters of a language model. Pretraining and supervised fine-tuning

both reduce to empirical risk minimization,

$$\min_{\theta \in \mathbb{R}^d} \mathcal{L}(\theta) = \frac{1}{N} \sum_{i=1}^N \ell(\theta; \mathbf{x}_i, \mathbf{y}_i), \quad (1)$$

where ℓ is usually a token-level cross-entropy or an instruction-tuning loss derived from it. At step t , the optimizer receives a mini-batch gradient,

$$g_t = \frac{1}{|\mathcal{B}_t|} \sum_{i \in \mathcal{B}_t} \nabla_{\theta} \ell(\theta; \mathbf{x}_i, \mathbf{y}_i), \quad (2)$$

where $\mathcal{B}_t \subset \{1, \dots, N\}$. When a stochastic-oracle model is needed, we write $\mathbb{E}[g_t \mid \theta_t] = \nabla \mathcal{L}(\theta_t)$ and $\mathbb{E}[\|g_t - \nabla \mathcal{L}(\theta_t)\|^2] \leq \sigma^2$. In practice, g_t reflects data sampling, sequence packing, distributed reduction, mixed precision, gradient accumulation, clipping, and loss scaling. These system details are not separate from optimizer behavior. In fact, they are what determine the noise level, numerical range, and memory traffic seen by the update rule.

Transformer parameter topology. Transformer-style LLMs [107] contain heterogeneous parameter tensors. For optimizer design, the most important distinction is not the layer name but the tensor geometry. Two-dimensional matrices $W \in \mathbb{R}^{m \times n}$, such as attention projections W_Q, W_K, W_V, W_O , feed-forward projections, and embedding tables, admit row-column operations including singular-value decompositions, Kronecker factorization, matrix orthogonalization, and low-rank projection. Vector-like parameters, such as biases and normalization gains or shifts, do not have the same matrix geometry and are usually routed to element-wise rules or excluded from weight decay. Some methods introduce finer scopes, e.g., attention-head blocks, per-layer groups, or module-specific rules. This parameter topology is the basis for the scoping-and-routing stage of the universal meta-pipeline in Section 3.1.

Memory budget under mixed-precision training. Under BF16 forward and backward computation with FP32 master weights, the training memory can be estimated as

$$M_{\text{train}} \approx 4d + 2d + 2d + S_{\text{opt}}d + M_{\text{act}}. \quad (3)$$

The first three terms correspond to FP32 master parameters, BF16 model copies, and BF16 gradients, S_{opt} is the optimizer-state footprint in bytes per parameter, and M_{act} denotes activation and temporary-buffer memory. Adam stores two FP32 state tensors m_t and v_t , so each parameter carries an extra 8 bytes. A 7B-parameter model therefore needs about 56 GB for Adam states alone, before activations, temporary buffers, and distributed-training overheads. State-compressed methods in Section 5.4 are therefore not merely engineering variants. Under a fixed hardware budget, reducing S_{opt} changes the feasible model size, batch size, and tuning regime.

2.2 Classical Optimization Background

The modern LLM optimizer literature can be read as a sequence of modifications to a small set of classical design choices. These choices are whether to smooth gradients, whether to maintain a curvature proxy, how to scale the direction, and how to regularize the final write. The following review fixes the baseline equations used by later sections.

Newton method and the perspective of preconditioning. A natural starting point for our subsequent preconditioning analysis is the Newton method. Near the current iterate, a second-order Taylor expansion yields:

$$\mathcal{L}(\theta_t + \delta) \approx \mathcal{L}(\theta_t) + g_t^\top \delta + \frac{1}{2} \delta^\top H_t \delta, \quad H_t = \nabla^2 \mathcal{L}(\theta_t). \quad (4)$$

Minimizing this local quadratic model gives the damped Newton update

$$\theta_{t+1} = \theta_t - \eta_t H_t^{-1} g_t, \quad (5)$$

where the scalar η_t absorbs damping, line search, or trust-region control. This equation gives the classical preconditioning viewpoint, since the optimizer does not only choose a gradient signal but also chooses the geometry in which that signal is scaled. SGD can be read as the first-order simplification that replaces H_t^{-1} by the identity. Modern large-model optimizers replace the exact inverse Hessian with tractable approximations or geometry-induced direction operators, where Adam uses a diagonal second-moment or Fisher-like proxy, Shampoo and SOAP use structured matrix factors or eigenbases, and Muon uses a polar or Gram-induced matrix direction. This connection motivates the preconditioned and matrix-structured views used throughout the rest of the survey.

SGD and momentum. Stochastic gradient descent (SGD) writes the raw mini-batch gradient into the parameters:

$$\theta_{t+1} = \theta_t - \eta_t g_t. \quad (6)$$

Momentum replaces the instantaneous gradient with an exponential moving average (EMA):

$$m_t = \beta_1 m_{t-1} + (1 - \beta_1) g_t, \quad \theta_{t+1} = \theta_t - \eta_t m_t. \quad (7)$$

SGD and momentum use one global scale, or a schedule of global scales, for all coordinates. They therefore do not adapt to coordinate-wise gradient magnitudes or curvature proxies. In the notation of Eq. (5), SGD corresponds to the identity preconditioner, $H_t = I$, so $H_t^{-1} g_t = g_t$. Momentum keeps the same identity geometry but replaces the instantaneous signal g_t with the smoothed signal m_t .

AdaGrad and RMSProp. AdaGrad [31] introduced a diagonal, history-dependent preconditioner by accumulating squared gradients:

$$G_t = \sum_{\tau=1}^t g_\tau^2, \quad \theta_{t+1} = \theta_t - \eta_t \frac{g_t}{\sqrt{G_t + \epsilon}}. \quad (8)$$

Here and below, powers and divisions are element-wise unless stated otherwise. The monotone accumulator is useful for sparse features but can make effective learning rates decay too aggressively in long training runs. RMSProp [105] replaces the cumulative sum with an EMA:

$$v_t = \beta_2 v_{t-1} + (1 - \beta_2) g_t^2, \quad \theta_{t+1} = \theta_t - \eta_t \frac{g_t}{\sqrt{v_t + \epsilon}}. \quad (9)$$

Equivalently, AdaGrad uses the effective diagonal metric $H_t^{\text{AdaGrad}} = \text{diag}(\sqrt{G_t + \epsilon})$, whereas RMSProp uses $H_t^{\text{RMSProp}} = \text{diag}(\sqrt{v_t + \epsilon})$. Both should be read as cheap diagonal preconditioners, that is, approximate proxies for Fisher or Hessian curvature.

Adam. Adam [54] combines momentum and RMSProp-style second moments, then corrects the initialization bias of both EMAs:

$$m_t = \beta_1 m_{t-1} + (1 - \beta_1) g_t, \quad v_t = \beta_2 v_{t-1} + (1 - \beta_2) g_t^2, \quad (10)$$

$$\hat{m}_t = m_t / (1 - \beta_1^t), \quad \hat{v}_t = v_t / (1 - \beta_2^t), \quad (11)$$

$$\theta_{t+1} = \theta_t - \eta_t \hat{m}_t / (\sqrt{\hat{v}_t + \epsilon}). \quad (12)$$

The diagonal preconditioner of Adam remains the reference point for most LLM optimizers. Later methods may alter the moment time scale, replace the gradient estimator, change the direction map, compress the state, or add a wrapper around the final update. Nevertheless, they are often compared against this Adam-like template. In the same preconditioning notation, Adam uses the effective signal \hat{m}_t and the diagonal metric $H_t^{\text{Adam}} = \text{diag}(\sqrt{\hat{v}_t + \epsilon})$, so the preconditioned direction is $H_t^{-1} \hat{m}_t = \hat{m}_t / (\sqrt{\hat{v}_t + \epsilon})$.

AdamW: decoupled weight decay. In Adam, adding ℓ_2 regularization to the loss causes the regularization gradient to be divided by the adaptive denominator. AdamW [70] decouples weight decay from this adaptive scaling:

$$\theta_{t+1} = \theta_t - \eta_t \frac{\hat{m}_t}{\sqrt{\hat{v}_t + \epsilon}} - \eta_t \lambda \theta_t. \quad (13)$$

This change is small at the formula level but important as a baseline convention: throughout the survey, an “Adam-like” optimizer means a method whose main state evolution is inherited from AdamW unless stated otherwise. AdamW retains the Adam diagonal preconditioner H_t^{Adam} for data-gradient components, moving weight decay outside the preconditioned update direction and incorporating it directly in the final parameter assignment step.

Natural gradient and the Fisher information matrix. The natural gradient [4] motivates many preconditioned updates. For a parameterized distribution $p_\theta(z)$, the Fisher information matrix is:

$$F(\theta) = \mathbb{E}_{z \sim p_\theta} \left[\nabla_\theta \log p_\theta(z) \nabla_\theta \log p_\theta(z)^\top \right]. \quad (14)$$

The corresponding update $\theta_{t+1} = \theta_t - \eta_t F(\theta_t)^{-1} \nabla \mathcal{L}(\theta_t)$ uses the geometry of the predictive distribution, whereas ordinary gradient descent uses the Euclidean geometry of raw parameters. Exact storage and inversion of F are infeasible for modern LLMs, so practical optimizers use diagonal, block-diagonal, Kronecker, low-rank, or stochastic approximations. Thus, natural gradient follows the same Newton-style template, but it replaces H_t with the Fisher metric $F(\theta_t)$. This makes it a useful bridge to later matrix and curvature-aware methods, which differ mainly in how they approximate, factor, or simplify this metric.

Gradient covariance and curvature. For negative log-likelihood objectives, the outer product of score gradients defines the Fisher matrix. Under standard regularity conditions, the gradient covariance, the Fisher matrix, and the Hessian are approximately equal, as given by

$$\mathbb{E} \left[g_t g_t^\top \mid \theta_t \right] \approx F(\theta_t), \quad F(\theta_t) \approx H(\theta_t) = \nabla^2 \mathcal{L}(\theta_t). \quad (15)$$

This distinction matters for a survey. The Adam $v_t = \text{EMA}(g_t^2)$ serves as a diagonal gradient-covariance estimate. The Shampoo factors $L_t = \text{EMA}(G_t G_t^\top)$ and $R_t = \text{EMA}(G_t^\top G_t)$ form a Kronecker-style curvature proxy [38], with $H_t^{\text{Shampoo}} \approx L_t^{1/4} \otimes R_t^{1/4}$. Sophia estimates a clipped diagonal Hessian using stochastic second-order information [65]. Section 3.2 turns these choices into Axis II (state and curvature estimator) and Axis III (geometry and precondition operator) of the LMO-driven four-axis decomposition.

Notation. Table 3 collects the mathematical symbols used throughout the paper and closes the preliminary setup before the meta-pipeline is introduced.

3 Unified Theoretical Framework for Optimizers

3.1 Universal Meta-Pipeline

3.1.1 Operational Steps

Modern LLM optimizers are usually named after their most visible local mechanism: an adaptive moment estimator, a matrix preconditioner, a low-rank projection, a sign map, a compressed state, or a sharpness-aware correction. Such descriptions are useful for implementation, but they make cross-method comparison difficult because they do not say *where* the mechanism enters the update.

Table 3: Summary of the mathematical notations used throughout this survey, including optimization variables, matrix operators, second-order quantities, and framework-specific symbols. The table serves as a reference for the formulations presented in the following sections.

Symbol	Meaning	Symbol	Meaning
d	Total number of model parameters	$W_t \in \mathbb{R}^{m \times n}$	Weight matrix
$\theta_t \in \mathbb{R}^d$	Parameter vector	$G_t \in \mathbb{R}^{m \times n}$	Gradient matrix
$\mathcal{L}(\theta)$	Training loss	$M_t \in \mathbb{R}^{m \times n}$	Matrix momentum
g_t	Mini-batch stochastic gradient	$W = U\Sigma V^\top$	Singular value decomposition
m_t	First-order momentum	$\langle A, B \rangle = \text{tr}(A^\top B)$	Matrix inner product
v_t	Second-order moment estimate	\odot	Hadamard product
η_t	Learning rate	$\ \cdot\ _p$	Vector ℓ_p norm
β_1, β_2	EMA decay coefficients	$\ \cdot\ _F$	Frobenius norm
λ	Weight-decay coefficient	$\ \cdot\ _{\text{op}}$	Spectral norm
ϵ	Numerical stability constant	$\ \cdot\ _*$ or $\ \cdot\ _*$	Nuclear or dual norm
$F(\theta)$	Fisher information matrix	Q_L, Q_R	Axis-I coordinate bases
$H(\theta) = \nabla^2 \mathcal{L}(\theta)$	Hessian matrix	Φ_t	Axis-III direction operator
\hat{H}_t	Axis-II curvature proxy	$\alpha \in [0, 1]$	Preconditioner exponent
$\text{EMA}_\beta(x_t)$	Exponential moving average	$\text{Imo}_C(s)$	Linear minimization oracle
\tilde{G}_t	Variance-reduced gradient estimate	$\rho^{(i)}$	Meta-pipeline routing label
$[\cdot]^\sharp$	Dual map	$T_1\text{--}T_5$	Dimension-A method families
		$O_1\text{--}O_6$	Dimension-B effect objectives

We therefore introduce a *Universal Meta-Pipeline*: a process-level abstraction that aligns the optimizers considered in this survey to a common single-step update template. Its purpose is to expose the operation site of each method, to separate primary mechanisms from defaults, and to prepare the bridge to the LMO-driven geometric view in Section 3.2.

Formal setup. Let $W_t \in \mathbb{R}^{m \times n}$ be a two-dimensional parameter tensor, $G_t \in \mathbb{R}^{m \times n}$ its training signal, and \mathcal{S}_{t-1} the optimizer state before the update. Five internal operators **S1–S5**, each of which may degenerate to the identity, transform G_t into a signed parameter increment Δ_t :

$$\Delta_t = \mathbf{S5}(\mathbf{S4}(\mathbf{S3}(\mathbf{S2}(\mathbf{S1}(G_t)); \mathcal{S}_{t-1}); \mathcal{S}_{t-1}); \mathcal{S}_{t-1}, W_t), \quad W_{t+1} = W_t + \Delta_t. \quad (16)$$

The internal state \mathcal{S}_t is updated within **S3** and is made available to all downstream stages. One-dimensional parameters (biases, normalization coefficients, and other vector-like tensors) follow the same pipeline, with matrix operations at **S2** and **S4** contracting to element-wise equivalents or identity maps. Figure 3 illustrates the pipeline for one training step.

S0: Training Signal Acquisition. Before the internal optimizer stages begin, the training system supplies a signal. We write this interface as **S0** because it determines what information the update pipeline is allowed to use. The standard case is *first-order backpropagation* (FO), $G_t = \nabla_W \mathcal{L}(W_t; \xi_t)$. Some optimizers replace G_t with a *variance-reduced* estimator, for example a STORM-style correction $\tilde{G}_t = G_t - G_{t-1}^{\tilde{t}} + M_{t-1}$. Others add *curvature-augmented* signals through Hessian-vector products or Hutchinson diagonal estimates, $h_t \approx u \odot (Hu)$ with $u \sim \mathcal{N}(0, I)$, as in Sophia [65]. Zeroth-order methods are treated as a boundary case in this paper: their main contribution is often signal acquisition from function values rather than the downstream update transformation, so they are not part of the main T1–T5 update-mechanism taxonomy.

S1: Parameter Scoping and Routing. The first internal stage partitions the full parameter set $\{\theta_{t-1}^{(i)}\}$ and assigns a routing label $\rho^{(i)}$ to each group based on tensor topology and module type:

$$\rho^{(i)} = \mathcal{R}(\text{shape}(\theta^{(i)}), \text{module-type}(\theta^{(i)})). \quad (17)$$

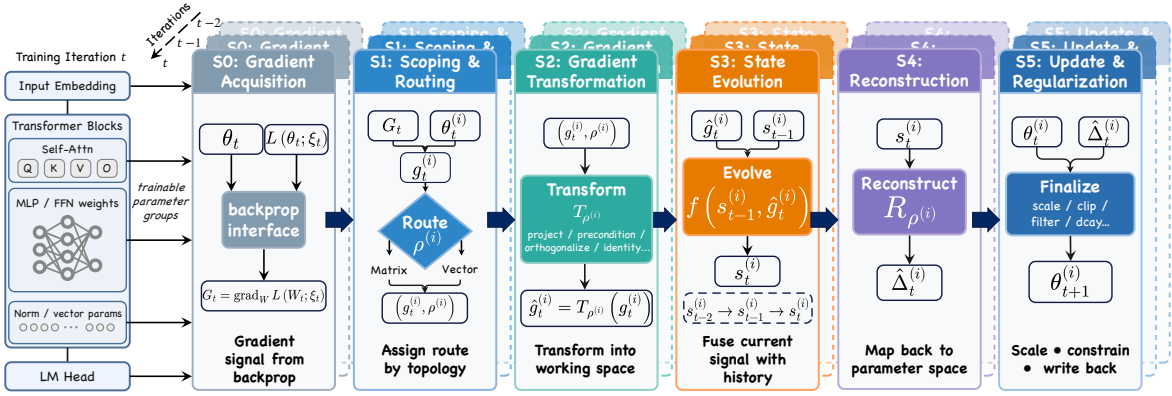


Figure 3: Universal meta-pipeline for one optimizer step. The training system provides a gradient or higher-order signal (S0), which the optimizer processes through five internal stages for each parameter group.

Equivalently, S1 outputs a partition $\mathcal{P} = \{P_k\}_{k=1}^K$ together with the processing rule attached to each group. All downstream stages condition on $\rho^{(i)}$. The common partition separates two-dimensional matrices—which admit matrix-geometric operations such as SVD decomposition, Kronecker factorization, and low-rank projection—from vector-like parameters handled by element-wise rules. Finer partitions include attention-head blocks, per-layer groups, and topology-dependent hybrid routes. When all parameters share a single route, S1 is an identity, as in standard AdamW. When routing is nontrivial, the same optimizer may apply different downstream operators to matrix, vector, or module-specific parameter groups.

S2: Gradient Transformation. This stage applies a structured operator \mathcal{T} to the routed gradient, potentially altering its dimension or manifold:

$$\hat{G}_t = \mathcal{T}(G_t; S_{t-1}) \in \mathbb{R}^{r \times s}. \quad (18)$$

When $r = m$ and $s = n$, the transformation is dimension-preserving. When $r \ll m$ or $s \ll n$, it is a compression. Representative transformations include: (i) the identity $\hat{G}_t = G_t$ (T1, T4, most T5 methods); (ii) Newton–Schulz spectral orthogonalization $\hat{G}_t = \text{NS}_k(M_t)$ such that $\hat{G}_t^\top \hat{G}_t \approx I$ (Muon, T2.1); (iii) Kronecker-factored preconditioning $\hat{G}_t = L_t^{-1/4} G_t R_t^{-1/4}$ where $L_t \approx \mathbb{E}[G_t G_t^\top]$ (Shampoo, T2.2); (iv) low-rank orthogonal projection $\hat{G}_t = P_t^\top G_t \in \mathbb{R}^{r \times n}$ with $P_t \in \mathbb{R}^{m \times r}$, $r \ll m$ (Galore, T2.3); (v) sign or quantized-direction discretization $\hat{G}_t = \text{sign}(\beta_1 m_{t-1} + (1 - \beta_1) G_t)$ (Lion, T3). Stages S2 and S4 form a mathematical dual: whenever S2 introduces a dimension-reducing or basis-rotating map, S4 must define the corresponding return map to the parameter space. This duality is exact for orthogonal basis rotations and approximate for projection or factorized-state methods.

S3: State Evolution. This stage updates the internal memory of the optimizer:

$$S_t = f(S_{t-1}, \hat{G}_t). \quad (19)$$

For Adam-family methods, S_t contains first- and second-order moment EMAs:

$$m_t = \beta_1 m_{t-1} + (1 - \beta_1) \hat{G}_t, \quad v_t = \beta_2 v_{t-1} + (1 - \beta_2) \hat{G}_t^{\odot 2}. \quad (20)$$

Alternative state forms include Kronecker factors $L_t = \text{EMA}_\beta(G_t G_t^\top)$, $R_t = \text{EMA}_\beta(G_t^\top G_t)$ (Shampoo, T2.2); row-column factored states $r_t \in \mathbb{R}^m$, $c_t \in \mathbb{R}^n$ with $v_t \approx r_t c_t^\top$ (AdaFactor, T4.1); INT8-quantized

states with error-feedback compensation (8-bit Adam, T4.2); and multi-timescale EMA streams (AdE-MAMix, T1.2). Stateless methods either bypass S3 or pass the current transformed signal directly downstream. As established in Section 2.2, the second-order moment $v_t = \text{EMA}(g_t^2)$ is an online estimator of the diagonal Fisher information matrix. This connects S3 to Axis III of the LMO-driven four-axis decomposition (Section 3.2.2).

S4: Update Reconstruction. If S2 introduced a change of representation, this stage applies the corresponding inverse operator \mathcal{R} to restore the full-space update:

$$\hat{\Delta}_t = \mathcal{R}(\tilde{\Delta}_t; S_t) \in \mathbb{R}^{m \times n}, \quad (21)$$

where $\tilde{\Delta}_t$ is the update direction derived from the evolved state. For low-rank methods, $\hat{\Delta}_t = P_t \tilde{\Delta}_t$; for Kronecker-factor methods, $\hat{\Delta}_t = Q_L \tilde{\Delta}_t Q_R^T$ (exact, as Q_L, Q_R are orthogonal); for row-column-factored preconditioners, the reconstruction is a rank-1 outer-product approximation. When S2 is the identity, S4 is also the identity. The exactness of the inverse map governs the fidelity of the final update direction and is analyzed per family in Subsections 5.2–5.4.

S5: Update Finalization. The reconstructed direction is converted into the actual parameter writeback by applying scaling, regularization, and geometric constraints:

$$W_{t+1} = W_t - \eta_t \cdot \phi_t^{(l)} \cdot \mathcal{C}(\mathcal{F}(\hat{\Delta}_t)) - \eta_t \lambda W_t, \quad (22)$$

where η_t is the global learning rate, $\phi_t^{(l)}$ is an optional layer-wise trust-ratio factor, \mathcal{F} is a post-update filter operator, \mathcal{C} is a clipping operator, and λ is the weight-decay coefficient. Representative sub-operations include: decoupled weight decay (AdamW [70]); global gradient clipping; element-wise trust-region clipping $\hat{\Delta}_t \leftarrow \text{clip}(\hat{\Delta}_t / \max(\gamma h_t, \epsilon), 1)$ (Sophia [65]); layer-wise trust-ratio scaling $\phi_t^{(l)} = \Phi(\|W^{(l)}\| / \|\hat{\Delta}^{(l)}\|)$ (LAMB); direction-consistency masking (Cautious Optimizers); and adversarial-perturbation final corrections (SAM [32], T5.1). These sub-operations are optional and often composable, but their order must be specified when two mechanisms modify the same quantity. Their shared role is to convert the update direction $\hat{\Delta}_t$ into the physically written parameter change.

Algorithm 1 gives the full abstract procedure. The operator names ROUTE, TRANSFORM, EVOLVE, RECONSTRUCT, and FINALIZE are abstract placeholders. A concrete optimizer family replaces one or two of them with a structured operator and leaves the remainder as identity maps or standard defaults.

The six stages should be read as an ordered checklist for locating non-identity operations. In the default path, S0 supplies a first-order mini-batch gradient, S1 assigns all parameters to a single element-wise route, S2 and S4 are identity maps, S3 is either stateless or a standard momentum buffer, and S5 writes the update with a global learning rate. Non-default optimizers deviate from this path by changing the acquired signal in S0, routing tensors or modules differently in S1, transforming the gradient representation in S2, storing richer temporal or curvature information in S3, reconstructing a full-space direction in S4, or applying decay, clipping, trust-ratio scaling, masks, or sharpness corrections in S5. Because practical optimizers often combine several such deviations, the meta-pipeline is not a one-to-one stage-to-family lookup. It is instead an operational vocabulary for describing where a method intervenes before the later taxonomy discusses families at a coarser mechanism level.

3.1.2 Identity Mapping and Representative Instantiations

A central consequence of the pipeline formulation is the *identity-mapping principle*: most optimizers make a nontrivial design choice at only one or two pipeline stages and leave the remaining stages as identity maps or standard defaults. This principle provides a compact characterization of representative optimizers and supports the methodological taxonomy in Section 4, while allowing individual families to span multiple stages when their mechanisms are coupled.

Algorithm 1 Universal Meta-Pipeline for Modern Optimizer Updates.

Require: Parameters Θ_0 , loss \mathcal{L} , learning-rate schedule $\{\eta_t\}_{t=1}^T$
Require: Initial optimizer state \mathcal{S}_0 , regularization coefficient λ
Ensure: Final parameters Θ_T

- 1: **for** $t = 1, \dots, T$ **do**
- 2: $G_t \leftarrow \text{ACQUIRE SIGNAL}(\Theta_{t-1}, \mathcal{L})$ ▷ S0: FO / VR / curvature-augmented
- 3: **for each** $\theta_{t-1}^{(i)} \in \Theta_{t-1}$ **do**
- 4: $g_t^{(i)} \leftarrow \text{SELECT}(G_t, \theta_{t-1}^{(i)})$
- 5: $\rho^{(i)} \leftarrow \text{ROUTE}(\theta_{t-1}^{(i)})$ ▷ S1: parameter scoping and routing
- 6: $\hat{g}_t^{(i)} \leftarrow \text{TRANSFORM}(g_t^{(i)}, \rho^{(i)})$ ▷ S2: gradient transformation
- 7: $s_t^{(i)} \leftarrow \text{EVOLVE}(s_{t-1}^{(i)}, \hat{g}_t^{(i)}, \rho^{(i)})$ ▷ S3: state evolution
- 8: $\hat{\Delta}_t^{(i)} \leftarrow \text{RECONSTRUCT}(s_t^{(i)}, \rho^{(i)})$ ▷ S4: update reconstruction
- 9: $\theta_t^{(i)} \leftarrow \text{FINALIZE}(\theta_{t-1}^{(i)}, \hat{\Delta}_t^{(i)}, \eta_t, \lambda)$ ▷ S5: update finalization
- 10: **end for**
- 11: $\mathcal{S}_t \leftarrow \{s_t^{(i)}\}_i$
- 12: **end for**

AdamW (T1). All parameters are assigned to a single element-wise route, so S1 is effectively an identity. Gradient Transformation (S2) is also the identity: G_t enters State Evolution (S3) unchanged. S3 maintains first- and second-order moment EMAs as in Eq. (20). This is the defining stage of the T1 family. Update Reconstruction (S4) is the identity because moment states reside in the full parameter space. Update Finalization (S5) applies bias-corrected adaptive scaling and decoupled weight decay. In the pipeline view, **AdamW is primarily an S3/S5 method.**

Muon (T2.1). Parameter Scoping and Routing (S1) separates two-dimensional weight matrices from vector parameters. Gradient Transformation (S2) applies Newton–Schulz orthogonalization to the gradient momentum, producing a spectrally normalized matrix \hat{G}_t with $\hat{G}_t^\top \hat{G}_t \approx I$. State Evolution (S3) maintains standard momentum. Update Reconstruction (S4) is trivially satisfied because the orthogonalization is dimension-preserving. Update Finalization (S5) follows an SGD-style writeback. **Muon is primarily an S1/S2 method.**

GaLore (T2.3). Routing (S1) identifies tensors eligible for low-rank treatment. Gradient Transformation (S2) projects gradients into an r -dimensional subspace via $\hat{G}_t = P_t^\top G_t$. State Evolution (S3) runs a full Adam update in the reduced space. Update Reconstruction (S4) maps the subspace update back via $\hat{\Delta}_t = P_t \tilde{\Delta}_t$. The primary contribution is the relocation of both computation and optimizer state into a lower-dimensional space through the S2/S4 dual. **GaLore spans S1–S4, with primary novelty at S2 and S4.**

Lion (T3). Gradient Transformation (S2) discretizes the momentum-interpolated gradient into the signed direction

$$d_t = \text{sign}(\beta_1 m_{t-1} + (1 - \beta_1) G_t), \quad (23)$$

whose entries lie in $\{-1, +1\}$ and whose writeback has an ℓ_∞ norm set by the learning rate. State Evolution (S3) maintains only a first-order momentum (no second-order state). Update Reconstruction (S4) is the identity since the discrete direction already has the parameter shape. **Lion is primarily an S2/S3 method.**

Table 4: Representative optimizer families viewed through the universal meta-pipeline. Only active stages and defining mechanisms are shown; inactive stages follow identity maps or standard defaults.

Method (family)	Active stages	Core mechanism
AdamW (T1.1)	S3, S5	Moment EMAs (S3) with decoupled weight decay (S5)
Muon (T2.1)	S1, S2	Matrix routing (S1) with Newton–Schulz spectral orthogonalization (S2)
GaLore (T2.3)	S1–S4	Low-rank projection (S1/S2), subspace Adam state (S3), and inverse projection (S4)
Lion (T3)	S2, S3	Momentum interpolation (S3) followed by sign discretization (S2)
SAM (T5.1)	S0, S5	Perturbation-induced gradient (S0) with neighborhood-regularized writeback (S5)

SAM (T5.1). A first backward pass computes the mini-batch gradient G_t . An adversarial perturbation $\epsilon^* = \rho G_t / \|G_t\|$ is then injected, and a second backward pass at $W_t + \epsilon^*$ supplies the sharpness-aware update signal. Stages S1–S4 execute default element-wise operations. The sharpness correction is realized entirely within the Training Signal Acquisition (S0) and Update Finalization (S5). **SAM is primarily an S0/S5 method.**

Table 4 summarizes these instantiations. Active-stage labels identify the pipeline positions that implement the defining mechanism of each method, and the family label in the method cell links each example to Subsections 5.1–5.5.

The same view also exposes composition constraints. Mechanisms placed in different stages are often naturally stackable. For example, a variance-reduced signal (S0) can feed AdamW, Lion, or Shampoo. Low-rank projection (S2/S4) can be combined with state quantization (S3/S4), and a final trust-ratio wrapper (S5) can be placed after a standard adaptive update. By contrast, mechanisms that occupy the same slot require an explicit ordering. For example, two S2 operations such as low-rank projection and spectral orthogonalization must specify whether the optimizer projects before orthogonalizing or orthogonalizes before projecting, because the resulting descent direction and state memory differ. This is why the meta-pipeline is useful not only for classification, but also for reasoning about optimizer composition.

The meta-pipeline answers an *operational* question: where does an optimizer intervene in the update process? The LMO-driven analysis in Section 3.2 answers a complementary *geometric* question: why does the resulting direction take a particular mathematical form? The two views are aligned. S2 corresponds to applying an analysis basis and a direction function (Axes I and III of the four-axis decomposition). S3 corresponds to maintaining a curvature estimate and its storage form (Axes II and III). S5 encompasses the weight-decay, clipping, and trust-ratio mechanisms orthogonal to direction geometry. This alignment allows each optimizer to be characterized by a concise four-axis coordinate tuple in addition to its active pipeline stages. The full instantiation table is given in Section 3.2.3.

3.2 A Mathematical Unification of Optimizer Updates

The universal meta-pipeline of Section 3.1 is an operational abstraction, because it only tells us at which step of a single update an optimizer intervenes. The shape of the resulting update direction is exactly what this section formalizes through a complementary mathematical view.

We take the linear minimization oracle, abbreviated LMO, as the central building block, and the reason is geometric. When the same gradient signal is fed into different norm balls, the extremal direction returned by the oracle changes with the shape of the ball, so the constraint geometry and the optimizer behavior become two readings of one object. This single idea is strong enough to place sign updates, spectral orthogonalization, Kronecker-factored preconditioning, curvature weighting, variance reduction, and state compression inside one compact coordinate system, and it lets us compare them without ever switching notation.

Building on this view, we organize every optimizer update along four axes, and we order them so that

they follow the actual pipeline of an optimizer. The first axis is the *update domain*, which asks where the update lives, whether in the original parameter space, in the matrix space, in a low-rank subspace, or in some projected coordinate system. The second axis is the *state estimator*, which asks how the effective signal, the momentum, the second-order state, the Gram Hessian, and the projection state are formed from the current gradient together with the accumulated history. The third axis is the *geometry and precondition operator*, which asks how the quantity produced by the state estimator becomes a direction, either through an LMO constraint set or through a Hessian-based preconditioner. The fourth axis is the *finalization wrapper*, which asks how the direction is written back to the parameters, and it absorbs the learning rate, the weight decay, the projection-back step, the routing rule, the fallback, and the refresh schedule. In short, the first axis fixes the space, the second estimates the state, the third generates the direction, and the last commits the update.

3.2.1 LMO Foundations and Norm-Induced Directions

Linear minimization oracle. Given a convex set \mathcal{D} and an input signal s , the LMO is defined as

$$\text{lmo}_{\mathcal{D}}(s) \in \arg \min_{x \in \mathcal{D}} \langle s, x \rangle. \quad (24)$$

Here \mathcal{D} can be any convex set, such as a simplex, a polytope, an ℓ_1 ball, a nuclear-norm ball, or, most importantly for this section, a norm ball. Norm balls are exactly the special case that connects the oracle to familiar optimizer directions, and they are the case we develop next.

Norm-constrained LMO. When the constraint set is a norm ball of radius ρ , written $\mathcal{D}_{\rho} = \{x : \|x\| \leq \rho\}$, the oracle returns the extremal descent direction of that particular geometry. To make this explicit, let $u^{\sharp}(s)$ denote the steepest-ascent direction on the unit ball,

$$u^{\sharp}(s) \in \arg \max_{\|u\| \leq 1} \langle s, u \rangle, \quad (25)$$

so that the oracle factorizes as

$$\text{lmo}_{\mathcal{D}_{\rho}}(s) = -\rho u^{\sharp}(s). \quad (26)$$

Now suppose the optimizer takes the descent form $W_{t+1} = W_t - \eta_t \Phi_t(s_t)$. Then the direction operator is exactly

$$\Phi_t(s_t) = u^{\sharp}(s_t) = -\frac{1}{\rho} \text{lmo}_{\mathcal{D}_{\rho}}(s_t), \quad (27)$$

which shows that the norm-constrained LMO and steepest descent share one geometric core. In words, the norm ball is what decides which direction counts as steepest. One caveat matters here, because the oracle reports a direction and a boundary point but discards magnitude, so any gradient scale that we wish to keep must be reintroduced through the learning rate, the radius, or a preconditioner.

Unconstrained update-direction view. For the rest of the section we adopt the direction-generator view of an unconstrained optimizer,

$$W_{t+1} = W_t - \eta_t \Phi_t(M_t), \quad (28)$$

where $W_t \in \mathbb{R}^d$ collects the parameters, M_t is the effective signal handed over by the state estimator, and Φ_t is the direction operator that the LMO geometry or the preconditioner induces.

Canonical norm geometries. Different norm balls give rise to different families of directions, and a few canonical choices already cover most optimizers. The Euclidean ball yields the normalized gradient,

$$\mathcal{D}_2 = \{x : \|x\|_2 \leq \rho\}, \quad \text{Imo}_{\mathcal{D}_2}(g) = -\rho \frac{g}{\|g\|_2}, \quad \Phi(g) = \frac{g}{\|g\|_2}. \quad (29)$$

The max-norm ball yields the sign direction, because every vertex of the hypercube is a sign pattern,

$$\mathcal{D}_\infty = \{x : \|x\|_\infty \leq \rho\}, \quad \text{Imo}_{\mathcal{D}_\infty}(g) = -\rho \text{sign}(g), \quad \Phi(g) = \text{sign}(g). \quad (30)$$

The spectral-norm ball yields the matrix polar direction, and writing $M = U\Sigma V^\top$ we obtain

$$\mathcal{D}_{S_\infty} = \{X : \|X\|_{S_\infty} \leq \rho\}, \quad \text{Imo}_{\mathcal{D}_{S_\infty}}(M) = -\rho UV^\top, \quad \Phi(M) = UV^\top. \quad (31)$$

We stress that the SVD here is only a device for computing the polar operator. Muon is the clearest example, because its update domain can stay in the original matrix space with $Q_L = Q_R = I$. Adam fits the same picture once the box is allowed to move with the state. If the state estimator outputs m_t and v_t , define the dynamic bound $b_{t,i} = |m_{t,i}| / \sqrt{v_{t,i}}$ and the adaptive box

$$\mathcal{D}_t^{\text{Adam}} = \{x : |x_i| \leq \rho_t b_{t,i}, \forall i\}, \quad \text{Imo}_{\mathcal{D}_t^{\text{Adam}}}(m_t) = -\rho_t \frac{m_t}{\sqrt{v_t}}. \quad (32)$$

Adam is therefore a dynamic-boundary LMO over an adaptive constraint set, and that constraint set is itself produced by the Axis II state estimator. Table 5 collects these correspondences between norms, analysis coordinates, direction operators, and representative optimizers, and it again records that Muon keeps the original update domain even though its direction is computed through an SVD.

3.2.2 A Four-Axis Decomposition of Optimizer Updates

The reorganization at the heart of this section is easy to state. The LMO reading and the preconditioning reading are two faces of one direction operator Φ_t , so we keep them together inside Axis III. At the same time, we move momentum, the second moment, variance reduction, and the projection state one step earlier into Axis II, because all of them are estimated before any direction is formed and all of them feed the operator. With this ordering the update takes a master form,

$$(M_t, H_t, \mathcal{D}_t) = \text{StateEstimator}_t(g_t, \text{State}_{t-1}), \quad (33)$$

$$D_t = \Phi_t(M_t; H_t, \mathcal{D}_t), \quad (34)$$

$$W_{t+1} = \text{Finalize}(W_t, D_t), \quad (35)$$

in which g_t is the current stochastic gradient, M_t is the effective signal, H_t is a Hessian, Gram, Fisher, or second-moment proxy, and \mathcal{D}_t is the LMO constraint set when one is used. Axis II produces these objects, and only Axis III turns them into a direction. We describe the four axes one by one below, and because each axis is a largely independent choice, a concrete optimizer follows once we settle on an update domain, a state estimator, a geometry-and-precondition operator, and a finalization wrapper.

Axis I: Update domain and support. This axis, written \mathcal{X}_t or (Q_L, Q_R) , fixes the space in which the update is expressed. For SGD, AdamW, and Muon the natural choice is to update directly in the original parameter or matrix space, whereas GaLore deliberately confines the update to a low-rank projected space. Whenever such a projection is present, we write $Z_t = Q_L^\top M_t Q_R$ and then carry the direction back through $D_t = Q_L \Phi_t(Z_t; \bar{H}_t, \bar{\mathcal{D}}_t) Q_R^\top$, so the direction is first formed in the small space and only afterwards returned to the full space. When there is no genuine subspace, however, no basis should be introduced artificially, and Muon makes the point concrete because it can simply take $Q_L = Q_R = I$. The representative choices are therefore the full space, the matrix space, and a low-rank projected subspace.

Axis II: State estimator. The state estimator, written StateEstimator_t , answers one question. Given the current gradient and the accumulated history, what signal does the optimizer actually hand to the geometry operator? Vanilla SGD keeps nothing, so $M_t = g_t$ and $H_t = I$. Momentum SGD keeps a first-order average, so $M_t = m_t$ with $m_t = \beta m_{t-1} + (1 - \beta)g_t$. Adam keeps both a first moment and a second moment,

$$m_t = \beta_1 m_{t-1} + (1 - \beta_1)g_t, \quad v_t = \beta_2 v_{t-1} + (1 - \beta_2)g_t^2, \quad M_t = m_t, \quad H_t = \text{diag}(v_t). \quad (36)$$

MARS [128] belongs here as well, even though it is usually described as a variance-reduction method, because in our framework its role is unambiguous. It first turns the raw stochastic gradient into a variance-reduced estimate, and only afterwards maintains the momentum and the second moment from that estimate. Concretely, writing $g_t^{\zeta_t} = \nabla f(W_t, \zeta_t)$ and $g_{t-1}^{\zeta_t} = \nabla f(W_{t-1}, \zeta_t)$, the corrected gradient is

$$c_t = g_t^{\zeta_t} + \gamma_t \frac{\beta_1}{1 - \beta_1} (g_t^{\zeta_t} - g_{t-1}^{\zeta_t}), \quad (37)$$

and the MARS-AdamW state then follows $m_t = \beta_1 m_{t-1} + (1 - \beta_1)c_t$ and $v_t = \beta_2 v_{t-1} + (1 - \beta_2)c_t^2$, again with $M_t = m_t$ and $H_t = \text{diag}(v_t)$. This makes the separation clean, because variance reduction in the style of MARS, STORM, or SVRG belongs to Axis II, whereas the geometry and preconditioning of AdamW, Shampoo, or Muon belong to Axis III.

Axis III: Geometry and precondition operator. The direction generator, written Φ_t , carries two readings at once, an LMO reading and a preconditioning reading, which is why we name the axis the geometry and precondition operator. From the LMO side it is $\Phi_t(M_t) = -\frac{1}{\rho_t} \text{Imo}_{\mathcal{D}_t}(M_t)$, and from the preconditioning side it is $\Phi_t(M_t) = H_t^{-\alpha} M_t$, where α is an internal exponent of Φ_t . The two readings agree on the familiar cases, since AdamW uses a diagonal second-moment metric, Shampoo uses a Kronecker-factored metric, and Muon uses the Gram Hessian of the current matrix. Muon is worth spelling out, because it shows the equivalence directly. Take $M_t \in \mathbb{R}^{m \times n}$ with $m < n$, and use the left Gram Hessian $H_t = M_t M_t^\top$ in the idealized full-rank case. Then

$$\Phi_t(M_t) = H_t^{-1/2} M_t = (M_t M_t^\top)^{-1/2} M_t, \quad \text{with} \quad M_t = U_t \Sigma_t V_t^\top, \quad \Phi_t(M_t) = U_t V_t^\top, \quad (38)$$

so the preconditioned form coincides exactly with the spectral-LMO polar form. Muon is therefore a spectral-norm LMO and a Gram-based preconditioner at the same time, and these are the two faces of Axis III.

Axis IV: Finalization and wrapper. The last axis, written Finalize , handles everything that happens after a direction has been produced, from the learning rate and the weight decay to the projection-back step, the layer-wise routing, the fallback rule, and the refresh schedule. The decoupled weight decay of AdamW lives here, the projection-back of GaLore lives here, and the unique Muon practice of treating different tensor types with different rules lives here as well.

Relation to the universal meta-pipeline. The mathematical framework of this section and the meta-pipeline of Section 3.1 describe the same update from two angles, and the two line up step by step. Choosing the update domain $W_t \in \mathcal{X}_t$ is the P1 step and corresponds to Axis I, estimating the optimizer state $(M_t, H_t, \mathcal{D}_t) = \text{StateEstimator}_t(g_t, \text{State}_{t-1})$ is the P2 step and Axis II, generating the direction $D_t = \Phi_t(M_t; H_t, \mathcal{D}_t)$ is the P3 step and Axis III, and finalizing the writeback $W_{t+1} = \text{Finalize}(W_t, D_t)$ is the P4 step and Axis IV. The ordering is the part worth remembering, because the state estimator always comes first and the geometry operator always comes second, so Axis II produces the triple $(M_t, H_t, \mathcal{D}_t)$ and Axis III then consumes that triple to form the direction $\Phi_t(M_t; H_t, \mathcal{D}_t)$.

3.2.3 Instantiations

We close the section by reading several representative optimizers through the four axes. The main table keeps only short labels, and the detailed formulas follow underneath so that the table stays legible.

AdamW. AdamW estimates two moments in Axis II, namely $m_t = \beta_1 m_{t-1} + (1 - \beta_1) g_t$ together with $v_t = \beta_2 v_{t-1} + (1 - \beta_2) g_t^2$. Axis III then turns these states into a direction through $D_t = \Phi_t(m_t; H_t) = H_t^{-1/2} m_t$ with $H_t = \text{diag}(v_t)$. Read as an LMO this is an adaptive ℓ_∞ box, and read as a preconditioner it is a diagonal second-moment metric, which is exactly the two-faced behavior described above.

MARS-AdamW. MARS-AdamW shares the Axis III form of AdamW and differs only in Axis II. It first builds a corrected gradient $c_t = g_t^{\xi_t} + \gamma_t \frac{\beta_1}{1 - \beta_1} (g_t^{\xi_t} - g_{t-1}^{\xi_t})$, then maintains the Adam states from the corrected c_t , with $m_t = \text{EMA}(c_t)$ and $v_t = \text{EMA}(c_t^2)$, and only afterwards forms the direction $D_t = \text{diag}(v_t)^{-1/2} m_t$. The variance reduction therefore sits squarely in the state estimator, while the preconditioning remains a later Axis III step.

Muon. In Muon the Axis II stage produces a momentum matrix M_t . The Axis III reading as an LMO is the spectral-norm ball, so $\text{lmo}_{\mathcal{D}_{S_\infty}}(M_t) = -\rho_t U_t V_t^\top$ with $M_t = U_t \Sigma_t V_t^\top$, which gives the direction operator $\Phi_t(M_t) = U_t V_t^\top$. The reading as a preconditioner instead uses the left Gram Hessian $H_t = M_t M_t^\top$, and then $\Phi_t(M_t) = H_t^{-1/2} M_t$. Both readings describe one update, and we keep the original matrix-space interpretation throughout.

GaLore-Adam. GaLore is the clearest case in which Axis I is nontrivial, because it places the whole update inside a low-rank projected subspace. The construction starts from a pair of projection matrices, $Q_L \in \mathbb{R}^{m \times r}$ and $Q_R \in \mathbb{R}^{n \times r}$, whose columns span the retained subspace and whose rank r is much smaller than the matrix dimensions m and n . Given the full-space momentum $M_t \in \mathbb{R}^{m \times n}$, the optimizer first compresses it into the subspace through

$$\bar{M}_t = Q_L^\top M_t Q_R, \quad (39)$$

where $\bar{M}_t \in \mathbb{R}^{r \times r}$ is the projected momentum and the bar notation marks every quantity that lives inside the subspace. The Axis II stage then runs an ordinary Adam state update on \bar{M}_t , maintaining a projected first moment \bar{m}_t and a projected second moment \bar{v}_t , where \bar{m}_t plays the role of the momentum and \bar{v}_t plays the role of the coordinate-wise variance estimate, both stored in the small $r \times r$ space so that the memory cost drops from $O(mn)$ to $O(r^2)$. The Axis III stage forms the direction inside the subspace exactly as AdamW would, namely

$$\bar{D}_t = \frac{\bar{m}_t}{\sqrt{\bar{v}_t}}, \quad (40)$$

where the division and the square root act entry by entry, so $\bar{D}_t \in \mathbb{R}^{r \times r}$ is the adaptive direction in the projected coordinates. Finally, the Axis IV stage lifts this direction back to the original space through

$$D_t = Q_L \bar{D}_t Q_R^\top, \quad (41)$$

where $D_t \in \mathbb{R}^{m \times n}$ is the update actually applied to the weight matrix. Read as an LMO the construction is a projected adaptive box, because the box geometry of Adam is simply expressed in the subspace coordinates, and read as a preconditioner it is a projected diagonal metric, because \bar{v}_t supplies a diagonal scaling that is later rotated back by Q_L and Q_R .

Table 5: Optimizer instantiations under the four-axis decomposition (Axes I–IV of Section 3.2.2), spanning all five families (T1–T5). Axis III shows two faces of the same direction operator Φ_t , the LMO constraint ball and the preconditioner H_t . The LMO direction is the steepest descent inside that ball, which is the ℓ_2 ball, the ℓ_∞ box, or the metric ball $\|\delta\|_{H_t} = \sqrt{\delta^\top H_t \delta} \leq 1$ induced by H_t . In the Domain column, \mathbb{R}^d means all parameters are flattened into d independent scalar coordinates and updated element-wise, while $\mathbb{R}^{m \times n}$ means the update operates on a whole weight matrix and couples its entries, with short tags for factored, INT8, block, row, or column variants. Here g_t is the gradient, m_t, v_t the first and second moments, c_t the MARS variance-reduced estimate, s_t the AdaBelief variance, h_t a diagonal Hessian estimate, M_t the matrix-form momentum, L_t, R_t the Shampoo row and column Kronecker factors, Q_L, Q_R their eigenvector matrices, P_t the low-rank projection onto the current subspace (learned for GaLore and Fira, random for APOLLO, column-orthogonal for Conda) with back-projection P_t^\top , and $\tilde{m}_t, \tilde{v}_t, \tilde{H}_t$ the quantities formed inside P_t . The tag +res marks Fira’s residual correction in the orthogonal complement of P_t , VR marks a variance-reduced (MARS) estimate, and matrix routing means only matrix parameters receive the matrix update while vector-like parameters follow an AdamW-style branch.

Optimizer	Axis I: Domain	Axis II: State estimator	Axis III (LMO)	Axis III (Precondition)	Axis IV: Finalization
T1: Element-wise adaptive moment and scalar control					
SGDM	\mathbb{R}^d	m_t	ℓ_2 ball	$H_t = I$	LR
Adam, AdamW	\mathbb{R}^d	m_t, v_t	adaptive ℓ_∞	$H_t = \text{diag}(v_t)$	LR + decoupled WD
NAdam	\mathbb{R}^d	Nesterov m_t, v_t	adaptive ℓ_∞	$H_t = \text{diag}(v_t)$	Nesterov + LR + WD
AdaBelief	\mathbb{R}^d	m_t, s_t	adaptive ℓ_∞	$H_t = \text{diag}(s_t)$	LR + WD
ADOPT	\mathbb{R}^d	ordered, delayed m_t, v_t	adaptive ℓ_∞	$H_t = \text{diag}(v_t)$	LR + WD
Adan	\mathbb{R}^d	m_t + grad-diff state	adaptive ℓ_∞	$H_t = \text{diag}(v_t)$	LR + WD
AdEMAMix	\mathbb{R}^d	short/long EMA	adaptive ℓ_∞	$H_t = \text{diag}(v_t)$	LR + WD
MARS-AdamW	\mathbb{R}^d	c_t, m_t, v_t	adaptive ℓ_∞ (VR)	$H_t = \text{diag}(v_t),$ $v_t = \text{EMA}(c_t^2)$	LR + decoupled WD
RAdam	\mathbb{R}^d	rectified m_t, v_t	adaptive ℓ_∞	$H_t = \text{diag}(v_t)$	LR + WD
Prodigy	\mathbb{R}^d	m_t, v_t + LR est. d_t	adaptive ℓ_∞	$H_t = \text{diag}(v_t)$	automatic LR + WD
T2: Matrix-level structural methods					
Muon	$\mathbb{R}^{m \times n}$	M_t	spectral (polar)	$H_t = M_t M_t^\top$	LR + matrix routing
MARS-Shampoo	$\mathbb{R}^{m \times n}$ (L_t, R_t)	c_t, m_t, L_t, R_t	metric ball (VR)	$H_t = L_t^{1/4} \otimes R_t^{1/4}$	LR + damping
Shampoo	$\mathbb{R}^{m \times n}$ (L_t, R_t)	m_t, L_t, R_t	metric ball	$H_t = L_t^{1/4} \otimes R_t^{1/4}$	LR + damping
SOAP	Q_L, Q_R	m_t, v_t, Q_L, Q_R	adaptive ℓ_∞ in Q_L, Q_R	$\text{diag}(v_t)$ in Q_L, Q_R	LR + WD
GaLore	P_t	\tilde{m}_t, \tilde{v}_t on $P_t g_t$	projected ℓ_∞	$\tilde{H}_t = \text{diag}(\tilde{v}_t)$	P_t^\top back + LR + WD
Fira	P_t (+res)	\tilde{m}_t, \tilde{v}_t + residual	projected ℓ_∞ (+res)	$\tilde{H}_t = \text{diag}(\tilde{v}_t)$	P_t^\top back + res + LR
RMNP	$\mathbb{R}^{m \times n}$ (row)	M_t	row-normalized	$H_t = \text{diag}(M_t M_t^\top)$	LR + matrix routing
T3: Discretization and directional quantization					
SignSGD	\mathbb{R}^d	g_t	fixed ℓ_∞	$H_t = \text{diag}(g_t)$	LR
Lion	\mathbb{R}^d	m_t	fixed ℓ_∞	$H_t = \text{diag}(m_t)$	LR + WD
MARS-Lion	\mathbb{R}^d	c_t, m_t	fixed ℓ_∞ (VR)	$H_t = \text{diag}(m_t)$	LR + WD
T4: State compression and structural aggregation					
AdaFactor	\mathbb{R}^d (factored)	row/col v_t factors	adaptive ℓ_∞	factored $\text{diag}(v_t)$	LR + factored update
CAME	\mathbb{R}^d (factored)	factors + confidence	adaptive ℓ_∞	factored $\text{diag}(v_t)$ (+conf.)	LR + factored update
Adam-mini	\mathbb{R}^d (block)	m_t, v_t (block)	block ℓ_∞	block-mean $\text{diag}(v_t)$	LR + WD
APOLLO	P_t (rand.)	\tilde{m}_t, \tilde{v}_t	projected ℓ_∞	$\tilde{H}_t = \text{diag}(\tilde{v}_t)$	P_t^\top back + LR
8-bit Adam	\mathbb{R}^d (INT8)	m_t, v_t (INT8)	adaptive ℓ_∞	$H_t = \text{diag}(v_t)$ in INT8	dequant + LR + WD
Conda	P_t (col)	v_t (col)	projected ℓ_∞	col-wise $\text{diag}(v_t)$	P_t^\top back + LR + WD
T5: Curvature-aware and geometric regularization					
Sophia	\mathbb{R}^d	m_t, h_t	clipped local	$H_t = h_t$	LR + WD
AdaHessian	\mathbb{R}^d	m_t, h_t (Hutch.)	metric ball	$H_t = h_t$	LR + WD
AdamP	\mathbb{R}^d	m_t, v_t	adaptive ℓ_∞	$H_t = \text{diag}(v_t)$	radial projection + LR + WD
LAMB	\mathbb{R}^d	m_t, v_t	adaptive ℓ_∞	$H_t = \text{diag}(v_t)$	trust ratio + LR + WD

SOAP. SOAP is the case in which the update domain is a rotated coordinate system. It keeps the two Shampoo factors $L_t = \beta_2 L_{t-1} + (1 - \beta_2) G_t G_t^\top$ and $R_t = \beta_2 R_{t-1} + (1 - \beta_2) G_t^\top G_t$, where $G_t \in \mathbb{R}^{m \times n}$ is the matrix gradient, and takes their eigenvectors as the orthogonal bases Q_L and Q_R that define Axis I. These bases are full rank, and they are refreshed only once every f steps, so the preconditioning frequency f is the one extra hyperparameter beyond AdamW. For Axis II the estimator keeps a first moment in the original space, $M_t = \beta_1 M_{t-1} + (1 - \beta_1) G_t$, together with a second moment that lives in the rotated space and is updated every step, $V_t = \beta_2 V_{t-1} + (1 - \beta_2) (G'_t \odot G'_t)$ with $G'_t = Q_L^\top G_t Q_R$. Axis III is then the ordinary Adam box read in the eigenbasis. It rotates the momentum through $M'_t = Q_L^\top M_t Q_R$ and forms

$$N'_t = \frac{M'_t}{\sqrt{V_t} + \epsilon}, \tag{42}$$

after which Axis IV rotates the direction back through $N_t = Q_L N'_t Q_R^\top$ and adds the learning rate and decoupled weight decay. The contrast with Shampoo is sharp. Shampoo bakes the curvature into a fixed inverse-root metric, whereas SOAP keeps the basis fixed for f steps and lets the per-step V_t carry the adaptivity. This is why SOAP tolerates a stale basis and stays robust at a low preconditioning frequency.

Summary. The section therefore reduces every optimizer to four decisions, namely where it updates, how it estimates the state, how it turns that state into a direction, and how it writes the result back. The most useful consequence is the clean split between the two middle axes. Momentum, the second moment, the projection basis, and the variance reduction of MARS, STORM, or SVRG all belong to Axis II, whereas the LMO geometry, the diagonal metric of Adam, the polar map of Muon, and the Kronecker metric of Shampoo all belong to Axis III. Keeping these two apart prevents state estimation from being confused with direction geometry, and at the same time it preserves both the LMO and the preconditioning readings of every method.

4 Dual-Dimension Taxonomy

Section 3 unifies modern LLM optimizers from two complementary views. The universal meta-pipeline asks where an optimizer intervenes in a single update, whereas the LMO-driven four-axis decomposition asks how the intervention changes the update direction, curvature estimate, gradient estimator, and state representation. This section turns those two views into a survey taxonomy that can also guide the benchmark design. The goal is not to list optimizers chronologically or to assign informal empirical labels. The goal is to construct a mechanism coordinate system that supports literature organization, fair experimental grouping, and interpretable trade-off analysis.

The taxonomy has two dimensions. *Dimension A* is a methodological taxonomy: each optimizer receives one primary mechanism label so that Section 5 can present T1–T5 as non-overlapping families. *Dimension B* is an effect-objective taxonomy: each optimizer may receive multiple objective labels describing the training properties it claims to improve or should be evaluated against, such as convergence, per-step cost, memory, stability, hyperparameter robustness, and generalization. The two dimensions answer different questions: what does the optimizer change, and what outcome is the change intended to improve?

4.1 Taxonomy Design Principles

A single tree taxonomy is not expressive enough for modern LLM optimizers. Lion, for example, can reasonably be described as an Adam alternative, a sign-based optimizer, and a memory-friendly optimizer. All three descriptions are defensible: Lion keeps a first-order momentum structure, replaces continuous-valued directions with a sign map, and removes Adam second-moment state. However, the labels answer different questions. The sign map is the primary update mechanism, whereas memory

saving is an effect of that mechanism. If Lion is placed only under “memory-efficient optimizers,” it is grouped with AdaFactor, 8-bit Adam, Adam-mini, and LOMO, although those methods mainly alter state storage, state sharing, or gradient lifetime. If Lion is copied into every relevant branch, the taxonomy loses its role as a clean survey organization and an experimental grouping rule.

The same ambiguity appears throughout the optimizer landscape. GaLore changes the subspace in which gradients and optimizer states live, whereas Q-GaLore adds low-bit state quantization on top of that subspace mechanism. SAM can wrap SGD or AdamW, but its defining contribution is a sharpness-aware perturbation and second gradient evaluation. LAMB first performs an Adam-style element-wise update and then applies a layer-wise trust ratio at writeback. Cautious AdamW and Cautious Lion inherit different base optimizers but share the same direction-consistency filter. These examples show why the taxonomy must separate primary mechanism, base optimizer, composable wrapper, and intended effect.

We therefore use three design principles.

First, Dimension A uses a single primary mechanism label. Each optimizer is assigned to exactly one main family. The assignment is not based on the name of the optimizer or chronology, but on the component whose removal would make the method collapse to a simpler baseline. Direct modifications of Adam-style moments, bias correction, time scales, iterate averaging, or global step-size adaptation belong to T1. Matrix routing, spectral orthogonalization, Kronecker-factored preconditioning, and low-rank subspace projection belong to T2. Sign maps and related irreversible direction discretization belong to T3. State sharing, compression, quantization, or elimination belong to T4. Perturbations, explicit curvature wrappers, post-update filters, and layer-wise trust-region rules belong to T5. Composite methods are classified by their incremental contribution and record secondary tags in the cross-dimension matrix.

Second, family boundaries are aligned with the meta-pipeline. The five families are not arbitrary names. T1 mainly modifies element-wise state evolution in S3 and local scaling in S5. T2 changes the update space through S1–S4 matrix routing, matrix transformation, structured state, and reconstruction. T3 introduces irreversible direction discretization in S2 and often simplifies S3. T4 acts on S3/S4 state representation and gradient lifetime. T5 acts near S5 through update writeback, post-processing, or geometric regularization. Given an update rule, locating its dominant non-identity pipeline operation is usually enough to assign the method label.

Third, Dimension B uses multi-label effect annotations. Effect objectives should not be mutually exclusive categories. A method may target convergence efficiency and hyperparameter robustness at the same time, or it may reduce memory while hurting convergence or stability. An effect label means that the method claims to improve, is designed to improve, or must be evaluated on that property. This separation avoids equating “designed to save memory” with “better under a fixed hardware budget,” and avoids assuming that every sharpness-aware method improves generalization under every protocol.

4.2 Methodological Taxonomy

Dimension A organizes the surveyed set of 108 optimizers into five families and fifteen subclasses. The five families correspond to the dominant mechanism that transforms a stochastic gradient into a parameter update. The main text keeps the organizing principles and family definitions that are needed for the survey chapters that follow, with a compact family-level summary given in Table 7.

T1: Element-wise adaptive moment and scalar control. T1 retains the Adam-style element-wise processing paradigm, but it is broader than a strict set of Adam variants. Its core members maintain first moments, second moments, or related variance surrogates and normalize each parameter independently. Its boundary members are scalar first-order predecessors or outer-control schemes that do not introduce matrix routing, sign quantization, state compression, or sharpness-aware wrapper

gradients. Differences within the family come from temporal structure, variance estimation, iterate averaging, corrected decay, and global step-size rules. In the four-axis view, most T1 methods use the identity analysis basis, a diagonal Fisher or variance estimate, square-root preconditioning for the Adam-like core, and full state storage.

T2: Matrix-level structural methods. T2 treats two-dimensional Transformer weights as matrices rather than as flattened vectors. The family includes spectral orthogonalization, Kronecker-factored preconditioning, and low-rank subspace projection. These methods share nontrivial S1 routing and S2 transformation: they either orthogonalize matrix momentum, maintain row/column curvature factors, or project gradients into a low-dimensional subspace before updating state. T2 is the family that most visibly changes Axis I. Muon-style methods use a dynamic SVD or polar basis, Shampoo and SOAP use Kronecker or Fisher eigenbases, and GaLore changes the effective optimizer-state space through projection.

T3: Discretization and directional quantization. T3 is defined by sign maps or related direction-discretization operations. The core idea is to keep coarse direction information while discarding or quantizing magnitude. Lion is the representative method: it forms a signed direction from a gradient-momentum interpolation and keeps only first-order momentum. Compared with T1, T3 is not merely a cheaper second-moment estimator. It changes the geometry of the update direction. In the LMO view, the family is naturally associated with ℓ_∞ -type direction selection and weak or absent Hessian preconditioning. Methods whose primary increment is a binary or stochastic mask applied to an already computed update are treated as T5.3 post-update filtering rather than as T3, even when the mask is motivated by directional agreement.

T4: State compression and structural aggregation. T4 directly targets the optimizer-state memory bottleneck. It includes row/column factorization, low-bit state quantization, block- or layer-level state sharing, and fused backprop-update schemes. Its distinction from T2.3 is the object being compressed. T2.3 first changes the mathematical subspace of the gradient signal and then runs an optimizer in that subspace. T4 mainly changes how the state itself is stored, shared, quantized, or released. In the four-axis view, T4 is the most direct instantiation of state compression in Axis II.

T5: Curvature-aware and geometric regularization. T5 does not primarily introduce a new element-wise moment estimator or matrix transform. Instead, it adds geometric constraints near update finalization. Sharpness-aware methods change the point at which gradients are evaluated. Hessian-guided methods replace or augment curvature signals and often add trust-region clipping. Post-processing methods centralize, project, normalize, mask, or sparsify an already computed update. Layer-wise trust-region methods rescale updates according to parameter and update norms. Because many T5 methods are wrappers around a base optimizer, the base optimizer and the T5 mechanism must be recorded separately.

Boundary cases are resolved by the primary incremental mechanism. Direct Adam variants remain T1 even if they claim stability or generalization benefits, because their main mechanism is still element-wise moment estimation or step-size control. Q-GaLore is T4.2 when the focus is the additional quantized-state mechanism, while base GaLore remains T2.3. Magma and MGUP are T5.3 because their primary operation is a selective update mask. SAM, Cautious optimizers, and LAMB are classified by wrapper-level contributions in T5 rather than by their possible AdamW or Lion base optimizers. This keeps the main survey families mutually exclusive while leaving room for secondary tags in the appendix-level optimizer matrix.

4.3 Objective-Oriented Taxonomy

Dimension B describes what an optimizer is intended to improve. We organize effect objectives by evaluation cost rather than by method mechanism, because the feasibility of a benchmark depends on how each objective is measured. We use six objectives: O1 convergence efficiency, O2 per-step

Table 6: Dimension-B effect objectives and measurement sources.

Definition	Data source	Extra cost	Typical outputs
O1: Convergence Efficiency			
Loss reduction and time-to-target under a fixed training budget	Train/validation logs	loss None	Final loss; steps-to-threshold; token efficiency
O2: Step Cost			
Extra per-step computation and synchronization relative to a baseline	Timers, FLOP analysis	Recorded training	during Step time; FLOPs; extra backward count
O3: Memory			
Memory from optimizer states and associated buffers	Memory profiler, model	byte Recorded training	during Peak memory; state and buffer bytes
O4: Stability			
Robustness to spikes, divergence, and gradient fluctuations	Loss and gradient curves	norm Offline processing	post- Spike rate; gradient CV; divergence rate
O5: Hyperparameter Robustness			
Sensitivity to learning rate, decay, batch size, and other knobs	Multiple training runs	Search or transfer experiments	ex- Usable LR interval; performance variance; tuning burden
O6: Generalization			
Quality beyond the training objective (validation, downstream, OOD, transfer)	Validation and stream evaluation	down- Low for validation, high for full evaluation	Validation loss; generalization gap; downstream score

computational cost, O3 memory overhead, O4 training stability, O5 hyperparameter robustness, and O6 generalization quality. These labels are not mutually exclusive and should not be read as intrinsic family rankings. They are evaluation axes for organizing experiments and interpreting trade-offs.

The six objectives form three measurement layers.

Layer 1: directly logged metrics. O1–O3 can be obtained from a single training run, timers, profilers, or analytic byte/FLOP models. O1 measures how fast loss decreases or a target quality is reached under a fixed step, token, wall-clock, or compute budget. O2 measures additional per-step computation relative to AdamW or SGD, including matrix multiplications, orthogonalization iterations, extra forward/backward passes, synchronization, and quantization/dequantization. O3 measures memory from parameters, gradients, optimizer states, temporary matrices, projection bases, and quantization buffers.

Layer 2: single-run derived metrics. O4 and the lightweight version of O6 require post-processing of standard training logs. O4 measures whether the trajectory is robust to loss spikes, gradient-norm bursts, overflow, divergence, and incomplete runs. The lightweight O6 signal comes from validation loss, train-validation gap, or a fixed validation protocol during pretraining.

Layer 3: cross-configuration metrics. O5 and the full version of O6 require multiple training runs or downstream evaluations. O5 measures sensitivity to learning rate, weight decay, momentum, warmup, batch size, and method-specific hyperparameters. Full O6 measures downstream transfer, out-of-distribution retention, scale transfer, or other quality metrics beyond pretraining loss.

Dimension B must remain neutral before benchmarking. T2 methods may improve O1 token efficiency through matrix structure, but their orthogonalization or Kronecker operations may hurt O2. T4 methods are designed for O3, but aggressive compression may degrade O1 or O4. T5 methods often target O4 and O6, but SAM-style extra gradient evaluations impose a clear O2 cost. Thus effect labels are measurement prompts rather than substitutes for empirical results.

For the family analyses in Section 5, each optimizer or subclass can be annotated by

$$\text{Effect}(A) \subseteq \{O1, O2, O3, O4, O5, O6\}, \tag{43}$$

where A denotes an optimizer or subclass. The annotation should distinguish design intent from experimentally verified effect. AdaFactor, for instance, can be marked as O3-targeting under an

Table 7: Compact cross-matrix between method families and effect objectives.

Family	O1	O2	O3	O4	O5	O6
T1 Element-wise adaptive moment and scalar control	↑↑	○	↓↓	↑↑	↑↑	↑↑
T2 Matrix-level structural methods	↑↑	↓↓	↓↓	↑↑	↑↑	↑↑
T3 Discretized directions	↑↑	↑↑	↑↑	↑↑	○	○
T4 State compression	↓↓	↑↑	↑↑	↓↓	○	↓↓
T5 Geometry regularization	↑↑	↓↓	↓↓	↑↑	↑↑	↑↑

Note. Dark double-line arrows denote strong priors: ↑ indicates a favorable target and ↓ a likely cost. Pale single-line arrows denote conditional or protocol-sensitive favorable/cost effects. The hollow gray circle ○ denotes protocol-dependent neutrality. Arrows indicate objective favorability rather than raw metric direction.

analytic memory model, but whether it also improves O1, O4, or O6 under a fixed training protocol must be decided by the benchmark.

4.4 Cross-Dimension Analysis

The value of the dual taxonomy appears in cross-dimension analysis. Dimension A gives mechanism labels, while Dimension B gives effect objectives. Table 7 provides a compact matrix of the objectives that each method family should emphasize in the benchmark. The matrix is a mechanism-informed prior, not a final empirical conclusion.

The symbols in Table 7 should not be read as a global performance ranking. A T2 method may be slower per step but still win in wall-clock time if token efficiency improves enough. A T4 method may look worse in a fixed-small-model loss comparison while enabling a larger batch or model under the same hardware budget. A T5 method may improve generalization only at particular data scales, training durations, or evaluation suites.

The cross view also identifies mechanisms that are likely to compose orthogonally. Low-rank projection and state quantization can be combined because T2.3 changes the signal subspace, whereas T4.2 changes the state representation. Variance-reduced gradient estimates can be layered onto AdamW, Lion, or Shampoo because variance reduction (Axis II) is mostly independent of basis choice and curvature representation. Post-update filters can wrap AdamW or Lion because T5.3 acts after the base direction has been computed. Layer-wise trust ratios can similarly wrap an element-wise adaptive update because they primarily act in S5.

Not every cross-family combination is natural. Mechanisms that occupy the same meta-pipeline slot require an explicit ordering and a descent-quality argument. Spectral orthogonalization and low-rank projection are both strong S2 constraints on a matrix signal, so combining them requires specifying whether projection precedes orthogonalization or vice versa. LOMO-style streaming updates can conflict with methods that need global gradient statistics, delayed basis updates, or a second gradient evaluation. SAM-style methods already require extra forward/backward computation, so adding expensive Kronecker-factored preconditioning may be mathematically valid but practically unattractive. These constraints are not implementation details. They are composition boundaries that the taxonomy should make explicit.

The full appendix-level matrix should therefore record, for each optimizer, three fields: the primary Dimension-A label, secondary mechanism tags, and O1–O6 effect annotations. The main text keeps only compact summaries such as Table 7; the family analyses instantiate the matrix progressively by describing each subclass’s meta-pipeline site, four-axis coordinates, and expected benchmark signature. In this way, the taxonomy is a mechanism-aware benchmark plan: a new optimizer entering the framework must specify which pipeline stage it modifies, which four-axis coordinates it changes, and which effect objectives it claims to improve.

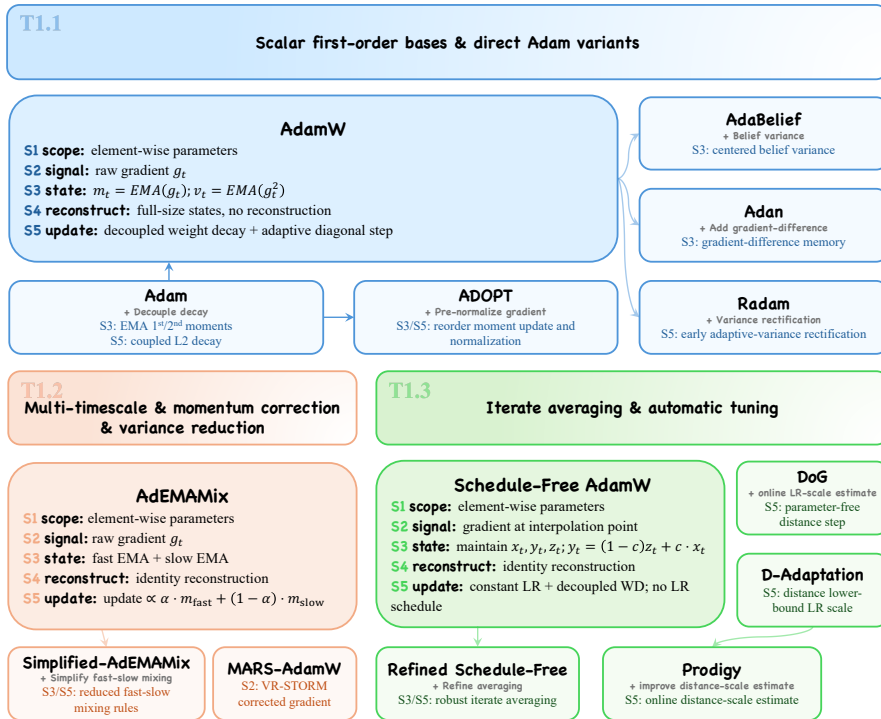


Figure 4: Mechanism overview of T1 element-wise adaptive-moment and scalar control methods. The family is organized by the dominant intervention in the update: direct scalar or Adam-style variants, additional temporal or estimator-correction channels, and outer iterate or global-scale control. Boundary methods are shown only when they preserve scalar or element-wise update topology.

5 Optimizer Method Families

The five method families below form the mechanism-oriented core of the survey. Rather than treating T1–T5 as separate top-level sections, we place them under one common section and use the same internal template for each family: meta-pipeline position, LMO-driven four-axis interpretation, representative methods, and effect-target assessment. This keeps the main progression of the paper compact while preserving the comparison granularity needed for method-level analysis and benchmark design.

5.1 T1: Element-Wise Adaptive Moment and Scalar Control

5.1.1 Family Overview and Meta-Pipeline Position

Element-wise adaptive-moment methods are the default optimizer family for modern Transformer training. Their defining property is not the mere presence of momentum, but the preservation of an element-wise update topology: the optimizer maintains scalar or coordinate-wise state, normalizes or controls each parameter independently, and avoids exchanging information across rows, columns, heads, or layers. T1 therefore contains the Adam-centered adaptive moment line together with scalar first-order predecessors and outer-control schemes whose primary mechanism remains element-wise or scalar. Methods whose main contribution is matrix routing, irreversible direction discretization, state compression, or sharpness-aware wrapper gradients are assigned to T2–T5 instead.

Subclass structure. Figure 5 gives the complete optimizer membership for T1. The three subclasses below are therefore used to interpret the taxonomy figure, rather than to repeat its entries. The split

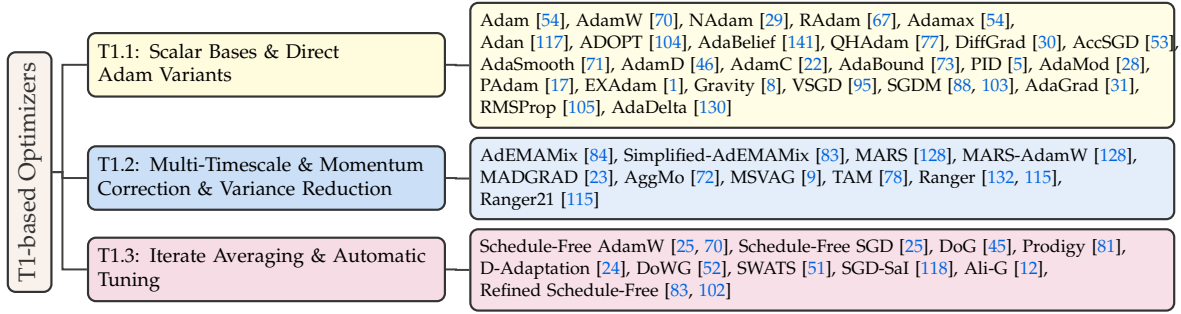


Figure 5: Taxonomy of element-wise adaptive-moment and scalar-control optimizers.

is mechanism-based rather than chronological: each subclass identifies the dominant non-identity operation added around the AdamW coordinate-wise template.

T1.1 Scalar bases and direct Adam variants. This subclass groups optimizers whose main change remains local to the coordinate-wise template: the numerator, diagonal scale, bias correction, decay finalization, or scalar control law. It includes both the AdamW line and historical scalar or diagonal predecessors, but the latter are used as conceptual anchors rather than as evidence that all T1 methods are modern large-model optimizers.

T1.2 Multi-timescale, momentum correction, and variance reduction. This subclass changes the signal that enters state evolution. Its members add fast/slow temporal channels, replace the raw mini-batch gradient with a corrected or variance-reduced estimator, gate momentum by temporal alignment, or bundle such components around an Adam or RAdam core.

T1.3 Iterate averaging and automatic tuning. This subclass leaves the scalar or element-wise base update largely intact and instead modifies the outer control system: iterate averaging, global learning-rate scale inference, initialization-time scaling, or optimizer-phase switching.

For a parameter vector $\theta_t \in \mathbb{R}^d$ and stochastic gradient g_t , the canonical AdamW update maintains

$$m_t = \beta_1 m_{t-1} + (1 - \beta_1) g_t, \quad v_t = \beta_2 v_{t-1} + (1 - \beta_2) g_t \odot g_t, \quad (44)$$

$$u_t = \frac{\hat{m}_t}{\sqrt{\hat{v}_t + \epsilon}}, \quad \theta_{t+1} = (1 - \eta_t \lambda) \theta_t - \eta_t u_t, \quad (45)$$

where hats denote bias correction and weight decay is decoupled from the adaptive direction [54, 70]. The update constructs a diagonal preconditioner from the second-moment state and leaves the parameter topology unchanged. This coordinate-wise invariance is the central commonality of T1: individual methods may change the numerator, the variance proxy, bias correction, decay finalization, temporal state, averaged iterate, or global step-size scale, but they do not introduce matrix-level basis changes, low-rank reconstruction, quantized state representation, or sharpness-aware auxiliary gradients. Scalar-control boundary methods can be viewed as setting the adaptive denominator to an identity scale, while historical adaptive-rate methods provide the diagonal-statistics lineage from which Adam-style updates emerged.

In the meta-pipeline of Section 3.1, T1 is mostly identity-like in S1, S2, and S4. Parameters are routed at their native coordinate granularity (S1), the stochastic gradient is usually passed directly into the update rule (S2), and the reconstructed update remains full-dimensional (S4). The primary non-identity operation is S3 state evolution: the optimizer specifies which moving averages, variance proxies, time scales, cross-moment corrections, variance-reduced estimators, or averaged iterates are maintained. S5 supplies the second locus of variation: AdamW decouples weight decay, RAdam rectifies early adaptive variance, AdamC adjusts decay–schedule interactions, D-Adaptation and Prodigy infer a

global learning-rate scale, and Schedule-Free methods internalize the role of an external learning-rate schedule through iterate averaging.

5.1.2 LMO-Driven Four-Axis Interpretation

In the four-axis view, the common T1 coordinate is

$$((I, I), \psi, \hat{H}_t, \alpha, \hat{g}_t, \text{Full}), \quad (46)$$

where the analysis basis is the identity, the curvature estimate is diagonal, and the state is stored at full coordinate resolution. AdamW corresponds to $\hat{H}_t = \text{diag}(\hat{v}_t)$ and $\alpha = \frac{1}{2}$, yielding the square-root preconditioned direction in Eq. (45). Under the Fisher identity discussed in Section 2.2, the EMA of $g_t \odot g_t$ can be read as a diagonal Fisher or Gauss–Newton surrogate. This makes the family a diagonal-curvature analogue of the matrix preconditioners in T2, but with no off-diagonal coupling and no basis change.

The LMO interpretation clarifies what is shared and what is not shared across T1. If the adaptive denominator is temporarily fixed, the numerator selects a coordinate-wise descent pattern. In the limiting normalized view, a signed coordinate direction is the LMO solution over an ℓ_∞ -type ball, and the diagonal denominator deforms that ball into an anisotropic, coordinate-wise trust region. AdamW should therefore not be reduced to either “sign descent” or “Newton descent.” Its practical update combines an element-wise directional component, a diagonal curvature scale, bias correction, damping, and a global step-size schedule. This is why T1 methods often share the same Axis I basis and Axis III exponent while differing mainly in Axis II curvature/variance estimation and gradient-estimation quality, and S5 step-size or regularization control. Boundary methods with no adaptive denominator can be viewed as using $\hat{H}_t = I$ and $\alpha = 0$; they are kept in T1 only as scalar first-order predecessors or control schemes, not as evidence that every T1 method is an adaptive-moment estimator.

This view also separates T1 from neighboring families. Lion belongs to T3 because its defining operation is an irreversible sign map and it removes the second-moment state, even though it inherits an Adam-like momentum interface [19]. AdaFactor belongs to T4 because its defining contribution is factorized storage of the second-moment state, not a new full-state moment estimator. Sophia belongs to T5 because it replaces the Adam variance proxy with an explicit curvature estimate and clipped trust-region update [65]. T1 is therefore the baseline coordinate system from which many later optimizers depart.

5.1.3 Representative Methods

Against the subclass map above, the representative methods are organized by three recurring mechanism patterns: local modifications of AdamW’s numerator, denominator, bias correction, or writeback; additional temporal or variance-reduced signals; and outer rules for averaging, global scale inference, or switching.

Scalar Bases and Direct Adam Variants. The first branch is the broadest part of T1. Its members are best read in tiers, because some are historical scalar bases, some define the modern Adam baseline, and some are local corrections to one term of the AdamW template: at the survey level, they can be summarized as

$$u_t = \frac{a_t}{b_t + \epsilon}, \quad \theta_{t+1} = \theta_t - \eta_t u_t - \eta_t \lambda_t \chi_t(\theta_t), \quad (47)$$

where a_t is a momentum-like numerator, b_t is a diagonal scale or variance proxy, and χ_t specifies whether decay is coupled to the gradient channel or decoupled at writeback.

- **Scalar and diagonal predecessors.** SGDM introduced a heavy-ball momentum buffer for smoother descent [88, 103]; AdaGrad accumulated squared gradients to produce coordinate-wise learning rates [31]; RMSProp replaced AdaGrad’s cumulative sum with a running average

[105]; AdaDelta used ratios of running RMS quantities to reduce manual learning-rate dependence [130]; and VSGD estimated local gradient statistics to adapt learning rates [95]. These methods are not all Adam-like, but they form the scalar and diagonal-control substrate from which Adam-style methods developed.

- **Adam baseline line.** Adam combined first-moment momentum, RMSProp-style second moments, and bias correction into a single adaptive method [54]; Adamax replaces the second-moment denominator with an exponentially weighted ℓ_∞ norm; and AdamW became the practical large-model baseline by decoupling weight decay from the adaptive gradient normalizer [70]. In the meta-pipeline, AdamW is mainly an S5 change: the direction u_t is computed as in Adam, while shrinkage is applied directly to parameters rather than being mixed into g_t .
- **High-salience direct Adam variants.** NAdam inserts a Nesterov-style lookahead term into Adam’s first-moment pathway [29]. RAdam adds a rectification factor for the high-variance early adaptive denominator [67]. AdaBelief replaces g_t^2 with the centered prediction-error statistic $(g_t - m_t)^2$ [141]. Adan adds a Nesterov-inspired gradient-difference channel using both g_t and $g_t - g_{t-1}$ [117]. ADOPT changes the ordering of second-moment update and normalization to obtain guarantees for arbitrary β_2 [104]. EXAdam adds adaptive cross-moment debiasing and gradient-based acceleration while remaining a direct Adam extension [1].
- **Local adaptivity and correction variants.** QHAdam interpolates between immediate and momentum-based directions through quasi-hyperbolic weighting [77]; AdaMod bounds Adam’s adaptive learning rates using a momental upper bound [28]; and PAdam interpolates between Adam (or AMSGrad) and SGDM through a partial-adaptivity exponent [17]. DiffGrad and AdaSmooth adapt learning rates from gradient-change or effective-ratio signals [30, 71]; AdamD modifies bias correction [46]; and AdamC corrects decay–schedule interactions near the end of long-duration training [22].
- **Boundary scalar-control methods.** AccSGD, PID, and Gravity remain in T1.1 only as scalar-control boundary cases [53, 5, 8]. They help explain the control-theoretic and acceleration background of the family, but they should not receive the same narrative weight as AdamW, RAdam, AdaBelief, Adan, or ADOPT when the target setting is modern LLM training.

This tiered reading prevents T1.1 from becoming a flat list of names. The central comparison is AdamW versus direct modifications of AdamW’s numerator, denominator, bias correction, or writeback rule; the historical and boundary methods provide context and ablation anchors. Several direct variants can be viewed as substitutions inside Eq. (47); for example,

$$v_t^{\text{Belief}} = \beta_2 v_{t-1}^{\text{Belief}} + (1 - \beta_2)(g_t - m_t) \odot (g_t - m_t), \quad (48)$$

$$u_t^{\text{RAdam}} = r_t \frac{\hat{m}_t}{\sqrt{\hat{v}_t + \epsilon}}, \quad u_t^{\text{PAdam}} = \frac{\hat{m}_t}{(\hat{v}_t)^p + \epsilon}. \quad (49)$$

These formulas do not make AdaBelief, RAdam, and PAdam the same method; they show that their primary changes remain local to the diagonal variance proxy, early-step rectification, or adaptivity exponent.

Multi-Timescale, Momentum Correction, and Variance Reduction. The second branch asks whether a single raw EMA stream is enough. A fast momentum reacts to the current mini-batch distribution but is noisy; a slow momentum is stable but can lag behind regime changes; and a variance-reduced or alignment-corrected signal can change the quality of the gradient entering state evolution. We therefore separate the branch into four mechanism groups:

$$\hat{g}_t = C_t(g_t, g_{t-1}, m_{t-1}), \quad m_t^{(k)} = \beta_k m_{t-1}^{(k)} + (1 - \beta_k) \hat{g}_t, \quad a_t = \sum_{k=1}^K \omega_k m_t^{(k)}. \quad (50)$$

Here \mathcal{C}_t denotes a possible estimator correction and the $m_t^{(k)}$ streams denote different temporal channels. Standard AdamW is the special case $K = 1$ and $\widehat{g}_t = g_t$.

- **Multi-time-scale momentum.** AdEMAMix maintains both a standard fast EMA and an older, slower EMA, then mixes them in the update direction [84]. This is especially relevant to LLM training, where long horizons can make old gradient information useful rather than stale. Simplified-AdEMAMix preserves the interpretation while exposing connections to schedule-free and accelerated SGD variants [83]. AggMo is the earlier multi-time-scale analogue, aggregating several momentum buffers with different decay rates [72].
- **Variance-reduced or corrected estimators.** MARS introduces a scaled stochastic recursive momentum estimator that can be paired with AdamW, Lion, or Shampoo-style bases [128]. In the AdamW instance, the signal entering S3 is no longer raw g_t but a gradient-difference corrected estimator, so the method changes Axis II while preserving the element-wise base update. MADGRAD combines AdaGrad-style accumulated curvature with a momentumized dual-averaged update [23]. MSVAG is more diagnostic than deployment driven: it decomposes Adam into sign, magnitude, and variance effects [9].
- **Alignment-aware momentum correction.** TAM is neither a multi-time-scale method nor a STORM-style variance-reduction method. It damps momentum injection according to the alignment between current gradients and historical momentum [78]. Its role in T1.2 is to show that momentum can be corrected by geometry of temporal agreement, not only by adding an older EMA or recursive estimator.
- **Composite optimizer bundles.** Ranger combines RAdam, Lookahead, and often gradient centralization; Ranger21 combines AdamW with a larger set of stabilization components [132, 115]. These methods are useful implementation bundles, but their components occupy different meta-pipeline slots. We keep them connected to T1 through their Adam or RAdam core and record Lookahead-style averaging or post-processing as secondary tags.

The common thread is that T1.2 no longer trusts one raw momentum stream as the only temporal signal. It either adds more time scales, corrects the estimator fed into S3, or gates momentum by temporal alignment while leaving routing and writeback largely element-wise. In this notation, AdEMAMix primarily changes K and ω_k ; MARS changes \mathcal{C}_t before the AdamW-like state update; and TAM can be read as inserting an alignment-dependent gate, e.g.,

$$\widehat{g}_t = \kappa_t g_t, \quad \kappa_t = f\left(\frac{\langle g_t, m_{t-1} \rangle}{\|g_t\| \|m_{t-1}\| + \epsilon}\right), \quad (51)$$

where Eq. (51) is a template for the class of alignment-aware corrections rather than a replacement for the exact algorithm in each paper.

Iterate Averaging and Automatic Tuning. The third branch does not primarily change the coordinate-wise denominator. Instead, it changes the outer control logic around a scalar or element-wise base optimizer: how iterates are averaged, how the global scale is chosen, or when the optimizer should change phase. The subclass has three readable groups:

$$y_t = (1 - \rho_t)x_t + \rho_t \bar{x}_t, \quad x_{t+1} = x_t - \eta_t u_t(y_t), \quad \eta_t = \eta_{\text{base}} d_t, \quad (52)$$

where y_t is an interpolation point, \bar{x}_t is an averaged iterate, and d_t is an inferred global scale. Schedule-free methods emphasize the first two terms; learning-rate-free methods emphasize the online construction of d_t ; switching methods change which base rule defines u_t .

- **Schedule-free iterate systems.** Schedule-Free optimization replaces an externally prescribed learning-rate schedule with an internal iterate-averaging mechanism [25]. In the AdamW instance, the optimizer maintains training, evaluation, and averaged iterates, evaluates gradients

at an interpolation point, and uses a constant learning-rate interface with decoupled weight decay. Refined Schedule-Free methods further analyze language-model trajectories and adjust the method for robustness to momentum and large-batch settings [102]. Schedule-Free SGD is kept in the same subclass as the scalar-base analogue.

- **Learning-rate-free scale inference.** D-Adaptation estimates a lower bound on the distance to the solution online and uses it to set the learning-rate scale without line search or extra gradient evaluations [24]. Prodigy estimates the same distance scale more aggressively and can be used with Adam-like adaptive methods [81]. DoG and DoWG form a related parameter-free path, setting dynamic step sizes from distance-over-gradient quantities rather than a user-specified learning rate [45, 52].
- **Switching, initialization-time scaling, and global clipping.** SWATS starts with Adam and switches to SGD when an estimated SGD learning rate becomes stable, aiming to combine Adam’s fast early progress with SGD-like later generalization [51]. SGD-SaI avoids Adam-like second-moment state during training and uses an initialization-time group signal-to-noise estimate to set learning-rate scales [118]. Ali-G computes adaptive global learning rates from interpolation assumptions and clipping [12].

T1.3 therefore records a different kind of contribution from T1.1. The base update can still be AdamW-like or scalar first-order, but the claimed gain comes from reducing schedule design, learning-rate search, or phase-selection burden. This is why its benchmark claim should be evaluated under O5 hyperparameter robustness as well as O1 convergence.

T1 is the calibration family for effect assessment. Its role comes less from minimal resource use than from the reliability of the AdamW-style control stack: coordinate-wise normalization, momentum smoothing, decoupled weight decay, and a mature schedule interface. This stack is expensive compared with SGDM because AdamW stores two full-size moment buffers, but it often provides strong early loss reduction and stable Transformer pretraining under sparse, heterogeneous, or scale-imbalanced gradients. For this reason, recent LLM optimizer studies treat AdamW not as a weak default but as the baseline whose tuning budget, schedule, weight decay, batch size, and model scale determine whether a proposed optimizer has actually improved the training procedure. Zhao et al. [139] make this point by decomposing AdamW under controlled substitutions, while the benchmarks of Semenov et al. [97] and Wen et al. [113] show that optimizer rankings move with scale and protocol choices.

Table 8 is therefore a mechanism-derived performance prior rather than an empirical ranking. Each entry states what the corresponding T1 mechanism is expected to improve, what trade-off follows from that mechanism, and where the later benchmark provides supporting evidence or a useful caution.

Table 8: Mechanism-informed effect assessment for T1 subclasses. The entries are design priors for benchmark planning, not final empirical conclusions.

Primary target	Likely cost	Benchmark focus
T1: Element-wise adaptive moment and scalar control		
T1.1 Scalar bases and direct Adam variants		
O1 convergence, O4 stability, O5 default robustness	O3 two-state memory (lower for scalar predecessors)	AdamW-normalized loss, warmup and β_2 sensitivity, decay coupling
T1.2 Multi-timescale and variance reduction		
O1 convergence, O4 smoother trajectories	Extra S3 state	Token efficiency, noise sensitivity, batch-size transfer
T1.3 Iterate averaging and automatic tuning		
O5 hyperparameter robustness (secondary O4)	Possible O1 loss when schedules are well tuned	LR sweep width, schedule transfer, constant-LR comparison

Performance implications. The three T1 subclasses produce different performance signatures even when they share an AdamW-like interface.

- **T1.1: scalar bases and direct Adam variants.** Coordinate-wise normalization explains the characteristic T1.1 profile: fast early loss reduction, stable behavior under heterogeneous coordinate scales, and a forgiving default interface. The cost is full element-wise state for Adam-like methods; scalar predecessors reduce state, but typically give up part of the robustness that makes AdamW a strong Transformer baseline. This is the role AdamW plays in Sec. 6.2.9: it is retained as the default reference, and T1 remains the stable baseline family rather than the strongest raw-quality family.
- **T1.2: multi-timescale and corrected estimators.** Adding temporal channels or corrected estimators mainly improves the quality of the signal entering the AdamW geometry. This predicts smoother trajectories and better token efficiency when stochastic gradients are noisy or temporally biased, but it also predicts extra state, additional update logic, or higher per-step cost. The Stage 2 analysis in Sec. 6.2.3 follows this pattern: MARS-AdamW is the most stable AdamW-style enhancement, but the gain comes with more state and compute than plain AdamW.
- **T1.3: averaging and automatic tuning.** These methods move the contribution from the local direction to the outer control loop. Their expected advantage is not necessarily a lower best-tuned loss, but a wider usable range of learning rates, fewer schedule decisions, or smoother phase behavior. The corresponding risk is that an automatic rule may trail a carefully tuned fixed schedule when the latter is allowed enough search budget.

Across all three subclasses, the central question is not whether Adam-style adaptivity is useful; it is which components of the AdamW control stack remain necessary once model scale, batch size, training length, and tuning budget are fixed. This framing keeps T1 from becoming a list of Adam variants and makes it the reference point for the remaining families.

5.2 T2: Matrix-Level Structural Methods

5.2.1 Family Overview and Meta-Pipeline Position

T2 contains optimizers whose primary operation uses the matrix structure of Transformer parameters. T1 methods flatten a weight tensor and treat it as a collection of independent coordinates. T2 methods instead work directly at the matrix level, coupling rows, columns, singular directions, Kronecker factors, or low-rank subspaces. The typical object is a two-dimensional weight matrix $W_t \in \mathbb{R}^{m \times n}$ with stochastic gradient $G_t \in \mathbb{R}^{m \times n}$. The family is therefore tied to parameter topology. Attention projections, MLP projections, and other dense matrix weights are natural targets, whereas biases, normalization parameters, embeddings, and sometimes output heads fall back to an element-wise optimizer such as AdamW or SGD. This matrix routing is the S1 (parameter scoping and routing) stage of the meta-pipeline, and by deciding which parameters are treated as matrices it determines whether matrix transforms such as orthogonalization or Kronecker-factored preconditioning can be applied at all.

Subclass structure and membership. Figure 7 gives the subclass-level optimizer list for T2, and the three subclasses below specify the corresponding optimizer membership. The split is based on the primary matrix operation: spectral direction selection, structured matrix preconditioning, or subspace projection.

T2.1 Spectral orthogonalization. This subclass contains Muon, RMNP [26], MOGA, Dion, AdaMuon, OrthoGrad, AdaGO, and Spectral Sphere. Its members construct an orthogonalized or spectral-geometry update from a two-dimensional gradient or momentum object, with Muon as the subclass’s central representative method for LLMs [48, 87, 98].

T2.2 Kronecker-factored preconditioning. This subclass contains SOAP, Shampoo, MARS-Shampoo, COSMOS, Kron, PSGD, SPlus, and RACS. Its members estimate row/column curvature, covariance, structured Fisher factors, or learned Kronecker-style preconditioners, with Shampoo and

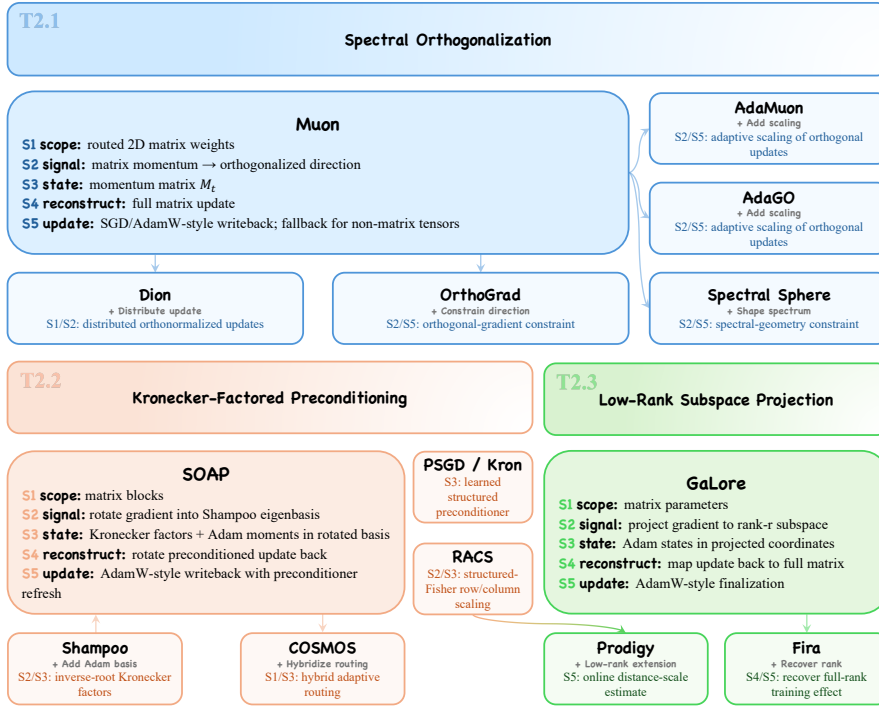


Figure 6: Mechanism schematic for T2 matrix-level structural methods. The schematic summarizes the three matrix routes used in this survey: spectral direction selection, Kronecker or structured-Fisher preconditioning, and low-rank subspace projection. It is a taxonomy guide rather than an empirical ranking.

SOAP as the subclass’s core representative methods, around which its mathematical framework is built [38, 108].

T2.3 Low-rank subspace projection. This subclass contains GaLore, Fira, and Alice. Its members project the gradient and optimizer state into a low-dimensional subspace, update there, and reconstruct a full matrix update, with GaLore as the canonical LLM example [138].

At the family level, a matrix-structured update can be summarized as

$$Z_t = B_t^\top G_t C_t, \quad \tilde{\Delta}_t = \Phi_t(Z_t; S_{t-1}), \quad \Delta_t = A_t \tilde{\Delta}_t D_t^\top, \quad (53)$$

where B_t, C_t are the left and right analysis bases that rotate or project the gradient into a new coordinate system, Φ_t is the direction or preconditioning rule applied in that coordinate system, S_{t-1} denotes the structured state, and A_t, D_t map the transformed update back to the parameter matrix. Muon uses an SVD or polar basis and flattens the singular values. Shampoo and SOAP use Kronecker or Fisher eigenbases. GaLore uses projection and reconstruction maps with rank $r \ll \min(m, n)$. This template is intentionally broader than any one algorithm. Its role is to make clear that T2 changes the geometry in which a matrix update is analyzed before the usual optimizer writeback is applied.

Together, these subclasses make T2 the family where S1 routing, S2 transformation, S3 structured state, and S4 reconstruction all become first-class design choices. S5 is usually less distinctive: many T2 methods still use SGD-style or AdamW-style final writeback after the matrix transform, possibly with decoupled weight decay, damping, or method-specific scaling.

This definition also fixes the boundary with neighboring families. Whether a method belongs to T2 depends on whether its update rule genuinely uses the matrix geometry. Conversely, whether

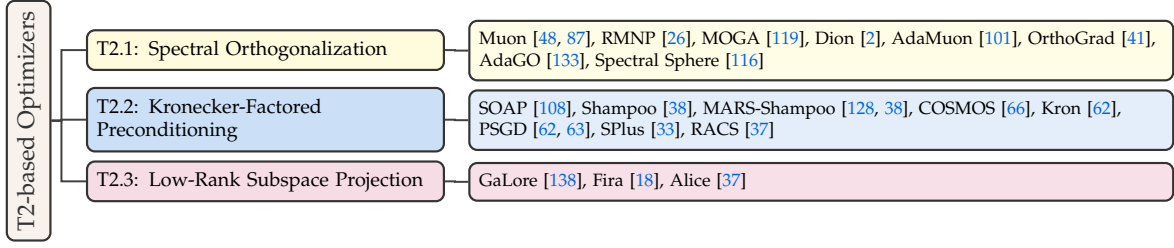


Figure 7: Taxonomy of matrix-level structural optimizers.

a method belongs to T4 likewise depends on its mechanism. GaLore does reduce optimizer-state memory, but it does so by changing the mathematical subspace in which the gradient and Adam state live, so its primary mechanism is T2.3 (low-rank subspace), and state compression is only an effect of that choice. If an additional contribution directly quantizes, shards, shares, or frees optimizer state, that contribution should be recorded as a secondary T4 tag. Likewise, sharpness-aware wrappers, layer-wise trust ratios, or post-update filters remain T5 unless the matrix transform itself is the primary new operation.

5.2.2 LMO-Driven Four-Axis Interpretation

The four-axis view in Section 3.2 is especially useful for T2 because it separates the basis used to analyze a matrix update from the state used to estimate its scale. A generic T2 coordinate can be written as

$$((B_t, C_t), \psi_t, \hat{H}_t, \alpha, \hat{G}_t, \mathcal{S}_t), \quad (54)$$

where B_t and C_t are left and right analysis bases, ψ_t is the matrix direction map, \hat{H}_t is a structured curvature or covariance proxy when present, and \mathcal{S}_t records whether the optimizer state is full-rank, factored, or projected. In T1, $B_t = C_t = I$ and \mathcal{S}_t is usually full coordinate state. In T2, the basis itself is part of the method.

For Muon-style spectral-normalization methods, the defining map is a polar or orthogonalized direction. With momentum matrix $M_t = \beta M_{t-1} + (1 - \beta)G_t$ and singular value decomposition $M_t = U_t \Sigma_t V_t^\top$, the update is

$$W_{t+1} = W_t - \eta_t U_t V_t^\top, \quad (55)$$

where $U_t V_t^\top$ is usually approximated by a few Newton–Schulz matrix multiplications rather than an explicit SVD. This direction is the full polar factor, so it keeps the singular vectors while flattening every singular value to one.

Axis III holds this direction in both the LMO and the preconditioner readings (Table 5), and the two agree on the same $U_t V_t^\top$. From the LMO side, it is the steepest matrix direction on the spectral-norm ball,

$$U_t V_t^\top = \arg \max_{\|X\|_{S_\infty} \leq 1} \langle M_t, X \rangle, \quad (56)$$

where $\|\cdot\|_{S_\infty}$ is the spectral norm and $\langle M_t, X \rangle = \text{tr}(M_t^\top X)$. By the von Neumann trace inequality $\langle M_t, X \rangle \leq \sum_i \sigma_i(M_t) \sigma_i(X) \leq \sum_i \sigma_i(M_t)$, with equality at $X = U_t V_t^\top$, the steepest direction is exactly the polar factor. From the preconditioner side, the same direction is a Gram preconditioning of the momentum,

$$\text{msign}(M_t) = (M_t M_t^\top)^{-1/2} M_t = U_t V_t^\top, \quad (57)$$

where $\text{msign}(\cdot)$ is the matrix sign function that sets all singular values to one, matching the Axis III metric $H_t = M_t M_t^\top$ in Table 5. The two readings are the two faces of the same operator Φ_t , and they differ only in whether the geometry is charged to the direction map ψ_t or to the metric H_t .

Kronecker-factored preconditioning occupies a different point in the same matrix space. For Shampoo, the matrix case maintains row and column factors

$$L_t = \beta L_{t-1} + (1 - \beta) G_t G_t^\top, \quad R_t = \beta R_{t-1} + (1 - \beta) G_t^\top G_t, \quad (58)$$

and applies an inverse-root preconditioner,

$$\Delta_t = L_t^{-1/4} G_t R_t^{-1/4}, \quad W_{t+1} = W_t - \eta_t \Delta_t. \quad (59)$$

As with Muon, Axis III holds this update in both the LMO and the preconditioner readings (Table 5). From the preconditioner side, the row and column factors combine into a Kronecker metric

$$H_t = L_t^{1/4} \otimes R_t^{1/4}, \quad \text{vec}(\Delta_t) = H_t^{-1} \text{vec}(G_t), \quad (60)$$

whose analysis basis is the eigenbasis of L_t and R_t . The curvature proxy is a Kronecker-structured matrix that captures coordinate coupling and is richer than the diagonal vector of Adam. From the LMO side, the same direction is the steepest matrix direction on the Kronecker-metric ball $\{X : \|L_t^{1/4} X R_t^{1/4}\|_F \leq \rho\}$, an ellipsoid (Mahalanobis ball) stretched and rotated by that metric, so Shampoo returns a continuous preconditioned gradient. SOAP keeps this basis idea but runs Adam-style coordinate adaptation after rotating the gradient into the Shampoo eigenbasis, then rotates the update back [108]. It is therefore a bridge between T1 and T2, with a coordinate-wise adaptive denominator whose coordinates have shifted from raw parameters to learned matrix-curvature coordinates.

Low-rank projection methods move along Axis I (Table 5), placing the whole update in a low-dimensional subspace while the curvature estimate largely follows Adam. GaLore is the representative example, choosing or refreshing a projection basis $P_t \in \mathbb{R}^{m \times r}$ with $r \ll \min(m, n)$ and projecting the gradient,

$$\tilde{G}_t = P_t^\top G_t, \quad (61)$$

running Adam or AdamW state evolution on \tilde{G}_t , and reconstructing a full update by $\Delta_t = P_t \tilde{\Delta}_t$. Because the optimizer state lives only in the projected low-dimensional coordinates, memory drops accordingly. The risk is approximation error. Useful high-rank gradient components may be removed unless the basis refresh, rank allocation, or residual pathway captures them.

5.2.3 Representative Methods

The following discussion follows the T2.1–T2.3 subclass order introduced above. Within each subclass, representative methods are grouped by the local matrix operation they modify rather than by chronology.

Spectral Orthogonalization. The spectral branch asks whether a matrix update should preserve the singular-vector frame but discard the singular-value scale. At the survey level, its core operation is

$$M_t = \beta M_{t-1} + (1 - \beta) G_t, \quad D_t = \text{Polar}(M_t) = U_t V_t^\top \approx \text{NS}_K(M_t), \quad (62)$$

where $M_t = U_t \Sigma_t V_t^\top$ and NS_K denotes a finite Newton–Schulz approximation to the polar factor. The resulting update is usually $W_{t+1} = W_t - \eta_t D_t$ on routed matrix parameters.

- **Canonical orthogonalized-update line.** Muon is the central T2.1 method because it turns the matrix momentum into an orthogonalized update rather than a coordinate-wise adaptive update. In practical LLM implementations, Muon is usually applied only to selected two-dimensional hidden-layer weights, while embeddings, scalar parameters, normalization parameters, and other excluded tensors use an SGD or AdamW-style fallback route [48].

- **Routing and scaling extensions.** Dion proposes distributed orthonormalized updates and broader parameter handling, making the S1 routing and systems pathway more explicit [2]. AdaMuon and AdaGO add adaptive scaling logic to orthogonalized updates, placing them at the boundary between T2.1 direction selection and T1-style step-size adaptation [101, 133].
- **Spectral-geometry boundary methods.** OrthoGrad and Spectral Sphere are useful boundary points rather than central LLM optimizer baselines: the former studies orthogonal-gradient constraints for calibration, while the latter studies controlled LLM training under spectral-sphere geometry [41, 116].

The common thread is a single direction choice, namely to preserve the singular-vector frame and flatten the singular spectrum. Whether it consistently beats AdamW, Shampoo, or SOAP depends on the setting. The open empirical question is whether the spectral direction remains beneficial after matching batch size, warmup, weight decay, fallback optimizer, matrix-only scope, step time, and tuning budget. Recent mechanism and fine-tuning studies already warn that Muon-style conclusions can be protocol-sensitive [89, 100].

Kronecker-Factored Preconditioning. The Kronecker branch asks whether a matrix update should be scaled in row and column curvature coordinates or kept in raw parameter coordinates. The shared template is

$$L_t = \beta L_{t-1} + (1 - \beta) G_t G_t^\top, \quad R_t = \beta R_{t-1} + (1 - \beta) G_t^\top G_t, \quad (63)$$

$$\bar{G}_t = P_{L,t}^\top G_t P_{R,t}, \quad \Delta_t = P_{L,t} \Psi_t(\bar{G}_t; \mathcal{S}_t) P_{R,t}^\top, \quad (64)$$

where $P_{L,t}$ and $P_{R,t}$ are eigenvectors or structured bases derived from row/column statistics. Shampoo instantiates Ψ_t as inverse-root preconditioning, whereas SOAP uses Adam-style coordinate adaptation in this rotated basis.

- **Inverse-root preconditioning base.** Shampoo is the mathematical base of T2.2. It stores per-mode row and column statistics and applies matrix inverse roots [38], approximating the full $(mn) \times (mn)$ curvature matrix with two small factors while keeping more coordinate coupling than Adam’s per-coordinate diagonal second moment. For matrices, this yields the factors and update in Eqs. (58)–(59). The benefit is a structured approximation to second-order information; the cost is nontrivial state, matrix-root computation, numerical damping, and a refresh schedule for the preconditioners.
- **Adam-in-eigenbasis and practical routing.** SOAP updates the Shampoo line by adding Adam-like adaptation in the Shampoo eigenbasis [108]. Conceptually, it first chooses the matrix basis from Kronecker factors and then applies diagonal adaptivity in that rotated coordinate system. COSMOS extends the practical branch by combining hybrid adaptive routing with memory-efficient LLM training goals [66].
- **Learned and structured-Fisher preconditioners.** PSGD and Kron-like instances form a broader learned-preconditioner branch. The early PSGD formulation and later Lie-group preconditioner view learn structured preconditioners rather than using Shampoo’s fixed inverse-root construction [62, 63]. RACS is placed in T2.2 because its row-and-column scaled SGD is based on a structured Fisher approximation, whereas the low-rank extension in the same source is represented by Alice [37].

The common thread is structured matrix scaling. T2.2 differs from T2.1 because it uses magnitude information in row/column or Fisher coordinates rather than only flattening a spectrum. It differs from T2.3 because it does not make low-rank projection the primary state space. Because Shampoo and SOAP tend to improve loss per token while paying a high per-step cost, benchmark claims for this subclass should report loss at a fixed token budget alongside loss normalized by wall-clock or

step time, so that the per-step overhead is counted, together with the preconditioner refresh frequency, damping, and memory overhead that drive this cost.

Low-Rank Subspace Projection. The low-rank branch asks whether the optimizer state should live in a projected matrix subspace. Its survey-level template is

$$\tilde{G}_t = P_t^\top G_t, \quad \tilde{\Delta}_t = \text{AdamW}_{\text{subspace}}(\tilde{G}_t), \quad \Delta_t = P_t \tilde{\Delta}_t + \mathcal{E}_t, \quad (65)$$

where $P_t \in \mathbb{R}^{m \times r}$, $r \ll \min(m, n)$, and \mathcal{E}_t denotes an optional residual or correction pathway. Plain GaLore uses the projection-reconstruction route without treating \mathcal{E}_t as the defining component. Follow-up methods modify the rank, refresh, or residual logic.

- **Projected Adam-state base.** GaLore defines the low-rank subspace branch for LLM optimization [138]. Its premise is that many large-model gradient matrices contain exploitable low-rank structure during training. GaLore periodically constructs a projection basis, runs the adaptive update in the projected coordinates, and maps the update back to the original matrix. Because its Adam states live only in this low-dimensional subspace, memory is much smaller than for the full matrix.
- **Residual and rank-allocation follow-ups.** If the rank is too small, the projection refresh interval is too long, or the basis misses changing gradient directions, a low-rank method may save memory while losing high-rank information. Fira directly addresses this concern by asking whether full-rank training quality can be recovered under a low-rank constraint, using residual or rank-allocation logic to reduce information loss [18].
- **Structured-Fisher low-rank extensions.** Alice is another low-rank extension, but its source begins from structured Fisher approximation and row/column scaling. Given this structured-Fisher origin, it is better described as a low-rank extension on a T2.2 background, whereas GaLore is the pure low-rank projection route [37].

The common thread is S2/S3/S4 subspace training, namely projection, subspace state evolution, and reconstruction. The memory benefit is an effect of this subspace choice, while the classification rests on the subspace mechanism itself. For benchmarking, T2.3 methods should be compared under explicit memory budgets against full-rank AdamW, T4 state-compression methods, and T2.2 matrix preconditioners under matched rank, refresh interval, batch size, and wall-clock accounting.

5.2.4 Effect-Target Assessment

T2 changes the unit of adaptation from coordinates to matrices. This shift can improve the direction itself: spectral methods choose a matrix-level orientation, Kronecker methods approximate curvature in row-column coordinates, and low-rank methods restrict state evolution to a cheaper subspace. The same shift also explains the family cost. Matrix operations, parameter routing, basis refresh, and structured state make T2 more dependent on layer topology and implementation details than T1. Table 9 summarizes these mechanism-derived performance priors.

The resulting performance profile is multi-objective. A spectral method can improve loss per token while increasing step time; a Kronecker method can improve conditioning but lose wall-clock advantage when inverse roots are too frequent; a low-rank method can save memory while requiring enough rank or refreshes to preserve high-rank gradient information. The family-level results in Sec. 6.2.8 therefore separate T2 into several regimes rather than treating it as a single upgrade over AdamW. The broad optimizer studies by several researchers [139] and Semenov et al. [97] already show that optimizer rankings move with scale, tuning effort, and training duration. T2 sharpens that dependence because its gains appear only when the exploited matrix structure is statistically useful and cheap enough to apply.

Table 9: Mechanism-informed effect assessment for T2 subclasses. The entries are design priors for benchmark planning, not empirical conclusions.

Primary target	Likely cost or failure mode	Benchmark focus
T2: Matrix-level structural methods		
T2.1 Spectral orthogonalization		
O1 token efficiency, O4 stability	O2 extra matrix multiplications, routing sensitivity	Matched LR/warmup/batch, matrix-only scope, step-time accounting
T2.2 Kronecker-factored preconditioning		
O1 convergence, O4 conditioning	O2 matrix roots, O3 Kronecker state, implementation complexity	Preconditioner update frequency, memory and wall-clock overhead, damping
T2.3 Low-rank subspace projection		
O3 memory reduction with possible O1 retention	Refresh cost, rank sensitivity, high-rank information loss	Rank and interval sweeps, memory budget vs. AdamW and T4

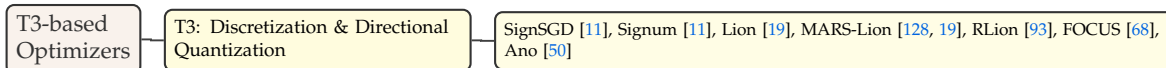


Figure 9: Taxonomy of discretized and directionally quantized optimizers.

5.3 T3: Discretization and Directional Quantization

5.3.1 Family Overview and Meta-Pipeline Position

T3 contains optimizers whose primary operation discretizes the update direction. The characteristic map is $\text{sign}(\cdot)$ or a close sign-like transformation: it keeps coordinate-wise orientation while discarding, clipping, or coarsening the continuous magnitude of the gradient or momentum signal. This makes T3 different from both T1 and T4. T1 methods may become sign-like in some coordinates after adaptive normalization, but their defining mechanism is still moment estimation and diagonal scaling. T4 methods may reduce memory, but their defining mechanism is state storage, sharing, quantization, or release. T3 instead changes the geometry of the direction itself.

Mechanism-group structure. Figure 9 gives the complete optimizer membership for T3. Because the current taxonomy treats T3 as one compact family-level subclass, the discussion below interprets the taxonomy figure through three sign-direction routes rather than restating the member list.

- **Pure sign directions.** The defining operation is a hard sign map applied to either the raw gradient or a momentum buffer before the update is formed. SignSGD is the canonical instance, and its momentum-sign variant is usually discussed as Signum [11].
- **Signed momentum.** The direction is the sign of an interpolated current-gradient and past-momentum signal, with only one persistent momentum buffer. Lion is the central large-model representative of this route [19]; MARS-Lion keeps the same sign map but feeds it a MARS-style corrected signal [128].

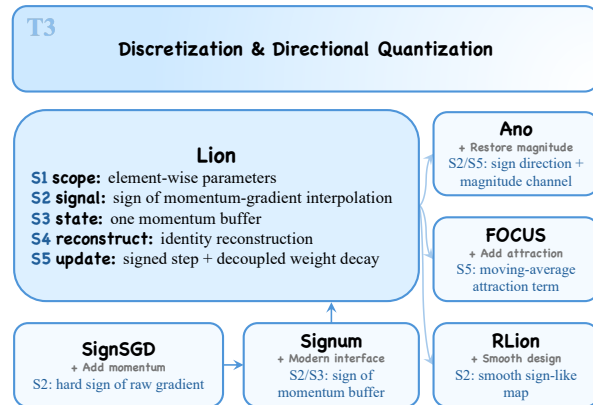


Figure 8: Mechanism schematic for T3 discretization and directional quantization. This schematic provides a taxonomy guide rather than an empirical ranking for the compact T3 family, grouping discretization and directional quantization mechanisms by their sign-direction generation methods.

- **Smooth and hybrid sign directions.** These methods preserve a sign-like core but soften discontinuities, add trajectory attraction, or reintroduce a limited magnitude channel. RLion smooths the sign decision [93]; FOCUS attracts iterates toward a running parameter trajectory [68]; and Ano restores a bounded magnitude channel without returning to a full Adam-style second-moment state [50].

At the family level, T3 can be summarized as

$$z_t = C_t(g_t, m_{t-1}, \theta_t), \quad d_t = q_t(z_t), \quad \theta_{t+1} = (1 - \eta_t \lambda) \theta_t - \eta_t (s_t \odot d_t + a_t), \quad (66)$$

where C_t forms the signal on which the directional decision is made, q_t is a hard or smooth sign-like map, s_t is a scalar or coordinate-wise magnitude channel, and a_t is an optional trajectory-control term. SignSGD sets $C_t(g_t) = g_t$, $q_t = \text{sign}$, $s_t = \mathbf{1}$, and $a_t = 0$. Lion sets $C_t = \beta_1 m_{t-1} + (1 - \beta_1) g_t$ and keeps the hard sign. Hybrid variants retain the same directional core while changing q_t , s_t , or a_t . Thus the transformed signal in S2 is already a discrete or near-discrete direction, S3 is usually a first-moment state or no second moment, S4 is identity, and S5 controls the learning-rate radius, weight decay, and any added trajectory or scale correction. Compared with AdamW, the persistent optimizer state can be reduced because no second-moment buffer v_t is stored. This memory benefit is important, but it is an effect of the sign-direction mechanism rather than the classification rule.

The family boundary is also important for masks and selective updates. A method belongs to T3 when the sign-like map directly defines the base update direction, as in SignSGD, Lion, RLion, FOCUS, and Ano. By contrast, methods whose primary increment is a binary or stochastic mask applied to an already computed AdamW-, Lion-, or Muon-style update are post-update filters. We therefore place Magma and MGUP in T5.3 rather than in T3; the same rule covers cautious and top- k update filters. This separation keeps “direction quantization” distinct from “selective writeback” even though both may use signs or binary decisions internally.

5.3.2 LMO-Driven Four-Axis Interpretation

In the four-axis view, the typical T3 coordinate is

$$((L, I), \text{sign}, L, 0, \hat{g}_t, S_t), \quad (67)$$

where the analysis basis remains the raw coordinate basis, the direction map is sign-like, the curvature proxy is absent or weak, and S_t records whether a first-moment buffer, no buffer, or an extra magnitude channel is stored. The LMO explanation comes from the ℓ_∞ ball. For the linearized problem

$$\min_{\|d\|_\infty \leq 1} \langle g, d \rangle, \quad (68)$$

the optimizer is $d^* = -\text{sign}(g)$. The extreme points of the ℓ_∞ ball are coordinate-wise sign patterns, so a sign update is the steepest linearized step under a fixed maximum coordinate displacement. This is the coordinate analogue of the spectral sign logic used by Muon in T2, but with the identity basis rather than an SVD or Kronecker basis.

SignSGD realizes this geometry directly by applying $d_t = \text{sign}(g_t)$ [11]. Lion replaces the raw stochastic gradient with a smoothed interpolation of current gradient and past momentum before applying the same vertex map. This modification is small in algebra but large in practice: the sign decision is made on a lower-variance temporal signal, while the state remains cheaper than Adam’s two-buffer design. Recent norm-LMO and stochastic Frank–Wolfe analyses make this connection explicit by treating sign, normalized, and orthogonalized updates as different norm-constrained direction choices rather than unrelated heuristics [10, 87, 98].

The same interpretation also clarifies what T3 does not cover. AdamW may look sign-like when the adaptive denominator largely cancels gradient magnitudes, but its update is still controlled by a diagonal curvature or variance estimate and exponent $\alpha = 1/2$. FOCUS and Ano are closer to T3

because they preserve a sign-direction core while adding trajectory attraction or an explicit magnitude channel [68, 50]. RLion sits on the boundary in the opposite direction: it smooths the hard sign into a bounded continuous map, so it is best read as a Lion-style regularization of the same direction geometry rather than as a separate adaptive-moment family [93].

5.3.3 Representative Methods

The following discussion follows the three-part organization introduced above. Within each group, representative methods are further separated by the local operation that changes the sign-direction template in Eq. (66).

Pure Sign Directions. The first branch applies a sign map with minimal additional optimizer state. At the survey level, it can be written as

$$d_t = \text{sign}(h_t), \quad h_t = \begin{cases} g_t, & \text{pure SignSGD,} \\ \beta h_{t-1} + (1 - \beta)g_t, & \text{momentum sign.} \end{cases} \quad (69)$$

- **Pure gradient sign.** SignSGD is the historical anchor for T3. Its update transmits and applies only the sign of each stochastic-gradient coordinate, and the distributed variant aggregates worker signs through majority vote [11]. The original motivation was partly communication efficiency: a sign vector is a 1-bit message per coordinate. For this taxonomy, the more important point is geometric: SignSGD removes continuous magnitude information before the update is formed.
- **Momentum sign.** Momentum sign methods, often referred to as Signum in benchmark and theory discussions, move the sign decision from g_t to a smoothed momentum buffer. This makes the direction less sensitive to a single noisy mini-batch while keeping the fixed-magnitude update structure.
- **Benchmark role.** SignSGD should not be evaluated as a modern LLM optimizer on historical status alone. Its communication advantages, convergence assumptions, and failure modes were developed before current Transformer pretraining protocols. It remains useful because it isolates direction discretization from Adam-style second moments; recent language-model optimizer studies use Signum-like variants to decompose how much of Adam’s behavior comes from signed momentum, layer-wise adaptivity, and other control components [139].

The common thread is the early removal of magnitude. In the notation of Eq. (66), pure sign methods set $s_t = \mathbf{1}$ and $a_t = 0$; all adaptation must therefore come from the signal h_t , learning-rate schedule, or external routing, not from a diagonal second-moment denominator.

Signed Momentum. The second branch is the modern signed-momentum line. Lion’s compact rule is

$$z_t = \beta_1 m_{t-1} + (1 - \beta_1)g_t, \quad d_t = \text{sign}(z_t), \quad (70)$$

$$m_t = \beta_2 m_{t-1} + (1 - \beta_2)g_t, \quad \theta_{t+1} = (1 - \eta_t \lambda)\theta_t - \eta_t d_t. \quad (71)$$

- **Search-discovered signed momentum.** Lion is the central T3 method for LLM training. It was discovered through symbolic optimizer search and then simplified into Eq. (71) [19]. The method retains several practical features of AdamW—a momentum interface, decoupled weight decay, and schedule compatibility—but it replaces Adam’s continuous adaptive direction by the sign of a momentum-gradient interpolation.
- **Interface, mechanism, and memory effect.** Lion is often described as an AdamW alternative, a sign optimizer, and a memory-friendlier optimizer. In this taxonomy, only the second description

is primary. The AdamW interface is inherited scaffolding, and the memory saving follows from removing v_t .

- **Protocol-sensitive tuning.** Because $\|d_t\|_\infty = 1$, the learning rate directly sets the largest coordinate movement, and gradient-magnitude outliers cannot enlarge individual update coordinates. This can improve robustness in some noisy regimes, but it can also make learning rate, weight decay, warmup, and schedule choices sharper than in AdamW. Recent LLM studies include Lion as an important baseline, but also show that rankings change with model scale, token budget, batch size, and tuning effort [139, 97, 113, 96].
- **Cross-family wrappers.** MARS-Lion changes the gradient-estimation axis by feeding a variance-reduced signal into a Lion-style sign map; it does not create a new T3 subclass. Cautious Lion applies a consistency filter after the base direction is computed, so its primary added mechanism is T5.3 post-update filtering.

The common thread is signed momentum under an AdamW-like training interface. Lion therefore functions as the central comparison point for T3: pure sign methods show what is lost without a temporal buffer, while hybrid variants test how much smoothing or magnitude information can be restored without leaving the sign-direction geometry.

Smooth and Hybrid Sign Directions. The third branch tests which parts of the hard-sign template can be softened or supplemented. A broad template is

$$d_t = q_\tau(z_t), \quad \theta_{t+1} = (1 - \eta_t \lambda) \theta_t - \eta_t (s_t \odot d_t + \rho_t (\theta_t - \bar{\theta}_t)), \quad (72)$$

where q_τ is a smooth or bounded sign-like map, s_t may restore a limited magnitude channel, and $\bar{\theta}_t$ is an optional moving-average trajectory reference.

- **Smooth sign maps.** RLion replaces the discontinuous sign function with a bounded smooth alternative based on an arctan-style transformation [93]. This keeps the update in the same sign-like direction family while reducing abrupt coordinate flips near zero. Its evidence is mainly outside LLM pretraining, so it is a boundary method rather than a coequal anchor with Lion.
- **Trajectory attraction around sign directions.** FOCUS starts from the observation that sign-momentum methods can move aggressively in noisy, flat, or low-curvature regions, then adds attraction toward a moving average of parameters to concentrate the trajectory [68]. The update still uses a sign-direction core, but S5 gains an additional trajectory-control term.
- **Magnitude side channels.** Ano separates direction from magnitude, using momentum to smooth the direction while using instantaneous gradient magnitudes to set step sizes in noisy landscapes [50]. It is best read as a sign-direction plus magnitude-channel hybrid, not as a return to full Adam-style second-moment adaptivity.

These methods show that T3 is not limited to hard binary updates. They also make the boundary sharper: methods dominated by update masks or writeback filters are better handled in T5.3, even when they use directional agreement signals, whereas RLion, FOCUS, and Ano still define the base direction through a sign-like route.

5.3.4 Effect-Target Assessment

T3 replaces continuous update magnitudes with sign-like directions. This creates a compact performance profile: the update is cheap, the persistent state can be smaller than AdamW, and the largest coordinate displacement is controlled directly by the learning rate. The same discretization removes amplitude information before the step is formed. SignSGD exposes this limit in its purest form [11];

Table 10: Mechanism-informed effect assessment for T3 methods. The entries are design priors for benchmark planning, not empirical conclusions.

Primary target	Likely cost or failure mode	Benchmark focus
T3: Discretization and directional quantization		
SignSGD / Signum		
O2 communication simplicity, O4 outlier robustness	Magnitude loss, sign-noise sensitivity	Pure vs. momentum sign vs. AdamW under matched settings
Lion		
O3 low state, O2 cheap updates	LR, WD, and warmup become protocol-sensitive	LR/WD/schedule sweeps against strong AdamW baselines
RLion / FOCUS / Ano		
O4 stability around sign directions	Extra knobs, limited LLM evidence	Source domains, extra-knob tuning, per-component ablations

Lion makes the route more practical by applying the sign map to a smoothed momentum-gradient signal [19]. Table 10 summarizes the mechanism-derived performance priors.

The first expected gain is resource efficiency rather than peak quality. Lion can reduce optimizer state by removing v_t , and sign updates avoid expensive direction construction, but neither fact guarantees a better loss trajectory. Fixed-magnitude updates can be tolerant to local magnitude outliers while remaining sensitive to learning rate, warmup, and weight decay. This distinction matches the benchmark narrative in Sec. 6.2.8: T3 is efficient and locally tolerant to learning-rate perturbations, yet its tuned perplexity is generally weaker than the best T1 and T2 alternatives.

5.4 T4: State Compression and Structural Aggregation

5.4.1 Family Overview and Meta-Pipeline Position

T4 contains optimizers whose primary contribution is to reduce the memory footprint, granularity, precision, or lifetime of optimizer state. For a model with d trainable parameters, AdamW stores at least two full-size state tensors, m_t and v_t , in addition to parameters, gradients, activations, and distributed-training buffers. This cost is significant in LLM training, because optimizer state competes directly with model size, sequence length, batch size, activation rematerialization, sharding, and communication buffers. The central issue is which optimizer histories must be retained, how faithfully they must be represented, and when they can be reconstructed, broadcast, dequantized, or discarded.

Subclass structure and membership. Figure 11 gives the subclass-level optimizer list for T4, and the four subclasses below specify the corresponding optimizer membership. The split follows the state representation being changed.

T4.1 Row-column factorization. This subclass contains AdaFactor and CAME. Its members replace a full matrix second-moment tensor with row and column summaries, then reconstruct an approximate denominator only when the update is formed [99, 74].

T4.2 Low-bit quantization and error compensation. This subclass contains 8-bit Adam and Q-GaLore. Its members store optimizer statistics, projection objects, or related accumulated information in low-bit form and rely on block-wise scaling, stochastic rounding, or compensation logic to control long-horizon numerical error [27, 137].

T4.3 Block- and layer-level state sharing. This subclass contains Adam-mini, APOLLO, SM3, Conda, and NovoGrad. Its members reduce the number or dimensionality of adaptive statistics by sharing them across blocks, covers, columns, layers, or low-rank auxiliary structures [136, 140, 6, 111, 35].

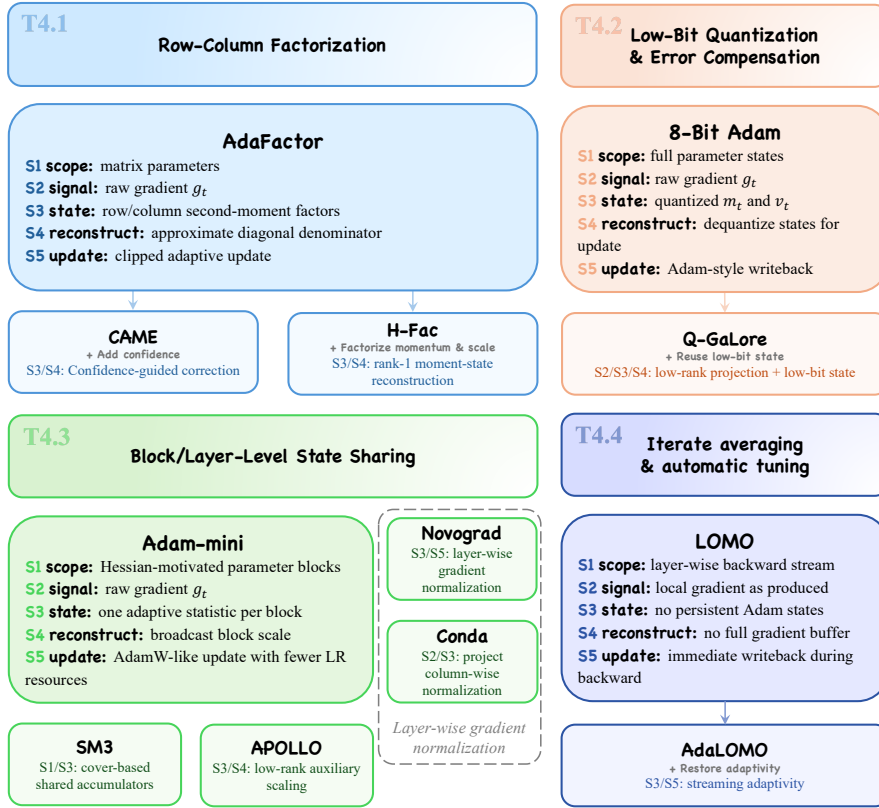


Figure 10: **Mechanism schematic for T4 state compression and structural aggregation.** The schematic organizes the family by the form of memory reduction: factored second-moment storage, low-bit state representation, shared adaptive statistics, and streaming gradient consumption.

T4.4 Fused backprop-update. This subclass contains LOMO and AdaLOMO. Its members change the optimizer pipeline so that gradients are consumed during backpropagation as soon as they are produced [76, 75].

At the family level, a compressed-state adaptive update can be summarized as

$$\mathcal{Z}_t = \mathcal{C}_t(\mathcal{S}_t), \quad \widehat{\mathcal{S}}_t = \mathcal{R}_t(\mathcal{Z}_t), \quad \theta_{t+1} = \theta_t - \eta_t \mathcal{U}_t(g_t, \widehat{\mathcal{S}}_t), \quad (73)$$

where \mathcal{S}_t denotes the full optimizer state that an AdamW-like method would store, \mathcal{C}_t is a compression, sharing, quantization, or lifetime-shortening map, \mathcal{R}_t reconstructs or exposes the usable state at update time, and \mathcal{U}_t is the base update rule. Full-state AdamW is the special case in which \mathcal{C}_t and \mathcal{R}_t are identities. T4 begins when at least one of them is nontrivial.

In the meta-pipeline, T4 primarily modifies S3 and S4. The state maintained by S3 may be factored, quantized, shared, reduced to a low-dimensional auxiliary object, or eliminated. S4 then reconstructs, broadcasts, dequantizes, or streams the required quantity into the update. T4.3 also uses S1 because the grouping of parameters into blocks, covers, columns, or layers determines which coordinates share statistics. T4.4 changes S5 as well because the writeback occurs during the backward pass, before all gradients have been materialized.

This definition separates T4 from nearby families. GaLore belongs to T2.3 because it changes the mathematical subspace in which gradients and Adam states are updated. Q-GaLore is discussed in T4.2 only for the additional quantization component on top of that low-rank mechanism [138, 137]. Lion

uses less memory than AdamW, but its primary mechanism is a sign-direction map, so it remains T3. ZeRO, activation checkpointing, CPU/NVMe offloading, and parameter-efficient fine-tuning can be combined with T4 optimizers, but they are systems or training-regime techniques in this taxonomy. T4 is reserved for methods that change the optimizer’s own state representation or gradient-consumption pipeline.

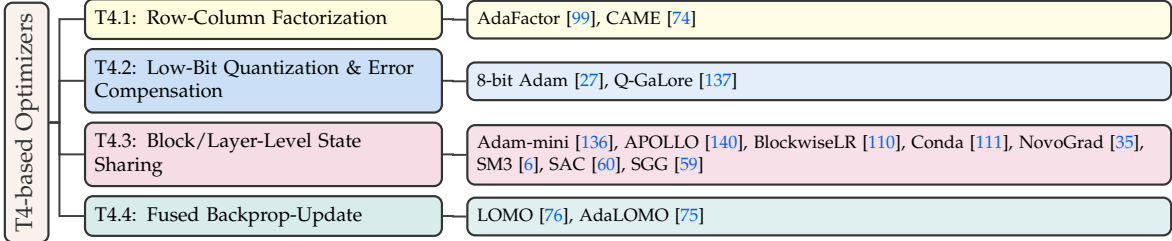


Figure 11: Taxonomy of state-compressed and structurally aggregated optimizers.

5.4.2 LMO-Driven Four-Axis Interpretation

In the four-axis notation of Section 3.2, T4 is the most direct instantiation of state compression in Axis II. A generic adaptive update can be written as

$$\theta_{t+1} = \theta_t - \eta_t \frac{\hat{m}_t}{\sqrt{\mathcal{R}(\mathcal{C}(v_t)) + \epsilon}}, \quad (74)$$

where \mathcal{C} compresses the second-moment state and \mathcal{R} reconstructs, broadcasts, or dequantizes it for the update. In full AdamW, \mathcal{C} and \mathcal{R} are both identities. In T4, at least one of them is nontrivial. The geometry of the base direction can remain coordinate-wise Adam-like, and the innovation is the representation of the statistics that control the denominator.

For matrix parameters $W_t \in \mathbb{R}^{m \times n}$, a factored method keeps row and column statistics, for example

$$r_{i,t} = \beta r_{i,t-1} + (1 - \beta) \frac{1}{n} \sum_{j=1}^n G_{ij,t}^2, \quad c_{j,t} = \beta c_{j,t-1} + (1 - \beta) \frac{1}{m} \sum_{i=1}^m G_{ij,t}^2, \quad (75)$$

and reconstructs an approximate matrix denominator such as $\hat{V}_{ij,t} \propto r_{i,t} c_{j,t}$. This lowers state from $O(mn)$ to $O(m+n)$, but it assumes that row and column summaries preserve enough information about the diagonal curvature proxy. For block sharing, the compression map is instead a partition $\{B_k\}_{k=1}^K$ with shared statistics

$$s_{k,t} = \beta s_{k,t-1} + (1 - \beta) \frac{1}{|B_k|} \sum_{i \in B_k} g_{i,t}^2, \quad i \in B_k, \quad (76)$$

which is then broadcast to all coordinates in the block. The compression quality depends on whether the partition aligns with the structure of the loss landscape.

Low-bit methods preserve the same state shape but change the value representation. With a b -bit block quantizer Q_b , the stored state is $Q_b(m_t)$ or $Q_b(v_t)$, and the update uses $\text{dequant}(Q_b(\cdot))$ at computation time. The key design choices are block size, dynamic range tracking, stochastic rounding, and special handling of sensitive tensors such as embeddings. Fused backprop-update methods change a different part of Axis II, namely that the state may not be stored at all. Gradients are consumed as soon as they are produced during backpropagation, which changes the lifetime of g_t and restricts operations that require global gradient visibility.

5.4.3 Representative Methods

The following discussion follows the T4.1–T4.4 subclass order introduced above. Within each subclass, representative methods are grouped by the local state operation they modify.

Row-Column Factorization. The first T4 branch replaces a dense matrix-valued second-moment state by two marginal summaries. For $G_t \in \mathbb{R}^{m \times n}$, the representative template is

$$R_t = \beta R_{t-1} + (1 - \beta) \text{rowmean}(G_t \odot G_t), \quad C_t = \beta C_{t-1} + (1 - \beta) \text{colmean}(G_t \odot G_t), \quad (77)$$

$$\widehat{V}_{ij,t} = \frac{R_{i,t} C_{j,t}}{\text{mean}(R_t)}, \quad \Delta_{ij,t} = \frac{\widehat{m}_{ij,t}}{\sqrt{\widehat{V}_{ij,t} + \epsilon}}. \quad (78)$$

- **AdaFactor base.** AdaFactor is the mathematical anchor of T4.1. It preserves the Adam and RMSProp intuition that recent squared gradients provide a useful scale estimate, but replaces the full $O(mn)$ matrix state with $O(m + n)$ row and column accumulators [99]. It reconstructs a cheaper approximation to a diagonal denominator while staying at the diagonal, coordinate-wise scale level.
- **Confidence-guided correction.** CAME starts from the same factored-state premise and adds confidence-guided correction to damp or reweight entries where the factorized surrogate is unreliable [74]. Its role is to show the second step in compressed optimization. Once state is approximated, the optimizer also needs a way to detect and control compression error.
- **Boundary to shared accumulators.** SM3 is adjacent because a matrix cover can resemble row-column accumulators, but its defining abstraction is a general cover-based shared state [6]. We therefore discuss SM3 in T4.3.

The common thread is an approximation to a diagonal second-moment tensor. The descent geometry itself is unchanged. The main benchmark question is therefore whether the row and column marginals preserve enough curvature heterogeneity for the target Transformer block, sequence length, and clipping rule.

Low-Bit Quantization and Error Compensation. The second branch preserves the shape of the base optimizer state but changes the numerical representation in which that state is stored. A block-wise quantized state can be written schematically as

$$z_{B,t} = Q_b(x_{B,t}; a_{B,t}), \quad \tilde{x}_{B,t} = \text{dequant}(z_{B,t}; a_{B,t}), \quad \Delta_t = \mathcal{U}_{\text{Adam}}(g_t, \tilde{m}_t, \tilde{v}_t), \quad (79)$$

where $x_{B,t}$ is a state block, $a_{B,t}$ records the local dynamic range, and Q_b is a b -bit quantizer.

- **Block-wise dynamic quantization.** 8-bit Adam is the central T4.2 method. It identifies optimizer statistics as compressible objects and stores them using block-wise dynamic quantization while maintaining an Adam-like update interface [27]. The block-wise range is essential, because a single global scale would be too coarse for tensors whose coordinates have heterogeneous magnitudes.
- **Quantized low-rank combinations.** Q-GaLore is the clearest cross-family member. Base GaLore is T2.3 because it projects gradients and Adam states into a low-rank subspace. Q-GaLore adds low-bit projection and weight representations, including INT4 projection matrices and stochastic rounding for accumulated information [138, 137]. It is therefore cited here only when the quantization component is under discussion.
- **Evaluation consequences.** Low-bit state storage preserves the base optimizer geometry, so an 8-bit Adam update is still Adam-like in direction and scaling. Its possible advantage is O3 memory

and sometimes bandwidth/cache behavior, while its risks are quantization noise, block-size sensitivity, dequantization overhead, and precision-sensitive tensors such as embeddings.

The defining taxonomy feature of T4.2 is the low-bit representation of optimizer history. Dynamic quantization, stochastic rounding, and compensation mechanisms are implementation-specific tools for making low-bit state usable.

Block- and Layer-Level State Sharing. The third branch reduces the number of adaptive statistics by sharing them over a partition or structural cover. The generic form is

$$s_{k,t} = \beta s_{k,t-1} + (1 - \beta) \mathcal{A}_{i \in B_k}(g_{i,t}^2), \quad \Delta_{i,t} = \frac{\widehat{m}_{i,t}}{\sqrt{s_{k(i),t}} + \epsilon}, \quad (80)$$

where B_k is a block, cover element, column, layer, or auxiliary state group, \mathcal{A} is an aggregation rule, and $k(i)$ maps coordinate i to the statistic that will be broadcast back to it.

- **Transformer block sharing.** Adam-mini is the central LLM-oriented T4.3 method. It argues that Adam’s coordinate-wise denominator contains more distinct learning-rate resources than many Transformer blocks require, partitions parameters using Hessian-motivated structure, and assigns shared adaptive scales to the resulting blocks [136]. In meta-pipeline terms, S1 selects the blocks, S3 maintains one statistic per block, and S4 broadcasts that statistic back to the block coordinates. Similar designs are appeared in Blockwise LR [110], SGG [59], and SAC [60], which rescales the learning rate of network blocks or the certain groups of parameters to obtain better parameter update controls.
- **Cover and layer extremes.** SM3 uses tensor covers to maintain shared accumulators, so a matrix may be covered by row and column sets while higher-order tensors use more general covers [6]. NovoGrad moves to a coarser layer-wise statistic or gradient normalization, keeping less second-moment state than Adam while retaining momentum and weight-decay controls [35]. These methods provide historical anchors for the aggregation continuum.
- **Low-dimensional and column-wise aggregation.** APOLLO approximates AdamW’s learning-rate adaptation with an auxiliary low-rank state based on random projection, aiming for an AdamW-like interface under SGD-like memory [140]. Conda uses column-wise second-moment normalization after projecting updates into an orthogonal subspace [111]. Conda remains in T4.3 because its stored adaptive statistics are column-level and coarser than coordinate-level, but it is a boundary member with a secondary T2 tag.

The shared-state branch is controlled by granularity. Fine blocks preserve more heterogeneity but save less memory. Layers or coarse covers save more state but risk underfitting heterogeneous curvature. Recent APOLLO and Conda claims should be read as source-reported preprint evidence until their status and LLM-scale comparison protocols are finalized.

Fused Backprop-Update. The fourth branch changes the lifetime of gradients, reaching deeper than the shape or precision of a persistent state tensor. A fused update can be schematized as

$$g_i^{(l)} = \text{backward}_i(\theta_t), \quad \theta_{i+1}^{(l)} = \theta_i^{(l)} - \eta_t \mathcal{U}^{(l)}(g_i^{(l)}, \ddagger_i^{(l)}), \quad \text{free}(g_i^{(l)}), \quad (81)$$

where layer l is updated while its gradient is still local to the backward pass and before a full-model gradient buffer is materialized.

- **Streaming state-free update.** LOMO defines T4.4. It updates parameters as soon as each layer’s gradient becomes available during backpropagation, shortening gradient lifetime and eliminating persistent Adam-style optimizer states [76]. This is an optimizer-level pipeline change because it determines when gradients are consumed and which global operations remain feasible.

- **Streaming adaptivity.** AdaLOMO keeps the fused low-memory pipeline but reintroduces adaptive learning-rate information through compressed second-moment estimation and grouped update normalization [75]. Its primary label remains T4.4 because the fused backprop-update interface is the defining operation, while the factored adaptive state is a secondary T4.1-like component.
- **Composition limits.** Streaming updates can conflict with global gradient clipping, delayed low-rank basis refresh, SAM-style second gradients, and matrix preconditioners that require complete gradient statistics. T4.4 therefore has stronger composition constraints than ordinary state compression.

This branch illustrates the most aggressive T4 trade-off. Removing state and shortening gradient lifetime can make full-parameter fine-tuning feasible under tight memory budgets, but the price is reduced access to global gradient information. Later streaming methods often reintroduce a small amount of structured state to recover stability or convergence behavior.

5.4.4 Effect-Target Assessment

T4 methods have the clearest primary objective among the method families, namely O3 memory reduction. The evaluation challenge is that O3 improvements change the feasible training regime. A method can look worse than AdamW at the same model and batch size but become useful when it enables a larger model, longer sequence, or larger batch on fixed hardware. Conversely, a memory-efficient optimizer can lose its advantage if compression slows each step or requires more tokens to reach the same loss. Table 11 summarizes the mechanism-informed benchmark prior.

The main benchmark rule is to report both absolute performance and memory-normalized performance. If AdamW fits comfortably, a compressed method must justify any approximation error or overhead through convergence, stability, or tuning benefits. If AdamW does not fit, the relevant baseline may be a smaller model, gradient accumulation, offloading, sharding, or parameter-efficient fine-tuning, and full-state AdamW alone is then no longer the right comparison. T4 evaluation should therefore include peak memory, persistent optimizer state, gradient-buffer lifetime, step time, token-normalized loss, wall-clock loss, and sensitivity to learning rate, weight decay, clipping, and quantization granularity. Recent optimizer and memory-efficient pretraining studies make this point explicit. Optimizer ranking is protocol dependent, and memory savings are only useful when the saved memory is converted into a better training configuration [139, 97, 113, 36].

Table 11: Mechanism-informed effect assessment for T4 subclasses. The entries are design priors for benchmark planning, not empirical conclusions.

Primary target	Likely cost or failure mode	Benchmark focus
T4: State compression and structural aggregation		
T4.1 Row-column factorization		
O3 second-moment memory reduction	Factorization error, possible O4 instability	AdamW vs. AdaFactor vs. CAME at matched clipping and memory
T4.2 Low-bit quantization and error compensation		
O3 state memory, sometimes O2 bandwidth	Quantization noise, block-size sensitivity, sensitive embeddings	Precision, block size, rounding, convergence at matched memory
T4.3 Block/layer-level state sharing		
O3 fewer adaptive statistics	Bad grouping underfits curvature, hurting O1/O4	Grouping granularity, partition choice, LR/WD robustness
T4.4 Fused backprop-update		
O3 peak memory via shorter gradient lifetime	Incompatible with global-gradient operations, possible convergence gap	Peak memory, buffer lifetime, clipping and sharding compatibility

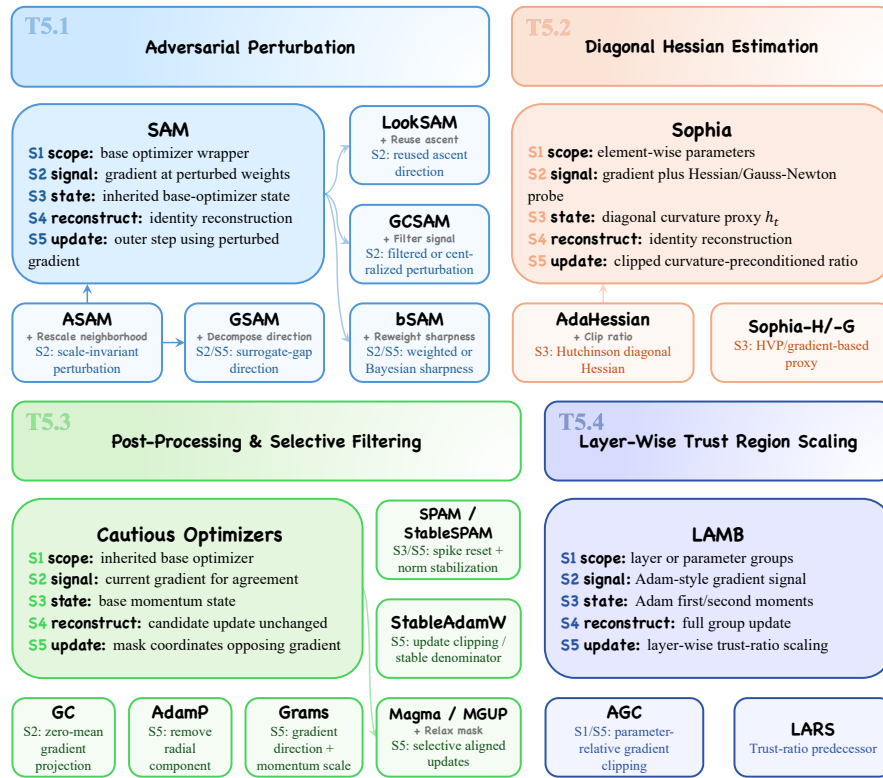


Figure 12: Mechanism schematic for T5 curvature-aware and geometric regularization methods. The schematic organizes the family by where the geometric intervention enters the update: perturbed-gradient evaluation, diagonal-curvature estimation, post-update filtering, or layer-wise trust-region scaling.

5.5 T5: Curvature-Aware and Geometric Regularization

5.5.1 Family Overview and Meta-Pipeline Position

T5 contains optimizers whose primary contribution is to impose a curvature or geometry constraint on the effective gradient, the candidate update, or the final parameter writeback. The family is broader than explicit second-order optimization. Some members estimate diagonal Hessian information, whereas others keep the base optimizer unchanged and act only through perturbations, projections, masks, norm controls, or layer-wise trust ratios. T5 therefore asks when a proposed step should be accepted, rescaled, clipped, filtered, or re-evaluated because of local sharpness, curvature, direction consistency, parameter scale, or update geometry.

Subclass structure. Figure 13 gives the complete optimizer membership for T5. The four subclasses below interpret that taxonomy by the dominant geometric operation.

T5.1 Adversarial perturbation (SAM family). SAM replaces the ordinary gradient by a gradient measured at a local adversarial perturbation [32]. ASAM changes the perturbation geometry [57]. Later variants modify the sharpness objective or its probabilistic interpretation [142, 129, 82], reduce perturbation frequency [69], separate stochastic-noise components in the perturbation [61], or combine SAM with gradient centralization [39].

T5.2 Diagonal Hessian estimation. Sophia maintains a diagonal Hessian or Gauss–Newton proxy

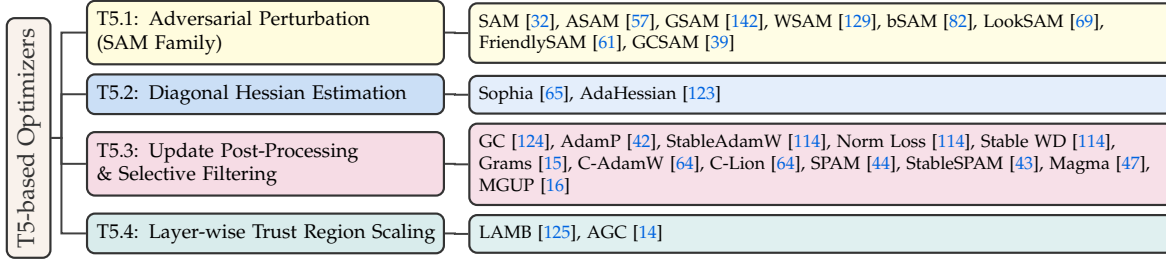


Figure 13: Taxonomy of curvature-aware and geometry-regularized optimizers. The prefix C- denotes Cautious.

and uses clipping to form an LLM-oriented trust-region-like update [65]. AdaHessian provides the earlier randomized diagonal-Hessian route [123].

T5.3 Update post-processing and selective filtering. This subclass centralizes, projects, normalizes, masks, stabilizes, or selectively amplifies a gradient or candidate update after the base direction has been defined. Gradient Centralization and AdamP are projection-style instances [124, 42], StableAdamW and its norm or decay components stabilize AdamW-style writeback [114], Cautious Optimizers instantiate direction-consistency masks [64], Grams separates direction and adaptive magnitude [15], SPAM and StableSPAM target spike-aware or norm-stabilized writeback [44, 43], Magma and MGUP occupy the selective-update and momentum-gradient-alignment corner of the subclass [47, 16].

T5.4 Layer-wise trust-region scaling. LAMB compares update and parameter norms to rescale Adam-style layer updates [125], whereas AGC clips gradients relative to the receiving parameter group [14].

At the family level, a T5 method can be summarized as

$$\tilde{g}_t = \mathcal{P}_t(g_t, \theta_t), \quad c_t = \mathcal{H}_t(\tilde{g}_t, \mathcal{S}_t), \tag{82}$$

$$\Delta_t^{\text{base}} = \mathcal{U}_{\text{base}}(\tilde{g}_t, \mathcal{S}_t, c_t), \quad \Delta_t = \mathcal{G}_t(\Delta_t^{\text{base}}, \tilde{g}_t, \theta_t, c_t), \tag{83}$$

$$\theta_{t+1} = \theta_t - \eta_t \Delta_t. \tag{84}$$

Here \mathcal{P}_t denotes the effective-gradient map, which is non-identity for SAM-style perturbations and some filtering methods, c_t is an optional curvature or scale signal, $\mathcal{U}_{\text{base}}$ is the underlying optimizer update, and \mathcal{G}_t is the T5 geometry operator. Ordinary AdamW with no wrapper is the identity case $\mathcal{P}_t = I$, $\mathcal{H}_t = \emptyset$, and $\mathcal{G}_t = I$.

In the meta-pipeline, T5 primarily acts near S5, but different subclasses enter through different interfaces. T5.1 reaches S5 through an S0/S2 perturbed-gradient evaluation. T5.2 modifies S3 by storing a curvature proxy and modifies S5 by clipping the resulting ratio. T5.3 uses S2 or S5 to filter the gradient or candidate update. T5.4 uses S1 to define layer or parameter-group routes and S5 to apply group-level trust ratios. S4 is usually identity-like because the update remains full-dimensional unless the method is primarily a T2 subspace method or a T4 state-compression method.

This definition fixes the boundary with the previous families. A direct AdamW variant remains T1 even if it improves stability, because its decisive change is still the element-wise moment formula. Muon, Shampoo, and GaLore remain T2 because they change the matrix basis or subspace before the update is formed. Lion remains T3 because its sign map defines the base direction. AdaFactor, 8-bit Adam, and Adam-mini remain T4 because they primarily alter state representation. By contrast, SAM can wrap SGD or AdamW, Cautious Lion can wrap Lion, and LAMB can wrap an Adam-style update. Their primary labels come from the wrapper-level geometry added around the base optimizer.

5.5.2 LMO-Driven Four-Axis Interpretation

T5 exposes the boundary between the LMO direction coordinate and the post-direction geometry of an optimizer. The LMO view explains how a base direction is selected under a norm constraint. T5 asks whether that direction should be evaluated at a different point, clipped by curvature, filtered by alignment, or rescaled by parameter-group geometry before it is written back. In four-axis notation, the base optimizer first supplies

$$((B_a, B_u), \psi_{\text{base}}, \widehat{H}_t, \alpha, \widehat{g}_t, \mathcal{R}), \quad (85)$$

and T5 appends an outer operator to the resulting step. For methods whose effective gradient is unchanged, Eq. (84) reduces to

$$\Delta_t^{\text{base}} = \mathcal{U}_{\text{base}}(g_t, \mathcal{S}_t), \quad \Delta_t = \mathcal{G}_t(\Delta_t^{\text{base}}, g_t, \theta_t), \quad \theta_{t+1} = \theta_t - \eta_t \Delta_t. \quad (86)$$

Here $\mathcal{U}_{\text{base}}$ may be SGD, AdamW, Lion, Muon, or another optimizer. For most T5.3 and T5.4 methods, the base optimizer’s four-axis coordinates remain intact, and the T5 mechanism is the additional S5 map \mathcal{G}_t .

SAM is different because it changes the point at which the gradient is measured. Its local objective can be written as

$$\min_{\theta} \max_{\|\epsilon\| \leq \rho} \mathcal{L}(\theta + \epsilon), \quad \epsilon_t \approx \rho \frac{g_t}{\|g_t\|_2}. \quad (87)$$

The update then uses $\nabla \mathcal{L}(\theta_t + \epsilon_t)$ in place of the ordinary mini-batch gradient. This makes SAM an S0/S5 wrapper, where the inner ascent direction is a local geometric probe, while the outer step can still be executed by SGD, AdamW, or another base optimizer. The price is the second forward-backward pass needed to evaluate the perturbed gradient.

Diagonal-curvature methods fit more directly into Axes II and III. Sophia-H uses a stochastic Hessian-vector product to estimate a diagonal curvature proxy, while Sophia-G uses a cheaper gradient-based proxy. Both use clipping to avoid unconstrained Newton-like steps [65]. In schematic form,

$$h_t = \beta_2 h_{t-1} + (1 - \beta_2) \widehat{\text{diag}}(H_t), \quad \Delta_t = \text{clip}\left(\frac{m_t}{\gamma h_t + \epsilon}, -1, 1\right). \quad (88)$$

AdaHessian is the earlier diagonal-Hessian route, using Hutchinson-style estimation and Hessian-powered adaptive scaling [123]. Compared with AdamW, T5.2 therefore changes both the curvature estimator and the final direction function.

Post-processing and layer-wise trust-region methods are simpler in the four-axis view but important in practice. A cautious filter can be expressed as

$$\mathcal{G}^{\text{cautious}}(\Delta, g) = \Delta \odot \mathbf{1}[\Delta \odot g > 0], \quad (89)$$

up to the sign convention used for Δ . The key property is that only coordinates whose proposed update agrees with the instantaneous gradient are kept [64]. A LAMB-style trust ratio instead rescales the whole layer:

$$\Delta_t^{(l)} = \phi_t^{(l)} \Delta_{t, \text{Adam}}^{(l)}, \quad \phi_t^{(l)} = \frac{\|\theta_t^{(l)}\|_2}{\|\Delta_{t, \text{Adam}}^{(l)}\|_2 + \epsilon}. \quad (90)$$

Both operations illustrate the same principle, namely that T5 often leaves the base direction geometry untouched, then constrains which parts of that direction are written into the parameters and at what group-level scale.

5.5.3 Representative Methods

The following discussion follows the T5.1–T5.4 subclass order introduced above. Within each subclass, representative methods are grouped by the local geometry operation they modify.

Adversarial Perturbation (SAM Family). The first branch changes the gradient evaluation point. At the survey level, SAM-style methods can be written as

$$\epsilon_t = \mathcal{A}_t(g_t, \theta_t; \rho), \quad \tilde{g}_t = \nabla_{\theta} \mathcal{L}(\theta_t + \epsilon_t), \quad \Delta_t = \mathcal{U}_{\text{base}}(\tilde{g}_t, \mathcal{S}_t), \quad (91)$$

where \mathcal{A}_t specifies the perturbation rule and $\mathcal{U}_{\text{base}}$ can be SGD, AdamW, or another first-order base optimizer.

- **Min–max anchor.** SAM instantiates \mathcal{A}_t by the approximate adversarial perturbation in Eq. (87), then updates with the perturbed gradient [32]. This directly connects optimization to flatness-motivated generalization, but it also changes the cost model, because without approximation or reuse, one step requires two sequential forward-backward passes.
- **Perturbation geometry and sharpness objective.** ASAM changes the neighborhood geometry to reduce sensitivity to parameter rescaling [57]. GSAM introduces a surrogate-gap objective and direction decomposition to balance loss decrease and sharpness reduction [142]. WSAM treats weighted sharpness as a regularization term [129]. bSAM links the SAM objective to a Bayesian relaxation and motivates Adam-like uncertainty-aware variants [82].
- **Perturbation frequency and signal composition.** LookSAM targets the extra-gradient bottleneck by periodically refreshing or reusing the ascent direction [69]. FriendlySAM separates full-gradient and stochastic-gradient-noise components in the perturbation signal [61]. GCSAM combines the perturbation route with gradient centralization before the ascent step [39].

The common thread is perturbed-gradient evaluation. Claims about this branch should therefore be read through the matched-compute lens: improvements under a fixed number of tokens do not automatically imply improvements under a fixed wall-clock or accelerator budget.

Diagonal Hessian Estimation. The second branch replaces AdamW’s squared-gradient denominator with a more explicit diagonal curvature proxy. A compact template is

$$q_t \approx \widehat{\text{diag}}(H_t) \quad \text{or} \quad \widehat{\text{diag}}(G_t^{\text{GN}}), \quad (92)$$

$$h_t = \beta_2 h_{t-1} + (1 - \beta_2) q_t, \quad \Delta_t = \Pi_{\gamma} \left(\frac{m_t}{h_t + \epsilon} \right), \quad (93)$$

where Π_{γ} denotes a clipping or trust-region map that prevents small or noisy curvature estimates from producing unbounded Newton-like coordinates.

- **LLM-oriented clipped curvature.** Sophia is the main representative method for LLM pretraining. Sophia-H estimates curvature with a stochastic Hessian-vector product, whereas Sophia-G uses a cheaper gradient-based proxy. Both combine the proxy with a clipped coordinate-wise update [65].
- **Diagonal-Hessian predecessor.** AdaHessian uses randomized Hessian-vector products to estimate diagonal curvature and smooths that estimate before applying Hessian-powered adaptive scaling [123]. It establishes the diagonal-Hessian route, but its target regime predates current LLM pretraining protocols.

T5.2 is adjacent to both T1 and T2 but distinct from each. It differs from T1 because its denominator is intended to approximate Hessian or Gauss–Newton curvature. It differs from T2 because it remains diagonal. Benchmark reports should therefore expose Hessian-estimation cadence, HVP batch, Sophia-H versus Sophia-G choice, clipping parameters, and mixed-precision behavior.

Update Post-Processing and Selective Filtering. The third branch acts after a base direction has been formed. The taxonomy figure lists methods whose surface forms differ substantially, but the common mechanism is an additional operator between the base optimizer and parameter writeback. At this level, the branch can be summarized as

$$\bar{\Delta}_t = \Pi_t(\Delta_t^{\text{base}}, g_t, \theta_t), \quad M_t = \mathcal{M}_t(\bar{\Delta}_t, g_t, \theta_t, \mathcal{S}_t), \quad \Delta_t = M_t \odot \bar{\Delta}_t, \quad (94)$$

where Π_t may centralize, project, normalize, or stabilize the candidate update, and M_t is a coordinate mask or selection weight. The all-ones mask recovers projection-only methods. This template deliberately separates post-processing from base-direction construction, because Δ_t^{base} may come from AdamW, Lion, Muon, or another optimizer, while the T5.3 contribution is the subsequent geometric test, projection, norm control, or selection policy.

- **Projection and radial control.** Gradient Centralization subtracts the mean from gradient vectors or convolutional kernels, placing the update in a zero-mean subspace that can be attached to SGD, Adam, or related optimizers [124]. AdamP addresses a different geometric failure mode by removing radial components for scale-invariant weights, so that accumulated momentum does not mainly increase parameter norms [42]. Both methods leave the base optimizer recognizable, and their contribution is the projection Π_t before writeback.
- **Stabilized writeback and norm control.** StableAdamW analyzes loss spikes caused by unstable AdamW-style update magnitudes and motivates stabilized denominators or AdamW–AdaFactor hybrids [114]. The Norm Loss and Stable WD entries in Figure 13 should be read as related S5 regularization components from the same stability-oriented design space. Their role in this taxonomy is to expose norm and decay control as writeback mechanisms that can change stability without changing the moment estimator.
- **Direction consistency and magnitude separation.** Cautious Optimizers apply the mask in Eq. (89) to a proposed update, keeping coordinates only when the update and instantaneous gradient agree under the paper’s sign convention [64]. This is why Cautious AdamW (C-AdamW) and Cautious Lion (C-Lion) share the same T5.3 label even though their base directions belong to T1 and T3, respectively. Grams makes a complementary separation, where the current gradient supplies direction, while momentum mainly supplies adaptive magnitude scaling [15].
- **Spike-aware and selective-update policies.** SPAM identifies gradient spikes in LLM training as a stability bottleneck and combines spike-aware clipping, momentum reset, and sparse momentum behavior [44]. StableSPAM broadens this idea into norm-stabilized writeback, keeping the instantaneous gradient direction while replacing unstable update magnitudes with running norm statistics [43]. Magma demonstrates that random or momentum-aligned masks can be effective when applied to adaptive optimizer updates [47], whereas MGUP assigns larger steps to momentum-gradient-aligned coordinates and smaller nonzero steps elsewhere [16].

The common thread is that T5.3 filters operate on gradients or candidate updates after the base optimizer’s core direction has been selected. This also fixes the boundary with T3. Sign methods define the base direction itself, whereas T5.3 methods accept, reject, rescale, or regularize an already computed direction. Consequently, a Lion wrapper with a cautious mask belongs to T5.3 as a wrapper-level contribution, while Lion itself remains T3.

Layer-Wise Trust-Region Scaling. The fourth branch uses parameter-group geometry to determine the step scale. For a layer or parameter group l , the representative form is

$$r_t^{(l)} = \frac{\|\theta_t^{(l)}\|_2}{\|\Delta_{t,\text{base}}^{(l)}\|_2 + \epsilon}, \quad \Delta_t^{(l)} = \Psi(r_t^{(l)}) \Delta_{t,\text{base}}^{(l)}, \quad (95)$$

$$g_t^{(l)} \leftarrow g_t^{(l)} \min\left(1, \frac{\tau \|\theta_t^{(l)}\|_2}{\|g_t^{(l)}\|_2 + \epsilon}\right), \quad (96)$$

where the first line is a trust-ratio update and the second line is an adaptive clipping rule.

- **Trust-ratio update.** LAMB first forms an Adam-style update and then rescales it by the layer-wise ratio in Eq. (90) [125]. Its contribution is the S1/S5 layer-wise grouping and trust-ratio writeback used for large-batch training.
- **Parameter-relative clipping.** Adaptive Gradient Clipping clips a layer or unit when the gradient norm is too large relative to the parameter norm [14]. Unlike fixed global clipping, the threshold scales with the receiving parameter group.

Layer-wise trust-region methods are syntactically easy to combine with Adam-style bases, but their behavior depends on parameter-group conventions. Benchmarks should state which tensors are excluded, how zero or near-zero norms are handled, whether trust ratios are clipped, and whether the ratio is applied before or after weight decay and global clipping.

5.5.4 Effect-Target Assessment

T5 acts on the geometry of the candidate step rather than on the base optimizer alone. The expected benefit is therefore stability or generalization: SAM-style perturbations seek flatter neighborhoods, diagonal curvature methods clip steps by local curvature, post-update filters suppress harmful components, and layer-wise trust ratios control scale mismatch across parameter groups. Each mechanism also adds a protocol-dependent cost. SAM spends extra forward-backward work [32]; Sophia-style updates rely on curvature proxies and clipping choices [65]; LAMB-style trust ratios depend on layer norms and excluded tensors [125]. Table 12 summarizes the mechanism-derived performance priors.

The distinction between mechanism and observed effect is especially important for this family. A method belongs to T5 because it imposes a geometric constraint; it need not improve generalization in every benchmark. Conversely, a T1 or T2 optimizer can be stable without becoming T5. Budgeted optimizer studies such as Schlotthauer et al. [96] make this point concrete: extra computation can

Table 12: Mechanism-informed effect assessment for T5 subclasses. The entries are design priors for benchmark planning, not empirical conclusions.

Primary target	Likely cost or failure mode	Benchmark focus
T5: Curvature-aware and geometric regularization		
T5.1 Adversarial perturbation (SAM family)		
O6 generalization, O4 flatness	Extra forward-backward pass, radius sensitivity, wall-clock loss	Matched-token vs. matched-compute curves, radius and frequency, downstream evaluation
T5.2 Diagonal Hessian estimation		
O1 convergence, O4 stability via clipped curvature	HVP overhead, clipping sensitivity, stale curvature	Estimation cadence, Sophia-H vs. Sophia-G, clipping rule
T5.3 Update post-processing and selective filtering		
O4 stability, O5 tuning width	May drop useful descent components, extra hyperparameters	Same base with/without filter, kept-coordinate ratio, spike rate
T5.4 Layer-wise trust-region scaling		
O4/O5 under large batch and heterogeneous layers	Trust-ratio instability at small norms, exclusion sensitivity	Layer-wise norms, excluded tensors, clipping order, large-batch scaling

change the apparent ranking if the comparison is made at fixed steps rather than fixed compute. The benchmark summary in Sec. 6.2.8 is consistent with this caution: T5 methods are competitive in limited regimes, but they do not show a uniform advantage under the current LLM benchmark.

6 Benchmark Study

This section presents a mechanism-aware benchmark of representative optimizers for LLM pretraining. Rather than treating the benchmark as a standalone leaderboard, we use the framework developed in the preceding sections—the universal meta-pipeline, the LMO-driven four-axis decomposition, and the dual-dimension taxonomy—to organize and interpret the empirical results. Each experiment is linked to a concrete framework question: which optimizer families perform well under controlled short-context pretraining, which quality–efficiency trade-offs emerge across optimization quality, runtime, and memory cost (O1–O3), whether short-context advantages transfer to long-context and cross-architecture settings (O6), and how training dynamics and hyperparameter perturbations reveal additional stability and robustness properties (O4–O5). We further use Muon as a representative matrix-structured optimizer to study how its sub-operations compose across scale and architecture.

Compared with existing LLM-pretraining optimizer benchmarks (e.g., *Fantastic Pretraining Optimizers* [113], *Benchmarking Optimizers for LLM Pretraining* [97]), our benchmark emphasizes three aspects. First, results are analyzed not only at the optimizer level, but also at the family and axis levels, so that empirical patterns can be mapped back to the methodological taxonomy. Second, we evaluate optimizers under a multi-objective protocol: final quality is measured by perplexity, Stage 2 additionally reports downstream Commonsense Reasoning average accuracy (CS Avg.), efficiency is measured by per-step runtime and optimizer-state memory, stability is analyzed through gradient-norm dynamics, robustness is probed by learning-rate perturbation, and generalization is evaluated by cross-scenario transfer. Third, we conduct a mechanistic ablation of Muon to examine how matrix-structured optimizer components—orthogonalization, scaling, momentum placement, and finalization—interact. In this way, the benchmark both evaluates practical optimizer choices and provides empirical feedback on the proposed framework.

6.1 Experimental Setup

Optimizer selection and taxonomy coverage. We instantiate the taxonomy by selecting 24 representative optimizers spanning all five methodological families (T1–T5) and the major regions of the four-axis coordinate space. Their four-axis coordinates are listed in Table 5 (Section 3.2.2), which places each optimizer in its family and records its update domain, state estimator, geometry-and-precondition operator, and finalization. This makes explicit that our optimizer set is a systematic coverage of the classification space.

Training protocol. Our evaluation comprises two complementary stages. Stage 1 sweeps all optimizers on C4 [90] under the LLaMA architecture at sequence length 256, across four model scales—60M, 130M, 350M, and 1B (trained for 10k, 20k, 60k, and 100k steps, respectively)—using final C4 validation perplexity as the quality metric. Stage 2 transfers the stronger Stage-1 optimizers to the higher-quality FineWeb-Edu corpus [86, 49] with long 32k sequences, at 340M and 1B (~30k steps), and across four architectures—Transformer++ [120] (standard attention) and three linear-attention variants (Gated DeltaNet [122], DeltaNet [121], GLA [120])—to probe portability across dataset, sequence length, and architecture. We weight the 350M and 1B results most heavily, as small-scale rankings are unreliable predictors of behavior at scale. To ensure that observed differences genuinely stem from the optimizers themselves, we adopt a strict *controlled-variable* principle: within each stage, only optimizer-related hyperparameters are tuned (betas, eps, 1r, and method-specific knobs such as APOLLO’s projection

rank and projection interval T), while all architectural, data, and schedule settings are held fixed across optimizers.

Stage-dependent regularization. The two S5 (Update Finalization) operations of the meta-pipeline—decoupled weight decay and gradient clipping—are treated differently across the two stages, by design. In Stage 1 both are *disabled*, so that the comparison isolates the S2/S3 machinery that distinguishes one family from another, and separates it from a generic finalization-stage regularizer. In Stage 2 both are *enabled* identically for all optimizers, to measure generalization under a realistic, production-style recipe. This also lets us distinguish whether an optimizer’s advantage is intrinsic to its S2/S3 design (surviving into the regularized regime) or merely an artifact of the unregularized Stage-1 setting.

Evaluation metrics (mapped to O1–O6). **O1 (optimization quality):** C4 validation PPL in Stage 1, while Stage 2 uses WikiText [79] test PPL and downstream Commonsense Reasoning average accuracy (CS Avg.). CS Avg. is evaluated with lm-eval-harness [34] and computed over ten tasks/splits: ARC-Easy, ARC-Challenge, HellaSwag, WinoGrande, PIQA, OpenBookQA, BoolQ, COPA, LAMBADA-OpenAI, and SciQ [21, 131, 94, 13, 80, 20, 92, 85, 112]. **O2 (per-step compute):** isolated wall-clock optimizer runtime per step (T , ms). **O3 (memory):** isolated optimizer-state memory (Mem, GB), excluding model parameters, activations, and gradients. **O4 (training stability):** long-context gradient-norm dynamics, mainly post-warmup GNormCV, with spike and NaN/Inf diagnostics. **O5 (hyperparameter robustness):** learning-rate perturbation around the tuned learning rate, using 1/5 and $5\times$ perturbations. **O6 (generalization):** cross-scenario transfer across dataset, context length, scale, and architecture, summarized by rank stability and sequence-length sensitivity. These measurements support the optimizer-level and family-level O1–O6 assessment below.

6.2 Results and Analysis

6.2.1 Stage 1: Broad Screening on C4

We first conduct a broad screening of all 24 optimizers on C4 under the LLaMA architecture. This stage is designed as a controlled short-context comparison, where the goal is to evaluate three directly measured quantities: validation perplexity (PPL), optimizer-state memory (Mem), and per-step optimizer runtime (T). These three metrics correspond to optimization quality (O1), per-step compute (O2), and memory efficiency (O3).

Table 13 reports the results at 60M, 130M, 350M, and 1B. Optimizers are grouped by methodological family (T1–T5) and sorted by 1B PPL within each family. This layout allows us to compare both individual optimizers and family-level tendencies without turning the table into a flat leaderboard.

Quality. At the 1B scale, the best PPL is achieved by APOLLO (13.53), followed by a group of matrix-structured methods, including MARS-Shampoo (13.72), Muon (13.72), and RMNP (13.87). This shows that the strongest short-context optimization quality is distributed across multiple families, because state-compressed optimization and matrix-structured optimization both produce highly competitive points. At smaller scales, however, the ranking is less stable. Muon leads at 60M and 130M, whereas APOLLO becomes strongest only at 350M and 1B. Therefore, Stage 1 already suggests that optimizer quality is scale-dependent and should be evaluated across multiple scales.

Runtime. The runtime column shows a different pattern. Lion is the fastest method at 350M and 1B, while AdamW remains one of the cheapest practical baselines. Several quality-oriented matrix methods are much more expensive: SOAP, Muon, MARS-Shampoo, and Shampoo¹ incur substantial per-step overhead due to matrix-level transformations or preconditioning. RMNP is the main exception

¹Our Shampoo implementation follows Meta’s [optimizers](#) library, incorporating the fix discussed in [this issue](#).

Table 13: **Stage-1 screening on C4 (LLaMA, seq. 256)**. C4 validation PPL, optimizer-state memory (Mem), and per-step runtime (T) at four scales; lower is better. Grouped by family, sorted by 1B PPL.

Optimizer	Venue	60M			130M			350M			1B		
		PPL ↓	Mem GB↓	T ms↓	PPL ↓	Mem GB↓	T ms↓	PPL ↓	Mem GB↓	T ms↓	PPL ↓	Mem GB↓	T ms↓
<i>T1: Element-wise adaptive moment and scalar control</i>													
Adan	TPAMI'24	30.25	0.433	2.32	22.84	1.000	4.72	17.29	2.742	12.06	14.35	9.977	39.67
RAdam	ICLR'20	30.12	0.217	1.53	23.22	0.500	3.07	17.34	1.371	7.64	14.47	4.989	23.79
AdamW	ICLR'19	30.08	0.217	1.14	23.18	0.500	2.31	17.78	1.371	5.97	14.48	4.989	18.62
NAdam	ICLR'16	33.72	0.217	3.45	24.51	0.500	4.93	17.90	1.371	9.96	14.67	4.989	20.91
MARS-AdamW	ICML'25	30.01	0.325	7.62	22.86	0.750	11.05	16.95	2.057	22.12	14.90	7.483	34.70
Prodigy	ICML'24	33.44	0.433	8.36	24.13	1.000	12.29	18.27	2.742	24.30	15.61	9.977	36.78
AdaBelief	NeurIPS'20	30.08	0.433	5.76	23.45	1.000	8.55	17.61	2.742	19.10	16.79	9.977	55.48
<i>T2: Matrix-level structural methods</i>													
MARS-Shampoo	ICML'25	30.03	0.325	26.27	22.56	0.750	37.94	16.82	2.057	78.71	13.72	7.483	513.7
Muon	arXiv'25	28.26	0.109	21.01	21.81	0.250	30.48	16.60	0.686	61.66	13.72	2.495	379.0
RMNP	ICML'26	29.88	0.109	3.26	22.54	0.250	4.63	16.85	0.686	9.32	13.87	2.495	16.94
SOAP	ICLR'25	29.47	0.731	50.58	22.67	2.214	110.4	17.14	7.465	302.5	14.04	29.299	1371.5
GaLore	ICML'24	34.56	0.062	4.21	25.32	0.199	5.88	19.18	0.426	11.85	14.29	0.790	15.29
Shampoo	ICML'18	30.22	0.217	22.36	22.56	0.500	33.27	17.03	1.371	66.05	14.29	4.989	389.4
<i>T3: Discretization and directional quantization</i>													
MARS-Lion	ICML'25	32.41	0.325	5.72	25.68	0.750	8.49	18.78	2.057	17.11	15.73	7.483	24.77
Lion	NeurIPS'23	35.94	0.109	2.07	25.56	0.250	3.01	19.30	0.686	5.80	17.02	2.494	12.48
<i>T4: State compression and structural aggregation</i>													
APOLLO	MLSys'25	30.86	0.062	8.62	22.74	0.149	12.65	16.43	0.426	26.21	13.53	0.790	28.65
Conda	arXiv'25	28.65	0.245	4.88	21.91	0.595	7.11	16.45	1.703	13.90	14.25	6.317	62.33
8-bit Adam	ICLR'22	30.46	0.110	4.11	23.30	0.254	7.27	17.67	0.697	16.89	14.53	2.534	42.38
CAME	ACL'23	31.40	0.218	14.99	23.79	0.502	21.76	17.60	1.376	44.89	14.53	4.997	87.46
AdaFactor	ICML'18	30.00	0.001	9.90	22.94	0.002	14.63	17.85	0.003	29.70	14.92	0.004	56.46
Adam-mini	ICLR'25	30.50	0.109	5.68	23.62	0.251	8.31	18.12	0.686	16.68	15.51	2.495	20.81
<i>T5: Curvature-aware and geometric regularization</i>													
AdamP	ICLR'21	30.21	0.217	12.82	23.07	0.500	19.13	17.39	1.371	39.98	14.57	4.989	64.69
LAMB	ICLR'20	30.03	0.217	9.14	23.40	0.500	13.17	17.25	1.371	26.62	16.09	4.989	44.18
Sophia	ICLR'24	36.27	0.217	3.92	25.76	0.500	5.66	18.86	1.371	11.06	16.45	4.989	20.05

among matrix-structured optimizers, achieving strong PPL while keeping runtime close to lightweight methods. Thus, Stage 1 reveals a clear separation between heavy matrix-structured optimizers and lightweight approximations.

Optimizer-state memory. The lowest-memory region is mostly occupied by state-compressed or subspace-based methods. AdaFactor has the lowest optimizer-state memory at all scales, while APOLLO and GaLore also use far less memory than AdamW at the 1B scale. However, the lowest memory does not necessarily imply the best quality. AdaFactor is extremely memory-efficient but only moderate in PPL. APOLLO is the most attractive Stage 1 memory point because it combines low memory with the best 1B PPL, but whether this advantage transfers beyond short-context C4 training must be tested separately.

Stage 1 takeaway. Short-context screening reveals different objective frontiers across T-families, and a universal winner does not exist. T4 shows the strongest advantage when memory efficiency is prioritized, T2 contributes the main high-quality and structured-update candidates, and T1 remains the most reliable balanced reference. Even in the same C4 short-context setting, different

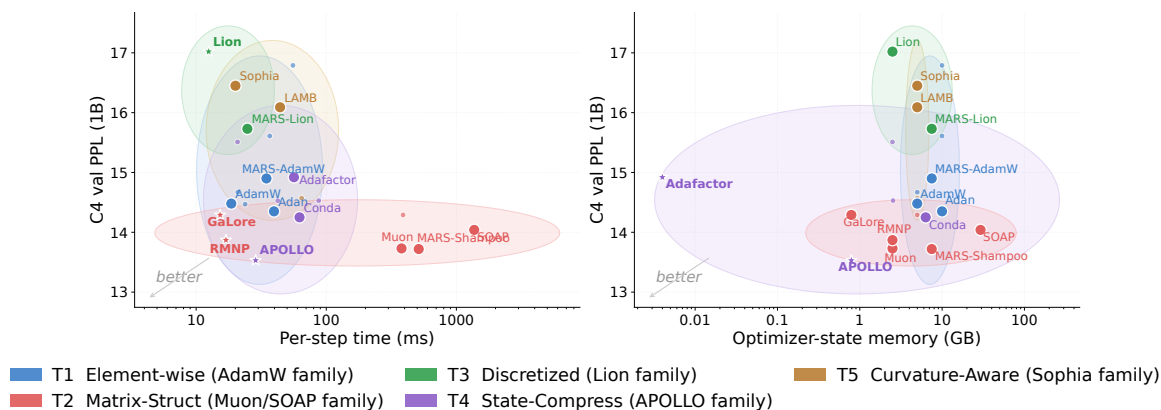


Figure 14: **Stage-1 Pareto frontiers (1B)**. PPL vs. per-step runtime (left) and vs. optimizer-state memory (right); lower-left is better. Colors denote families, stars mark frontier members.

families therefore occupy different favorable regions in quality, runtime, and memory. Optimizer choice is consequently objective-dependent.

6.2.2 Stage 1 Pareto Analysis over PPL, Runtime, and Memory

The Stage 1 results are inherently multi-objective. A method with lower PPL may become unattractive if it requires substantially higher runtime or optimizer-state memory, whereas a highly efficient method may be unusable if its quality degradation is too large. We therefore analyze the short-context C4 results through Pareto frontiers over the three directly measured objectives, namely optimization quality (O1), per-step compute (O2), and optimizer-state memory (O3).

PPL–runtime and PPL–memory frontiers. We plot two Pareto views at the 1B scale: PPL versus per-step optimizer runtime, and PPL versus optimizer-state memory. An optimizer is Pareto-optimal if no other optimizer achieves both lower PPL and lower cost along the corresponding efficiency axis.

Figure 14 shows that the runtime frontier is not occupied by the heaviest quality-oriented methods. Lion is the fastest point, but its PPL is too high to make it a strong overall choice. GaLore is also efficient in runtime, but its quality remains behind the best optimizers. RMNP occupies the most important middle region, where it is much faster than heavy matrix-structured methods while still achieving strong PPL. APOLLO appears as the best short-context quality point and remains non-dominated in runtime.

This pattern separates matrix-structured methods into two regimes. SOAP, Muon, MARS-Shampoo, and Shampoo improve quality through matrix-level operations or preconditioning, but they pay substantial runtime overhead. RMNP, in contrast, retains a large part of the matrix-structured quality benefit while staying close to the efficient frontier. It therefore represents the clearest quality–runtime compromise among matrix-structured methods in Stage 1.

The memory frontier is more concentrated. AdaFactor achieves the smallest optimizer-state memory, but its PPL is only moderate. APOLLO is the strongest memory-frontier point in Stage 1, achieving the best 1B PPL while using much less optimizer-state memory than AdamW. This result demonstrates the potential of state-compressed optimization under short-context training. However, it should be read as a local Stage 1 optimum.

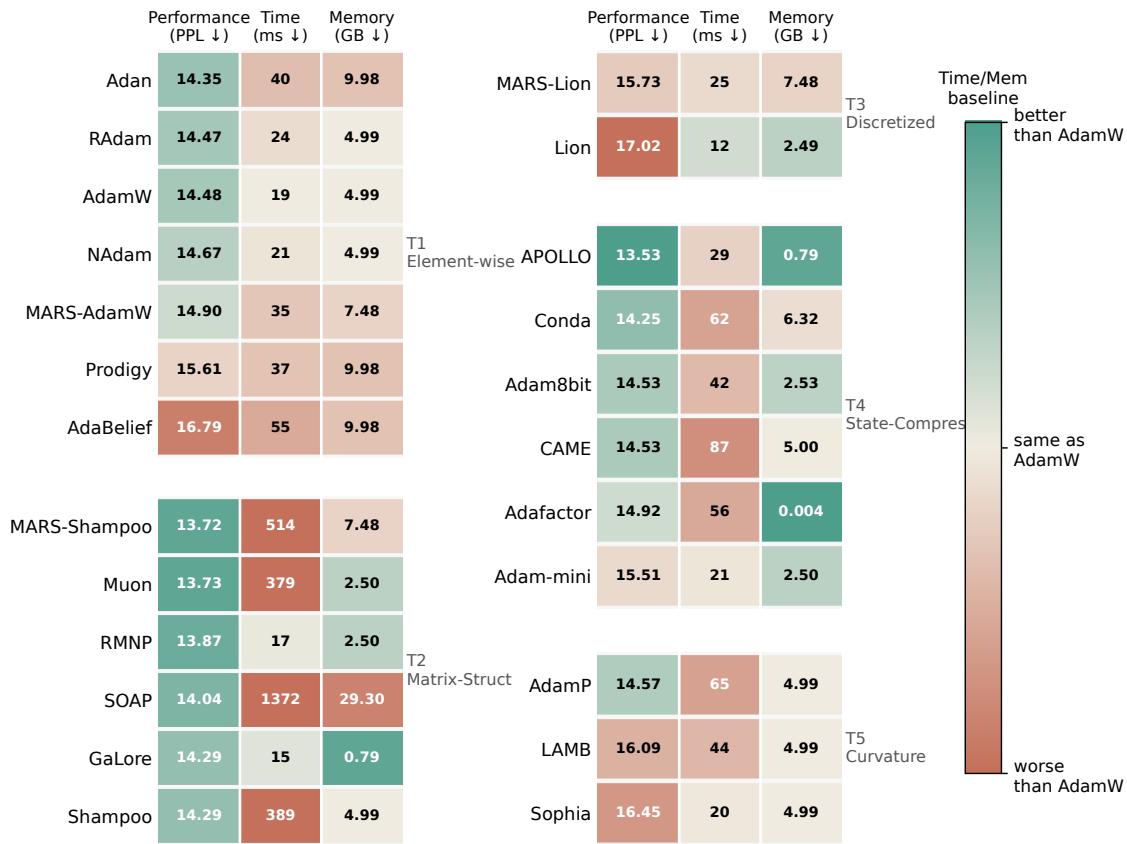


Figure 15: **Optimizer-level heatmap of the three Stage-1 metrics (1B)**. Rows are grouped by family, and columns are C4 PPL, runtime, and optimizer-state memory. Green is favorable, red unfavorable.

Optimizer-level heatmap. To complement the Pareto plots, Fig. 15 summarizes the three Stage 1 metrics at the 1B scale for all 24 optimizers. This figure keeps the analysis at the optimizer level and shows that even within the same family, methods can occupy very different quality–efficiency regimes.

The heatmap highlights substantial within-family variation. RMNP and SOAP both belong to the matrix-structured family, but RMNP is a balanced method whereas SOAP is a quality-oriented but expensive outlier. APOLLO and AdaFactor both belong to state-compressed optimization, but APOLLO achieves much better PPL whereas AdaFactor is more extreme in memory reduction. Similarly, AdamW and MARS-AdamW belong to the same element-wise family, yet they differ in the quality–runtime balance. Therefore, family labels are useful for organizing the benchmark, but optimizer selection still requires metric-level analysis.

Stage 1 Pareto takeaway. The Pareto frontier should be read as each T-family’s best attainable trade-off. T4 is most competitive when optimizer-state memory is the main constraint, lightweight T2 variants are more attractive when runtime matters, and T1 provides the stable reference region when neither cost dimension dominates. Heavier T2 methods can improve quality, but their benefit must be evaluated together with the runtime and memory cost needed to obtain it.

Table 14: **Stage-2 cross-architecture generalization (FineWeb-Edu, 32k)**. Left block: WikiText test PPL (lower is better). Right block: downstream commonsense-reasoning accuracy (CS Avg, %, average over ten lm-eval-harness tasks; higher is better). Both at 340M and 1B across four architectures. Per-scenario best in green. Absolute PPL is not comparable across architectures; rows are ordered by PPL-based cross-scenario stability. Gray row = AdamW. Note that the best PPL is almost always SOAP, whereas the best CS is spread across SOAP, MARS-AdamW, RMNP, and Muon.

Optimizer	WikiText PPL (↓)								Commonsense Reasoning Avg (↑)							
	Tr++		GDN		Delta		GLA		Tr++		GDN		Delta		GLA	
	340M	1B	340M	1B	340M	1B	340M	1B	340M	1B	340M	1B	340M	1B	340M	1B
<i>T1: Element-wise adaptive moment and scalar control</i>																
MARS-AdamW	24.57	18.94	24.17	20.04	26.79	20.67	28.28	21.89	52.50	57.46	54.91	58.18	51.69	56.80	51.24	55.71
AdamW	24.62	18.90	24.47	20.33	27.16	20.66	28.67	22.06	52.28	56.55	53.67	57.01	51.74	55.56	51.06	56.69
Adan	25.55	19.41	24.78	20.55	27.28	20.88	29.00	22.51	52.48	57.21	52.83	57.93	51.78	56.50	51.01	55.07
<i>T2: Matrix-level structural methods</i>																
SOAP	23.90	18.72	23.85	19.86	26.02	20.38	27.04	20.62	53.75	57.71	54.77	57.22	52.60	56.49	52.21	57.57
RMNP	24.37	19.40	23.65	20.26	26.80	21.06	28.60	22.23	53.35	57.12	54.45	57.30	53.25	57.32	50.72	55.79
Muon	25.05	19.86	24.34	20.32	27.18	21.18	27.47	21.54	53.25	56.36	54.45	57.20	52.00	56.65	52.50	56.85
MARS-Shampoo	26.43	19.74	25.99	24.87	28.26	21.25	29.20	21.53	51.96	57.30	53.37	57.58	51.43	56.74	52.01	57.33
<i>T3: Discretization and directional quantization</i>																
Lion	26.02	20.26	24.76	20.38	28.20	21.44	29.47	22.40	51.07	55.22	53.24	55.74	49.96	54.22	50.14	53.96
MARS-Lion	26.20	21.17	25.24	22.20	28.25	22.72	29.67	23.79	51.61	54.51	52.96	55.50	50.94	53.65	50.69	53.91
<i>T4: State compression and structural aggregation</i>																
Conda	28.30	19.86	26.11	21.07	29.09	21.75	37.38	22.89	51.61	57.24	53.45	57.18	51.46	56.10	48.28	54.95
APOLLO	34.08	25.29	30.36	29.29	34.73	25.58	37.75	27.78	48.19	53.61	50.92	53.73	49.04	53.88	48.38	52.33
<i>T5: Curvature-aware and geometric regularization</i>																
AdamP	24.68	19.04	24.32	20.29	26.77	20.68	28.66	21.86	51.69	56.82	53.82	57.07	51.53	56.73	51.14	55.31

6.2.3 Stage 2: Generalization across Data, Context Length, and Architectures

We migrate the stronger optimizers from Stage 1 to a substantially more demanding regime: the higher-quality FineWeb-Edu corpus, a 32k context length, two model scales (340M and 1B), and four architectures—Transformer++ (standard attention) together with three linear-attention variants (Gated DeltaNet, DeltaNet, GLA). This setting changes three factors at once relative to Stage 1: the data distribution, the sequence length, and the parameter topology induced by the token-mixing architecture.

Because different architectures have different modeling capacity, absolute perplexity is incomparable across them. Comparing raw PPL between, say, Transformer++ and GLA would conflate the optimizer with the architecture. We therefore analyze *within-architecture ranking* and its stability across architectures. For each architecture-scale pair, optimizers are ranked by WikiText test PPL, and an optimizer that holds a similar position everywhere is broadly generalizable, whereas one whose position swings sharply is architecture-sensitive. This rank-based view is the direct empirical proxy for the generalization objective (O6). To check whether the PPL-based picture is consistent with downstream behavior, we additionally report the average Commonsense Reasoning score (CS Avg.) over lm-eval-harness tasks for every scenario. Table 14 gives both PPL and CS Avg. across the eight scenarios. Figure 16 visualizes the resulting within-architecture PPL ranks.

Rank-stability visualization. Figure 16 complements Table 14 by visualizing how optimizer ranks change across the eight architecture-scale scenarios. Panel (a) compares AdamW with other element-wise adaptive methods, showing whether improvements within the AdamW family are stable. Panel (b)

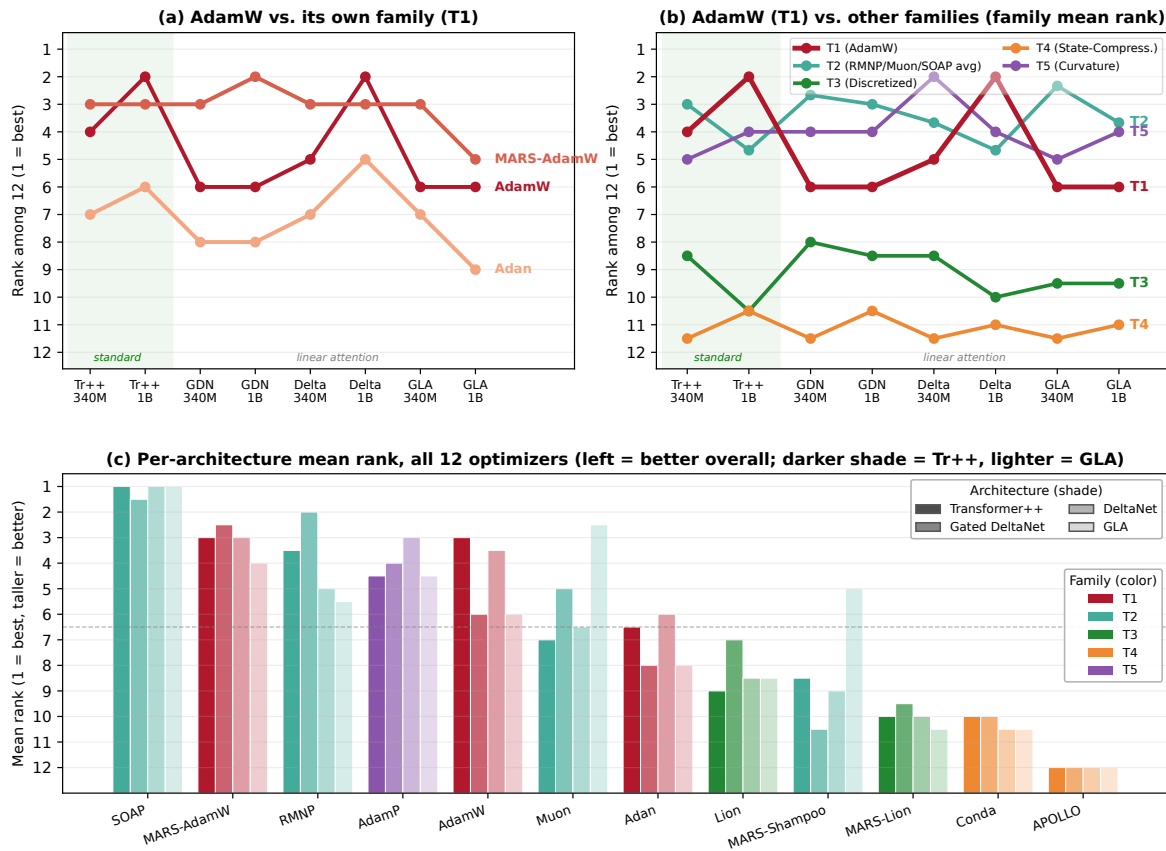


Figure 16: **Cross-scenario rank stability (FineWeb-Edu, 32k)**. Absolute ranks among all twelve optimizers per scenario. (a) AdamW vs. its T1 family; (b) AdamW vs. other families’ mean rank; (c) per-architecture mean rank per optimizer (color = family, hatch = architecture).

aggregates optimizers by family to reveal the broader ranking bands across architectures. Panel (c) returns to the optimizer level and summarizes each method’s per-architecture mean rank, making architecture sensitivity visible within a single optimizer. Together, the table and figure separate three phenomena: consistently transferable methods, methods that are strong only on specific architectures, and methods that systematically fail to transfer.

SOAP is the most stable cross-scenario optimizer. SOAP (T2) holds the top PPL position in seven of the eight scenarios and never leaves the top two, giving it an almost flat top line in Figure 16(b). Its advantage is therefore highly stable across both architecture and scale, which suggests that, in this benchmark, SOAP’s Kronecker or Fisher basis preconditioning transfers across both standard-attention and linear-attention architectures. We treat SOAP as the strongest quality-oriented generalization baseline on perplexity, while noting that its lead becomes less exclusive under CS Avg. and that its runtime and memory costs remain substantial in Stage 1.

MARS-AdamW is the most stable AdamW-style enhancement. Within the element-wise family, MARS-AdamW is consistently ahead of plain AdamW and far ahead of Adan, as panel (a) shows. It also attains the best CS Avg. on both Gated DeltaNet columns of Table 14. This pattern is consistent with the framework interpretation that the STORM-style variance-reduced estimator (Axis II) can improve the gradient signal while largely preserving the AdamW update geometry. This improvement

has a cost. MARS-AdamW introduces additional state and computation, so its runtime and optimizer-state memory exceed AdamW’s in Stage 1. We therefore read it as a stable quality-oriented AdamW extension.

Muon shows architecture-dependent behavior. Muon sits in the middle of the field on standard attention but moves toward the top on GLA, where it also attains the best CS Avg. at 340M. Panel (c) makes the pattern explicit. Among its four architecture-level bars, the GLA bar is the best while the Transformer++ and DeltaNet bars are worse. This trajectory suggests that Muon’s spectral/polar direction geometry (Axis III) interacts with the parameter topology of the target architecture. It also motivates the cross-architecture ablation below, where we test whether Muon’s component-wise gains remain stackable outside the standard Transformer setting.

State-compressed methods generalize worst. The two T4 members sit at the bottom of the table. APOLLO is last or near-last in every one of the eight scenarios under both PPL and CS Avg., despite having been the single best optimizer in the Stage-1 short-context screening. This reversal—from short-context champion to long-context worst—is the sharpest generalization failure in the benchmark, and we isolate its cause next.

CS Avg. corroborates the PPL ranking, with informative exceptions. The CS Avg. results in Table 14 largely track the PPL ordering, but the two views are not identical, and the mismatches are informative. Agreement is strongest at the extremes. APOLLO is last or near-last under CS Avg. in every scenario, confirming that its long-context collapse is not a PPL-only artifact, while SOAP remains in the top tier. The divergences are equally telling. SOAP’s near-exclusive lead on PPL does not fully carry over to CS Avg., where MARS-AdamW tops both Gated DeltaNet columns, RMNP tops both DeltaNet columns, and on Gated-DeltaNet-340M the best PPL and the best CS Avg. belong to different optimizers. In short, even when downstream average accuracy is considered alongside perplexity, the best optimizer remains scenario-dependent.

Stage 2 takeaway. *Long-context generalization is a stress test for T-families, and whether an optimizer generalizes is ultimately determined by the specific optimizer mechanism.* T1 and T2 form the strongest quality bands in the long-context setting, while T4 exposes the clearest transfer boundary from short to long context. At the same time, variation within the same family remains substantial. One representative may transfer well, whereas another can be sensitive to architecture. Generalization should therefore be understood as an interaction between optimizer mechanism and target model topology.

6.2.4 Scenario Sensitivity of Memory-Efficient Optimizers

The Stage-1 screening showed that an aggressive state-compression method, APOLLO, can be the single best optimizer under short-context training, yet Stage 2 showed it generalizing worst under long context. Short-context performance alone therefore overestimates the practical value of such methods. To isolate this effect as much as possible, we conduct a controlled sequence-length ablation that changes exactly one variable: we fix the dataset (C4) and the LLaMA architecture, and vary only the context length from 256 to 32k (Table 15). The short-context points come from the Stage-1 LLaMA setting at sequence length 256, and the long-context points from the same LLaMA architecture on C4 extended to a 32k context length. We compare AdamW (the element-wise baseline), Lion (a sign-based efficient method, T3), and APOLLO (state compression, T4). The question is whether an optimizer’s degradation from short to long context tracks the AdamW baseline or grows disproportionately.

Finding and framework attribution. The result is unambiguous from Table 15. At 256 tokens, APOLLO is the best optimizer in the table (13.53). At 32k, it collapses to 35.40, a degradation of +21.87

PPL, roughly three times the AdamW baseline increase of +7.39. It is the only clear outlier. Lion, by contrast, degrades by +6.29, slightly *less* than AdamW.

The framework explains the contrast through Axis II. APOLLO compresses its optimizer state by random projection into a low-dimensional subspace.

Under long context, the gradient’s effective rank rises and its structure becomes more complex, so a fixed low-dimensional projection discards proportionally more information, and the compression that was nearly lossless at short context becomes lossy at long context. Lion (T3) does not compress state and only discretizes the direction (Axis III), so its degradation tracks AdamW. This turns an isolated empirical surprise into a mechanistic statement, namely that the benefit of aggressive state compression (Axis II) is bounded by the rank and structure of the gradient statistics, and that boundary becomes visible when the context length grows.

Table 15: **Sequence-length effect.** PPL at 256 vs. 32k context, lower is better.

Optimizer	256	32k	Δ
APOLLO	13.53	35.40	+21.87
Muon	13.72	22.54	+8.81
SOAP	14.04	21.62	+7.58
AdamW	14.48	21.87	+7.39
Lion	17.02	23.31	+6.29

A note on matched conditions. The short-context points are taken from the Stage-1 C4 configuration (LLaMA, sequence length 256), and the long-context points from the same LLaMA architecture on C4 extended to a 32k context length. The architecture and dataset are therefore held fixed and context length is the only varied factor. Where training budget or token count differs between the two configurations, the comparison should be read as a qualitative indication of the degradation *trend*, and the reported ranking of degradations (APOLLO \gg Muon \approx SOAP \approx AdamW $>$ Lion) is robust to these differences.

Sequence-length takeaway. *T4 is constrained by the structure and effective rank of long-context gradients.* A T4 optimizer can look highly competitive under short-context training, where compressed states may still preserve the dominant gradient information. As the context length increases, however, the gradient statistics become more complex and the same compression can become lossy. In contrast, T3 methods reduce update complexity without directly compressing optimizer state, making them less exposed to this particular sequence-length failure mode. Short-context quality alone therefore cannot certify the long-context reliability of T4.

6.2.5 Optimizer Robustness Across Vision Backbones

Unlike the language-model experiments where context length is the primary source of variation, the CIFAR100 benchmark fixes the dataset and training protocol while varying the backbone from a CNN (ResNet50 [40]) to a Vision Transformer (DeiT-S [106]) and a MetaFormer architecture [126] (CAFormer-S12 [127]). This setting allows us to isolate whether optimizer improvements transfer across architectural families or are tied to specific gradient structures. The image classification experiments on CIFAR100 follow the settings of BOCB [58].

No optimizer dominates all vision backbones. Table 16 shows that the best optimizer changes across architectures. AdaBelief achieves the highest accuracy of 80.53% on ResNet50, Muon is the strongest optimizer on DeiT-S, achieving 77.38%, and Adan obtains the best result of 84.89% on CAFormer-S12. The identity of the top-performing optimizer therefore depends on the backbone, suggesting that optimizer quality is closely coupled to the specific architecture.

Matrix-structured optimizers favor Transformer architectures. The most notable trend is the performance of Muon. Compared with AdamW, Muon improves DeiT-S by more than five percentage points (77.38% *vs.* 72.15%) while providing only modest gains on ResNet50. Within the four-axis

framework, Muon modifies both the update domain (Axis I) and direction construction (Axis III), preserving matrix-level gradient structure and treating parameters as correlated wholes. This design appears particularly well aligned with the correlated gradients of attention layers, explaining its clear advantage on Transformer-style backbones.

Adaptive moment methods remain the most robust family. Although methods such as Muon achieve the highest peak performance, AdamW, Adan, and AdaBelief consistently remain competitive across all three architectures. In contrast, some efficiency-oriented methods exhibit much stronger backbone sensitivity. The most extreme example is MARS-Lion, whose accuracy drops to 33.70 on DeiT-S despite achieving reasonable results on ResNet50 and CAFormer-S12. This suggests that aggressive approximations in state estimation or direction construction can interact poorly with the more complex gradient geometry of Transformer architectures.

Vision-backbone takeaway. Optimizer performance is strongly architecture-dependent. Matrix-structured methods such as Muon achieve substantial gains on Transformer-style models, while adaptive-moment methods remain the most robust across CNNs, Transformers, and MetaFormers. The large performance variance observed for methods such as MARS-Lion further indicates that single-backbone evaluations can substantially overestimate optimizer generality.

6.2.6 Auxiliary Stability Analysis from Gradient-Norm Dynamics

The preceding analyses cover optimization quality (O1), runtime (O2), memory (O3), and cross-scenario transfer (O6). To evaluate training stability (O4), we analyze the gradient-norm trajectories logged during the FineWeb-Edu long-context runs. Gradient-norm spikes and large gradient-scale fluctuations are increasingly used as direct indicators of training instability in modern LLM pretraining, including gradient-norm statistics, spike diagnostics, and the coefficient of variation (CV) of raw gradient norms [43, 7, 109, 56].

For each run, we compute the coefficient of variation of the gradient norm,

$$GNormCV = \frac{\text{std}(\|g_t\|)}{\text{mean}(\|g_t\|)}, \tag{97}$$

together with auxiliary diagnostics: clipping rate, spike rate, maximum consecutive spike length, tail trend, and NaN/Inf count. We adopt GNormCV as the primary O4 statistic for three reasons. First, it is scale-free and thus comparable across optimizers whose absolute gradient norms differ by orders of magnitude. Second, it captures *relative* volatility while remaining decoupled from absolute magnitude, which suits cross-architecture and cross-scale comparison. Third, it exposes *soft instability*, meaning that a run may complete without any

Table 16: CIFAR100 Top-1 Accuracy (%) across CNN, ViT and MetaFormer architectures.

Optimizer	ResNet50	DeiT-S	CAFormer-S12
<i>T1: Element-wise adaptive moment and scalar control</i>			
AdaGrad	73.30	67.24	38.09
AdaDelta	75.07	65.44	82.08
RMSProp	74.25	70.71	81.83
Adam	74.55	71.04	82.18
AdamW	75.56	72.15	83.60
Adamax	75.21	73.31	82.50
NAdam	74.82	72.75	82.83
RAdam	75.19	72.41	82.35
AdaBelief	80.53	70.66	83.56
Adan	77.08	76.33	84.89
AdaBound	78.11	68.59	82.38
NovoGrad	79.36	73.13	82.98
MARS-AdamW	74.19	71.57	80.48
<i>T2: Matrix-level structural methods</i>			
RMNP	73.39	71.83	82.44
Muon	75.25	77.38	84.43
GaLore	73.53	70.88	82.19
MOGA	63.20	62.48	79.00
<i>T3: Discretization and directional quantization</i>			
MARS-Lion	71.53	33.70	77.02
Lion	75.28	74.57	79.59
<i>T4: State compression and structural aggregation</i>			
AdaFactor	75.41	74.02	82.36
APOLLO	74.09	71.24	82.00
CAME	66.62	71.05	81.83
Conda	73.87	70.76	82.45
<i>T5: Curvature-aware and geometric regularization</i>			
LAMB	77.19	75.39	83.74
AdamP	78.17	71.55	83.40
Sophia	75.19	71.47	82.96



Figure 17: Auxiliary O4 stability analysis from gradient-norm dynamics across architectures. Each cell shows the coefficient of variation of the gradient norm (GNormCV) for one optimizer in one architecture-scale scenario of the FineWeb-Edu long-context benchmark. Lower GNormCV indicates smoother relative gradient-norm dynamics and thus better auxiliary stability. The bar chart on the right reports the mean stability rank across the eight scenarios (lower is better).

NaN/Inf event yet still exhibit highly volatile gradient dynamics. The remaining diagnostics serve to localize the source and persistence of that instability.

Figure 17 shows that O4 gives a different view from final PPL. All statistics are computed on *pre-clip* gradient norms, so that GNormCV reflects each optimizer’s own raw dynamics. Muon attains the best aggregate stability rank, placing first or second in every one of the eight scenarios. This is consistent with its spectral orthogonalization, which decouples the update scale from gradient magnitude and so damps relative gradient-norm fluctuation. RMNP, AdamP, and MARS-AdamW form a moderate band, and AdamW is a reliable reference on the standard- and DeltaNet-style architectures—though, as shown below, no optimizer is immune to architecture-induced volatility.

Completion status does not certify stability. Every summarized run finishes with zero NaN/Inf events, yet GNormCV spans more than two orders of magnitude, from ~ 0.32 to >160 . The conventional “did it diverge?” criterion would rate all of these runs equally stable, whereas GNormCV instead exposes the soft instability they hide. The auxiliary diagnostics pinpoint its source. For SOAP and Conda—and, on two architectures, MARS-Shampoo—the large GNormCV is driven by *rare single-step bursts*. In the affected scenarios the gradient-norm std is large (e.g. SOAP on Transformer++/1B reaches $\text{std} \approx 52$ at $\text{mean} \approx 0.76$) while the spike rate stays below 10^{-3} , the maximum consecutive spike length is 1, and the tail trend is near zero ($|\text{slope}| \sim 10^{-6}$). These are isolated outlier steps that a NaN/Inf check misses but GNormCV makes visible.

Volatility is architecture-driven, and its form matters. Stability is strongly architecture-dependent. On Transformer++, DeltaNet, and Gated DeltaNet, most optimizers keep GNormCV in the 0.3–2 range, and the matrix methods Muon and MARS-Shampoo are often the smoothest. GLA is the clear exception: nearly every optimizer jumps to GNormCV of 10–160, including AdamW (113.7 at 1B) and RMNP (121.8 at 340M). Crucially, these GLA blow-ups again share the single-step-spike signature—spike rate $\sim 10^{-4}$ and maximum consecutive spike = 1—with the tail trend staying flat, so the linear-attention topology amplifies *occasional extreme steps* while the overall training trajectory still converges stably. This mirrors the Stage-2 rank-stability finding, namely that both generalization and stability are shaped by the interaction between optimizer geometry and model architecture.

O4 takeaway. *Training stability must be measured from gradient dynamics, not inferred from whether a run finishes.* T2 can improve gradient-norm smoothness when its matrix-level direction construction regularizes the update geometry, but the same family can also contain methods that produce rare burst-like spikes under certain architectures. Since all tuned runs may finish without NaN/Inf while showing very different GNormCV profiles, stability is a mechanism-level property that must be evaluated directly and cannot be inferred from final PPL or T-family membership.

6.2.7 Auxiliary Learning-Rate Perturbation Robustness

We next probe hyperparameter robustness (O5) through a local learning-rate perturbation test. While O1–O3 are measurable from a single tuned run, O5 asks whether an optimizer remains usable when the learning rate departs from its tuned value—a practical concern in LLM pretraining, where exhaustive retuning is often too expensive when scaling the model, changing the dataset, or transferring to a new architecture.

The test is conducted on the FineWeb-Edu Gated DeltaNet/340M setting. For each optimizer o , let η_o^* denote its tuned learning rate, and evaluate three points, $0.2\eta_o^*$, η_o^* , and $5\eta_o^*$. The sensitivity score s_{LR} is the larger relative WikiText-PPL increase of the two perturbed runs over the tuned run, reported as a percentage. A smaller s_{LR} means a flatter local response and stronger robustness. A perturbed run that diverges or produces an invalid loss is assigned the maximal sensitivity (treated as the most sensitive case), so that instability is penalized and made explicit. We stress that this is a deliberately *local* diagnostic over three points around the tuned value. The $5\times$ point is merely an aggressive local stress test.

Figure 18 shows that tuned quality and learning-rate robustness are distinct. Lion and MARS-Lion have the flattest local response curves ($s_{LR} = 0.7\%$ and 7.7%), consistent with sign-direction methods bounding the per-coordinate step by the learning rate and so absorbing moderate LR misspecification. We read this as local tolerance. The response is flat in part because the fixed-magnitude update keeps quality weak across a wide LR range (cf. Lion’s Stage-1/Stage-2 PPL), so a flat curve here should not be equated with a strong optimizer. Adan, SOAP, AdamP, RMNP, Conda, MARS-AdamW, and Muon form a moderate-sensitivity band, where their degradation stays bounded but shows visible, direction-dependent dependence on the perturbation.

The sensitive group exposes a different failure mode. AdamW, MARS-Shampoo, and APOLLO reach reasonable tuned quality, but their PPL rises sharply under at least one perturbed LR. For AdamW the sensitivity is concentrated on the *over-large* ($5\times$) side, i.e. it remains well-behaved when the LR is reduced but degrades when pushed past its tuned value—so its placement here reflects the aggressive upper stress point. APOLLO is the extreme case, with its response rising steeply at $5\times$, yielding the largest s_{LR} . This is consistent with APOLLO’s broader profile in the benchmark—strong short-context quality and low memory, yet poor long-context transfer and high sensitivity—reinforcing that favorable tuned quality or memory says nothing about behavior under imperfect hyperparameter transfer.

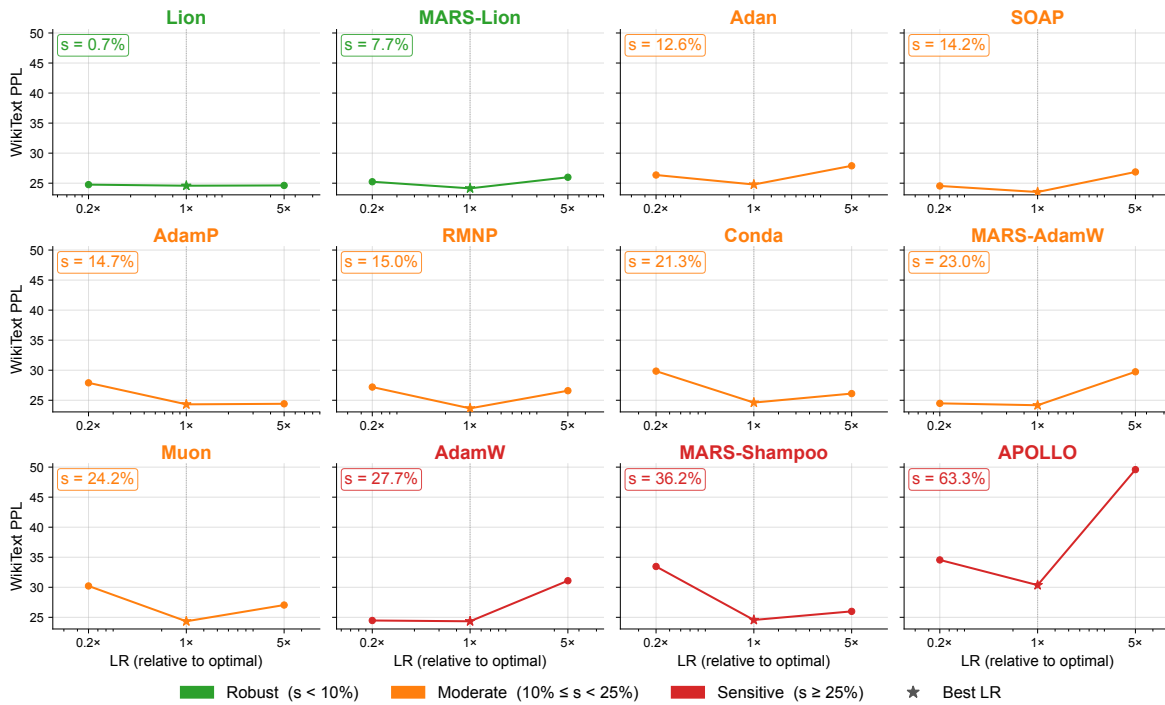


Figure 18: **Auxiliary learning-rate perturbation robustness.** Each panel shows WikiText PPL under $0.2\times$, $1\times$, and $5\times$ the tuned learning rate. The star marks the tuned learning rate. The sensitivity score s_{LR} is shown as s in each panel title and measures the worst relative PPL degradation from the tuned point, where lower is more robust. Green, orange, and red titles indicate robust, moderate, and sensitive learning-rate response regimes.

O5 takeaway. *Learning-rate robustness is not implied by tuned quality.* T3 tends to be locally tolerant to learning-rate perturbation because its direction-bounded updates limit the effect of moderate LR misspecification, but this tolerance can coexist with weaker tuned quality. T1 and T2 usually show a more moderate sensitivity profile, while T4 can be fragile when the tuned learning rate is transferred imperfectly. Thus, a T-family’s best quality or memory profile does not necessarily imply robustness under hyperparameter mismatch.

6.2.8 Family-Level Objective Summary

After Stage 1 analyzes the directly measured quality–efficiency trade-offs, Stage 2 evaluates cross-scenario transfer, and the auxiliary analyses cover training stability and learning-rate perturbation robustness, we summarize the results at the optimizer-family level. This summary connects the empirical benchmark back to the objective-oriented taxonomy. Unlike the Stage 1 Pareto plots, which only cover O1–O3, the family-level view in Figure 19 summarizes the broader objective profile, namely quality, runtime, memory, training stability, hyperparameter robustness, and generalization.

Figure 19 consolidates the preceding evidence. T1 methods form the stable baseline. They are not the strongest in raw PPL, but they remain moderate in runtime and memory, transfer reasonably across architectures, and provide a reliable reference for stability and robustness comparisons. T2 methods provide strong matrix-structured quality and generalization potential, but they are internally heterogeneous, where SOAP gives the strongest long-context quality at high cost, RMNP provides the most balanced quality–efficiency trade-off, and Muon shows the strongest observed gradient-norm



Figure 19: **Family-level objective summary.** Per-family profile over $O1$ – $O6$. $O1$ – $O3$ are directly measured from Stage 1; $O4$ is measured from gradient-norm stability; $O5$ is probed by an auxiliary learning-rate perturbation test; $O6$ is measured through Stage 2 rank stability and sequence-length sensitivity. Green indicates a more favorable profile and red indicates a less favorable profile.

stability profile while remaining architecture-sensitive. $T3$ methods are efficient and locally robust to learning-rate perturbation, but their tuned PPL is generally weaker. $T4$ methods achieve attractive short-context memory efficiency, but their Stage 2 behavior reveals a clear generalization boundary. APOLLO is the most representative case, where a favorable short-context quality–memory trade-off does not transfer reliably to long-context training. $T5$ methods remain competitive only in limited regimes and do not provide a consistent advantage under the current benchmark.

The family-level summary reinforces the main message of the benchmark, namely that optimizer selection is not a single-axis ranking problem. Different families occupy different regions of the $O1$ – $O6$ objective space, and an optimizer that is strong in one objective can be weak in another. Quality, cost, stability, robustness, and transfer must therefore be evaluated jointly. In particular, $O5$ should be interpreted as a local learning-rate robustness diagnostic whose scope is limited to local perturbations of the learning rate.

6.2.9 Tiered Optimizer Summary

Combining the Stage 1 short-context screening, the Stage 2 long-context generalization study, and the sequence-length sensitivity analysis, we organize the evaluated optimizers into three tiers. These three tiers are a grouping from three perspectives that summarizes the overall empirical evidence, namely short-context quality–efficiency behavior, cross-scenario transfer, and mechanistic value for further analysis. Interpreting them as a strict global leaderboard would be misleading.

Tier I: primary candidates. Tier I contains the optimizers that are most important for practical baselines and subsequent mechanistic analysis. AdamW is

Table 17: **Tiered classification of the benchmarked optimizers.**

Tier	Optimizers
Tier I	Muon, RMNP, AdamW
Tier II	MARS-Lion, MARS-Shampoo, APOLLO, Conda, AdamP, MARS-AdamW, SOAP, Adan, Lion
Tier III	RAdam, NAdam, Prodigy, AdaBelief, GaLore, Shampoo, 8-bit Adam, CAME, AdaFactor, Adam-mini, LAMB, Sophia

retained as the default reference because it is stable, efficient, and widely used, even though other methods surpass it in some settings. RMNP is selected as the most balanced matrix-structured optimizer, because it achieves strong quality while avoiding the prohibitive runtime and memory cost of heavier matrix methods. Muon is included because it combines strong Stage 1 performance with a clean matrix-structured mechanism that can be decomposed into orthogonalization, learning-rate scaling, momentum placement, and operator-order choices. Although Muon shows architecture-dependent behavior in Stage 2, this sensitivity is itself mechanistically informative and motivates the ablation study below.

Tier II: scenario-dependent methods. Tier II contains optimizers with clear strengths but stronger dependence on the training regime, context length, architecture, or efficiency budget. SOAP achieves the strongest long-context cross-scenario quality, but its runtime and optimizer-state memory costs make it less attractive as a default choice. APOLLO is the best short-context quality–memory point in Stage 1, but its long-context collapse shows that aggressive state compression does not transfer automatically. MARS-AdamW and AdamP are stable in Stage 2, yet they do not dominate the Stage 1 quality–efficiency frontier. MARS-Shampoo, Conda, Adan, Lion, and MARS-Lion similarly provide useful comparison points, but their advantages are limited by cost, transferability, or final quality. We therefore treat this tier as a set of important conditional baselines whose applicability depends on the specific training scenario.

Tier III: diagnostic failure cases. Tier III contains methods that are weak, dominated, or insufficiently robust under the current benchmark protocol. Some methods retain isolated advantages, where AdaFactor has extremely low optimizer-state memory, GaLore has low runtime and subspace compression, and 8-bit Adam reduces state precision. However, these advantages do not yield a consistently favorable trade-off across quality, efficiency, and transfer. Other methods, such as Sophia, LAMB, Prodigy, RAdam, NAdam, and AdaBelief, do not improve sufficiently over stronger baselines in the evaluated regimes. Their value is mainly diagnostic, because they help identify failure modes associated with direction discretization, noisy curvature estimation, aggressive state compression, or insufficient scaling behavior.

Selection guidance. The tiered summary leads to a constraint-driven view of optimizer selection. For general-purpose LLM pretraining, AdamW should remain the default reference, because although it is not the strongest method in every metric, it is stable, inexpensive, and consistently interpretable across settings. When a better balance between quality and efficiency is required, RMNP is the most attractive alternative in this benchmark. It preserves much of the benefit of matrix-structured optimization while avoiding the extreme runtime and memory overhead of heavier matrix methods.

When final quality is the dominant objective and compute or optimizer-state memory is not the bottleneck, SOAP provides the strongest long-context quality reference. Its Stage 2 rank stability suggests that it transfers well across the tested architectures, but its high cost makes it better suited as a quality ceiling. Muon occupies a different role, namely that it is a strong and interpretable matrix-structured optimizer, but its architecture-dependent behavior suggests that it should be used with awareness of the target model topology.

For memory-constrained short-context training, APOLLO and AdaFactor are useful candidates, but they should be separated carefully. AdaFactor is the safer low-memory baseline with moderate quality, whereas APOLLO is a high-reward but high-risk compressed-state method. It is excellent in the Stage 1 quality–memory trade-off, yet its advantage does not survive the long-context setting. For low-cost exploratory runs, Lion can reduce per-step overhead, but the quality gap should be expected. Overall, the benchmark does not identify a universal best optimizer. It shows that optimizer choice should be made by matching the method’s dominant strength to the binding constraint of the training regime: stability, quality, runtime, memory, or cross-scenario transfer.

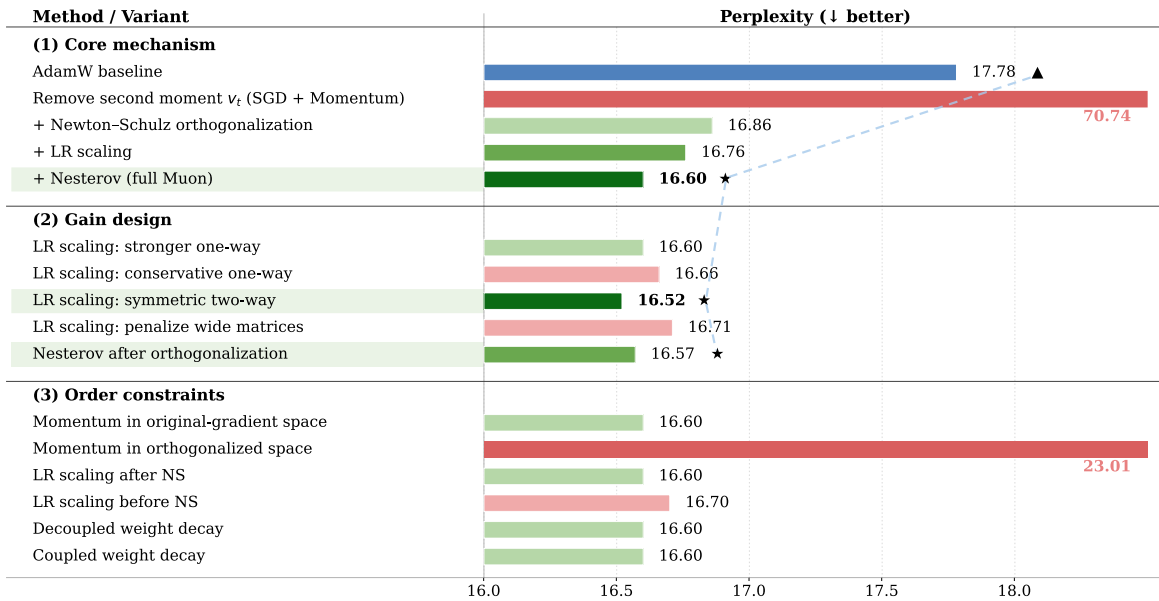


Figure 20: **Mechanistic ablation of Muon (C4, 350M)**. Decomposition into core operations, gain operations, and operator-order constraints, with bars showing absolute PPL (lower is better). The 70.74 bar is truncated off-scale.

Tiered-summary takeaway. Optimizer selection should be matched to the dominant constraint of the training regime. T1 is the safest reference family. T2 provides the strongest quality or stability ceiling when matrix-level cost is acceptable, while lightweight T2 variants offer a more practical balance between quality and efficiency. T3 is useful when runtime or local LR tolerance matters more than peak quality. T4 is attractive mainly under short-context memory pressure, but requires additional long-context validation. Overall, the benchmark supports mechanism-aware optimizer selection.

6.3 Mechanistic Ablation of Muon

The benchmark identifies Muon as a strong and mechanistically clean matrix-structured optimizer. Muon is commonly understood as a momentum-based matrix optimizer whose key operation is Newton–Schulz (NS) orthogonalization [48]. However, this description leaves open three questions: whether NS is truly indispensable, which auxiliary operations provide additional gains, and whether the sub-operations can be reordered freely. We therefore use Muon as a controlled case study for the meta-pipeline view.

6.3.1 Single-scene decomposition on C4-350M

We first perform a controlled decomposition on C4-LLaMA at the 350M scale, matching the Stage 1 screening setting. Figure 20 summarizes the results as absolute validation PPL, where lower is better. The three blocks correspond to core mechanism recovery, gain design, and operator-order constraints.

NS orthogonalization is the core mechanism. The first block shows that simply removing AdamW’s second moment is catastrophic, since PPL increases from 17.78 to 70.74. Adding NS orthogonalization immediately recovers performance to 16.86, already better than AdamW. This identifies NS as Muon’s

Table 18: **Cross-scale and Cross-Architecture Validation for Gain Operations in Muon.** Standard Muon, symmetric two-way LR scaling, post-NS Nesterov, and their combination; lower PPL is better. Gains stack on the standard Transformer but not on Gated DeltaNet.

Scenario	Standard Muon	Symmetric LR Scaling	Post-NS Nesterov	Both combined	Best config.
<i>Standard Transformer: gains are stackable</i>					
C4-LLaMA, 350M	16.60	16.52	16.57	16.51	Both combined
C4-LLaMA, 1B	13.72	13.64	13.64	13.58	Both combined
<i>Linear attention: stacking effect disappears</i>					
FineWeb-Edu 32k, GDN-340M	24.26	24.02	24.12	24.12	Symmetric LR Scaling

core replacement for AdamW-style diagonal adaptive scaling.

Scaling and Nesterov are secondary gains. Once NS orthogonalization is present, LR scaling and Nesterov correction provide smaller but consistent improvements. LR scaling improves PPL from 16.86 to 16.76, and adding Nesterov gives the full Muon result of 16.60. Thus, these operations refine the orthogonalized direction, but they are not responsible for the main recovery from the failed no- v_t variant.

The best gains are geometry-aware. The second block shows that the form of the gain operation matters. Symmetric two-way LR scaling gives the best single-scene result, reaching 16.52, whereas penalizing wide matrices worsens PPL to 16.71. Post-NS Nesterov also improves over the standard ordering, reaching 16.57. These results suggest that gain operations should be designed around the geometry of the NS-orthogonalized direction.

Operator order is constrained. The third block shows that Muon’s operations are not freely permutable. Accumulating momentum in the orthogonalized space degrades PPL to 23.01, whereas accumulating momentum in the original-gradient space keeps PPL at 16.60. Similarly, applying LR scaling before NS worsens PPL to 16.70, indicating that spectral normalization can absorb or distort the intended scale correction. Weight-decay ordering is less important in this specific C4-350M setting, where coupled and decoupled variants are nearly equivalent.

Single-scene Muon takeaway. Muon’s main improvement comes from NS orthogonalization, which replaces AdamW’s diagonal second-moment scaling with a matrix-level direction. LR scaling and Nesterov further refine this direction, but only when placed after the appropriate upstream operations. The ablation therefore supports the meta-pipeline view: Muon changes only a few stages, yet the location and order of those changes are essential.

6.3.2 Cross-scale and cross-architecture validation

The single-scene ablation identifies the core and gain operations, but it does not tell us whether the gain operations transfer. We therefore validate the two best gains—symmetric two-way LR scaling and post-NS Nesterov—across scale and architecture. Table 18 compares standard Muon, each gain alone, and their combination on C4-LLaMA at 350M and 1B, as well as on FineWeb-Edu 32k with Gated DeltaNet at 340M.

On standard Transformer models, the two gains are transferable and partially stackable. At 350M, symmetric LR scaling improves PPL from 16.60 to 16.52, post-NS Nesterov reaches 16.57, and combining both gives 16.51. At 1B, both individual gains reach 13.64, and the combined variant further

improves to 13.58. This indicates that the two gains act through mostly separable mechanisms on standard Transformer architectures.

On Gated DeltaNet, the behavior is different. Both gains remain useful individually, with symmetric LR scaling improving PPL from 24.26 to 24.02, and post-NS Nesterov reaching 24.12. However, their combination no longer improves over the best single gain, remaining at 24.12. This suggests that the orthogonality of optimizer components is architecture-dependent, meaning that operations that are separable on standard Transformers can interact on linear-attention parameter topologies.

Cross-validation takeaway. The Muon gains transfer across scale on standard Transformers, but lose additivity on Gated DeltaNet. Thus, LR scaling and post-NS Nesterov are useful refinements, but their interaction depends on the target architecture. This explains Muon’s role in the benchmark: it is not a universally best optimizer, but it is strong, interpretable, and exposes where matrix-structured optimizer design meets model topology.

7 Discussion

This paper was organized around three questions about where an optimizer acts, why its update takes a particular geometric form, and what training objective it is meant to improve. We answered them through three layers. The first is the meta-pipeline of Section 3.1, the second is the four-axis decomposition of Section 3.2.2, and the third is the dual-dimension taxonomy of Section 4. All three are grounded in the benchmark of Section 6. This section steps back from those instruments and asks what they collectively do and do not establish. We first delimit the scope of the present study (Section 7.1), then use the framework to extract technique-level lessons about benefit, composition, and conflict (Section 7.2), and finally distill the open directions that follow (Section 7.3).

7.1 Limitations

The introduction framed optimizer selection as a jointly empirical, mathematical, and engineering problem. A modern training run is constrained by more than whether an update reduces the loss. Compute, optimizer-state memory, tuning budget, and task diversity all bound it. The literature is also hard to navigate because mechanisms are named locally, empirical claims are protocol-sensitive, and mathematical accounts are fragmented (Section 1.1). Our framework targets exactly these gaps, and the benchmark supplies controlled evidence for them. The same framing, however, makes the boundaries of the current study explicit.

Empirical scope. The empirical study substantiates the framework primarily on language-model pretraining, covering four model scales from 60M to 1B parameters, four architectures spanning standard and linear attention, and context lengths from 256 to 32k tokens. In addition, the benchmark includes a CIFAR100 vision-backbone study across ResNet50, DeiT-S, and CAFormer-S12. This study tests whether optimizer behavior transfers across architecture families within image classification. Thus, claims about *domain-dependent crossings* are supported by the language-modeling regime and by a targeted CIFAR100 cross-architecture check. In future work we will add validation on ImageNet-scale vision and additional modalities, extending these into a full cross-modality conclusion.

Mechanism attribution. Every effect-target assessment in Section 6 is deliberately a mechanism-informed prior. The mechanistic explanations we give are also *qualitative*. They cover APOLLO’s rank-bounded compression, Muon’s interaction with architecture topology, and MARS’s variance reduction on the state estimator while preserving base geometry. We can say *why* an optimizer plausibly behaves as observed. In future work we will develop metrics that quantify these explanations, measuring quantities such as the effective rank of the gradient as context grows, the staleness of a preconditioning

basis, and the fraction of a technique’s benefit that is intrinsic to the algorithm versus induced by the tuning protocol. Such interpretability metrics must be designed and validated carefully, and we will provide a quantitative interpretability evaluation in a subsequent version of this work. For future work, we plan to add heavy-tailed self-regularization indices as training-quality metrics and to evaluate optimizers on downstream commonsense reasoning benchmarks.

Protocol dependence. Our conclusions are tied to a strict controlled-variable protocol, in which only optimizer-related hyperparameters are tuned while architecture, data, and schedule are held fixed. This isolates optimizer mechanism, but it also makes several findings protocol-relative. Many apparent improvements over AdamW shrink or disappear once the baseline is returned. The learning-rate robustness objective (O5) is reported as a *local* diagnostic. The long-context comparison is matched on dataset and architecture family but not on token budget, so it certifies a degradation *trend*. A few memory-efficient methods are drawn from recent preprints whose broader LLM-scale behavior is still being established. Their results should therefore be interpreted under the present protocol and remain preliminary for the method class.

Method coverage. We instantiate 24 representative optimizers chosen to cover the major regions of the four-axis space (Table 5), but the surveyed literature exceeds one hundred methods, and not every axis combination is realized by an existing optimizer or exercised by our benchmark. Consequently, family-level statements should be read as conclusions about the *tested* instances and protocol. This caution is especially important for the claim that curvature-aware and geometry-regularized methods (T5) are competitive only in limited regimes under the current benchmark. These boundaries motivate the technique-level reading and the open directions that follow.

7.2 Technique-Level Lessons

A central payoff of the framework is that it shifts attention from *which optimizer is the best* to a more tractable set of technique-level questions. Which mechanisms carry the gains? Which ones can be stacked? Which ones interfere? The governing principle, established by the meta-pipeline and the cross-dimension analysis (Section 4.4), is one of *locality*. Mechanisms that act on different pipeline stages or different axes tend to compose, whereas mechanisms that contend for the same slot require an explicit ordering and may conflict.

Benefit carriers. Under the tested protocol, the strongest gains are associated with *geometry-sensitive direction maps* (Axis III) and with the *structured state* that feeds them (Axis II). Scalar control tweaks alone contribute little. The Muon ablation makes this concrete. Removing the diagonal second moment alone collapses quality (PPL 17.78 \rightarrow 70.74), whereas replacing it with Newton–Schulz orthogonalization recovers and then surpasses the AdamW baseline (\rightarrow 16.86). This identifies spectral orthogonalization as the indispensable core. Kronecker-factored preconditioning is another strong carrier. SOAP attains the strongest transferable quality profile in Stage 2, with a mean rank near the top across architectures. This comes at the cost of the highest per-step runtime and the highest memory use. Variance reduction in the style of MARS is a genuine, reusable improvement to the state estimator. It improves the gradient signal while preserving the base update geometry, which makes MARS-AdamW the most stable AdamW-style enhancement in Stage 2. The gain comes with extra state and computation, so MARS is better read as a quality-oriented extension. Finally, simple memory techniques that *preserve* geometry, such as row/column factorization (AdaFactor) and low-bit state (8-bit Adam), deliver reliable memory savings without changing the descent direction, which is why they are safe defaults when memory is the binding constraint.

Limited returns. Conversely, several techniques are marginal in the tested regime. Small element-wise refinements of the AdamW template land in the weakest tier for tuned perplexity. These include

early-variance rectification (RAdam), Nesterov lookahead (NAdam), and prediction-error variance (AdaBelief). Automatic step-size tuning (Prodigy) lands in the same tier. This is consistent with their stated targets of robustness or convenience. Diagonal curvature proxies and geometric wrappers (Sophia, LAMB) are likewise weak or only situationally competitive here. They add cost through an extra Hessian-vector product, clipping or trust-ratio parameters, or a second gradient evaluation, yet they do not deliver a consistent quality return under matched tuning. These mechanisms still have value. Their advantage is simply conditional, and the benchmark is meant to expose that condition.

Compatible compositions. Locality predicts, and the survey confirms, several orthogonal compositions. (i) A variance-reduced signal (Axis II) can feed essentially any base direction, because it is largely independent of basis and curvature choice. This is exactly the pattern behind the MARS-AdamW, MARS-Lion, and MARS-Shampoo constructions. (ii) Low-rank projection (T2.3, acting on the signal subspace across S2 and S4) and state quantization (T4.2, acting on the state representation across S3 and S4) modify disjoint objects and combine cleanly, as in Q-GaLore. (iii) Post-update filters (T5.3) wrap a base optimizer because they act *after* the core direction is chosen. This yields the cautious variants of AdamW and Lion from a single mechanism. (iv) Layer-wise trust ratios (T5.4) act at finalization (S5) and can therefore wrap an element-wise adaptive update without touching its direction. (v) Even within a single method, the Muon ablation shows that smaller gain operations can act through partially separable mechanisms. In Muon, symmetric two-way learning-rate scaling and post-orthogonalization Nesterov momentum stack across model scales on the standard Transformer.

Conflicts and limits. The same locality principle predicts where stacking fails. (i) Two strong S2 matrix constraints, spectral orthogonalization and low-rank projection, contend for the same slot. Combining them is therefore not free. The result depends on whether projection precedes orthogonalization or vice versa, and the two orders yield different directions and state footprints. (ii) Fused backprop-update streaming (LOMO-style, T4.4) shortens the gradient’s lifetime and thereby conflicts with any mechanism that needs complete gradient statistics, including global clipping, delayed low-rank basis refresh, SAM-style second gradients, or matrix preconditioners. (iii) Some compositions are valid but impractical. Stacking SAM’s double forward-backward on top of expensive Kronecker-factored preconditioning multiplies cost for little expected return. (iv) Most importantly, two conflicts are *empirical and quantitative*. Aggressive state compression is *rank-bounded*. APOLLO is the single best optimizer at 256 tokens but the worst at 32k. Its degradation is +21.87 PPL, which is roughly three times the AdamW baseline degradation. The reason is that a fixed low-dimensional projection discards proportionally more information as the gradient’s effective rank rises with context (Section 6.2.4, Table 15). Muon’s spectral geometry is also *architecture-conditional*. The gain operations that stack on the standard Transformer no longer improve beyond the best single gain on Gated DeltaNet. The operator order matters as well. Accumulating momentum in the orthogonalized space hurts, and so does scaling the learning rate before orthogonalization (Section 6.3, Table 18).

Design takeaway. Read together, these results recommend treating the four-axis coordinate of a method as a practical compatibility test. Techniques that occupy different axes or pipeline stages are good candidates for composition. Techniques that share a slot demand an explicit ordering. Benefits that depend on gradient rank or architecture topology, especially compression and spectral geometry, must be validated in the target regime, and their transfer must be confirmed. The implication is that optimizer geometry must be matched to model structure and training dynamics. This is the sense in which no single optimizer dominates the multi-objective frontier. The unit of design is a *composition* chosen against a specific budget, context length, and architecture.

7.3 Open Problems and Future Directions

The limitations and the technique-level reading point to a coherent agenda for LLM optimizer design and evaluation.

Diagnostics and adaptive compression. The most direct gap is the absence of measures that turn our qualitative mechanism attributions into testable quantities. Useful examples include an effective-rank estimate that predicts when compression will become lossy, a basis-staleness measure that predicts when a Kronecker or low-rank preconditioner should refresh, and an intrinsic-versus-protocol decomposition that separates genuine algorithmic gains from tuning artifacts. Such metrics would convert the present coordinate system into a predictive diagnostic, and they point to a concrete algorithmic target. The APOLLO collapse shows the payoff of an effective-rank estimate, namely compression schemes whose retained rank or projection adapts to the rising effective rank of the gradient as context length grows, so that short-context memory wins do not become long-context quality failures.

Architecture-aware geometry and transfer. Rankings cross across dataset, context length, and architecture in ways that no single-setting comparison anticipates, and the two clearest mechanisms behind those crossings, compression versus gradient rank and spectral geometry versus attention topology, are understood only post hoc. This motivates a predictive account of *when* a given geometry transfers, tied to measurable properties of the model and data, which would let practitioners select an optimizer without an exhaustive sweep. The same handle suggests a design principle, namely to choose optimizer geometry from measurable properties of the architecture and the evolving training dynamics. RMNP [26] is one example. Under row-wise block-diagonal dominance in the layer-wise Hessian and diagonal dominance in the momentum Gram matrix, its row normalization is a structure-aware specialization of Muon-style preconditioning, and future optimizers should co-design the preconditioner with the architecture and the statistics that emerge during training.

Multi-objective selection. Because the O1–O6 objectives genuinely trade off and no method is uniformly best, optimizer choice is a multi-objective problem that the field still treats as a single-number leaderboard. Cost-aware comparison (token efficiency versus wall-clock and memory), Pareto-aware selection, and optimizer designs that target a specified region of the frontier are all open.

Compositional search. The framework identifies compatible and conflicting compositions by hand. Automating this would mean searching axis-compatible combinations, resolving same-slot ordering, and co-designing variance reduction, direction geometry, and state compression. It also includes the under-explored question of how to combine two S2 constraints without sacrificing either.

Cost-effective curvature. Methods that use curvature across T2 and T5 show the same cost tension. Sophia follows a T5 diagonal-curvature route, while Shampoo and SOAP follow T2 Kronecker-basis routes. They deliver either inconsistent gains or strong gains at prohibitive cost. Cheaper and more stable curvature estimation would help determine when these mechanisms become default tools and when they remain specialist choices. The same is true for a clear characterization of the regimes in which curvature information is worth its overhead.

Matched protocols. Finally, the protocol sensitivity documented throughout argues for standardized, matched-budget evaluation. Useful examples include full learning-rate-transfer studies, matched-token long-context comparisons, and reporting conventions that make the controlled-variable assumptions explicit. This would make it easier to separate intrinsic algorithmic progress from tuning and protocol effects.

8 Conclusion

Optimizer selection for large-scale model training has become a system-level, multi-objective decision, yet the field offers more than one hundred methods described in incompatible vocabularies and supported by protocol-sensitive evidence. This paper set out to make this body of work navigable and, ultimately, actionable. We treated every optimizer as a structured transformation of a stochastic training signal and showed that modern methods are sparse modifications of a shared five-stage meta-pipeline. We then used norm-constrained linear minimization oracles to place sign, spectral-orthogonalized, Kronecker-factored preconditioned, and projected updates inside a single four-axis decomposition. Finally, we organized the resulting mechanisms into a dual-dimension taxonomy that records both where a method acts and which training objective it targets. A controlled benchmark over language-model pretraining then turned this framework from a descriptive device into an evaluative one. The benchmark spans four scales from 60M to 1B parameters, four architectures, and context lengths from 256 to 32k tokens, with a targeted CIFAR100 vision-backbone study used to probe architecture-dependent optimizer behavior beyond language modeling.

Our main conclusion is simple. There is no universal best optimizer, and the practical question is which mechanism’s strength matches the binding constraint of the training regime. Under the tested protocol, the strongest quality gains are associated with geometry-sensitive direction maps and the structured state that feeds them. Scalar refinements of the adaptive-moment template alone contribute little. Most element-wise variants of AdamW do not survive a retuned baseline. Two empirical regularities sharpen this picture and should be treated as design constraints. Aggressive state compression is rank-bounded and degrades sharply as the gradient’s effective rank rises with context length. Spectral matrix geometry is architecture-conditional, so its gains must be validated on the target topology, and their transfer must be confirmed. Composability, in turn, is governed by locality on the four axes. Techniques on different axes or pipeline stages stack, while techniques that contend for the same slot require an explicit ordering. The unit of design is therefore a composition chosen against a budget.

These findings translate into concrete guidance. Across the benchmarked methods, the mainstream choices and the regime each one fits (Table 17) are the following.

- **AdamW** is the default reference for general-purpose pretraining. It is not the strongest on any single metric, but it is stable, inexpensive, interpretable, and the baseline every other choice should be measured against.
- **RMNP** [26] is better read as a practical, architecture-aware step beyond standard Muon-style preconditioning. It targets a better quality–efficiency balance by using architecture-induced row-wise structure. When the relevant curvature and momentum statistics are diagonally dominant in a row-wise sense, a Muon-style matrix direction can be implemented through a cheaper row-normalized form.
- **SOAP** is the quality ceiling for long-context training and the most transferable method across architectures. It is too costly to be a default, but it is useful when final quality dominates and compute and memory are not the bottleneck.
- **Muon** is a stable, mechanistically transparent matrix method. It should be used with awareness of the target model topology.
- **AdaFactor** is the safe low-memory baseline at moderate quality. **APOLLO** is a high-reward, high-risk compressed-state method that excels at short context but collapses at long context, so its short-context wins do not certify it.
- **Lion** is a cheap exploratory option with an expected quality gap. Curvature-aware and geometry-regularized methods such as Sophia and LAMB remain situational under the current protocol.

In short, the decision rule is to identify the single binding constraint of a run, such as stability, quality,

runtime, memory, or cross-scenario transfer, and select the method whose dominant strength addresses it. Starting from AdamW, move to RMNP, SOAP, or a memory-efficient method only when a specific constraint demands it.

Beyond these recommendations, the framework's main contribution to the community is an operational coordinate system. Any optimizer, including methods that have not yet been proposed, can be located by its pipeline stages and its four-axis coordinate. Its composability with other techniques can be predicted from that location, and competing methods can be compared under explicit mechanism and objective assumptions. This gives practitioners a shared vocabulary and a constraint-driven decision procedure. For method designers, it maps crowded regions, unexplored compositions, and empirical boundaries that any new method must respect, such as rank-bounded compression and architecture-conditional geometry. A further lesson, developed in Section 7.3, is that optimizer geometry should be coupled to the model architecture and training dynamics, with RMNP as one concrete example. The same coordinate system marks where this study should grow next. One direction is to develop quantitative interpretability metrics that turn the present qualitative mechanism attributions into predictive diagnostics. A second direction is to extend the study beyond language modeling, building on the foundation established here.

References

- [1] Ahmed M Adly. Exadam: The power of adaptive cross-moments. *arXiv preprint arXiv:2412.20302*, 2024.
- [2] Kwangjun Ahn, Byron Xu, Natalie Abreu, Ying Fan, Gagik Magakyan, Pratyusha Sharma, Zheng Zhan, and John Langford. Dion: Distributed orthonormalized updates. *arXiv preprint arXiv:2504.05295*, 2025.
- [3] Doğay Altınel. Development of deep learning optimizers: Approaches, concepts, and update rules. *arXiv preprint arXiv:2509.18396*, 2025.
- [4] Shun-Ichi Amari. Natural gradient works efficiently in learning. *Neural computation*, 10(2):251–276, 1998.
- [5] Wangpeng An, Haoqian Wang, Qingyun Sun, Jun Xu, Qionghai Dai, and Lei Zhang. A pid controller approach for stochastic optimization of deep networks. In *Proceedings of the IEEE conference on computer vision and pattern recognition*, pages 8522–8531, 2018.
- [6] Rohan Anil, Vineet Gupta, Tomer Koren, and Yoram Singer. Memory efficient adaptive optimization. *Advances in Neural Information Processing Systems*, 32, 2019.
- [7] Jeongin Bae, Baeseong Park, Gunho Park, Minsub Kim, Joonhyung Lee, Junhee Yoo, Sunghyeon Woo, Jiwon Ryu, Se Jung Kwon, and Dongsoo Lee. Affine-scaled attention: Towards flexible and stable transformer attention. *arXiv preprint arXiv:2602.23057*, 2026.
- [8] Dariush Bahrami and Sadegh Pouriyari Zadeh. Gravity optimizer: a kinematic approach on optimization in deep learning. *arXiv preprint arXiv:2101.09192*, 2021.
- [9] Lukas Balles and Philipp Hennig. Dissecting adam: The sign, magnitude and variance of stochastic gradients. In *International Conference on Machine Learning*, pages 404–413. PMLR, 2018.
- [10] Jeremy Bernstein and Laker Newhouse. Old optimizer, new norm: An anthology. *arXiv preprint arXiv:2409.20325*, 2024.
- [11] Jeremy Bernstein, Yu-Xiang Wang, Kamyar Azizzadenesheli, and Animashree Anandkumar. signsgd: Compressed optimisation for non-convex problems. In *International conference on machine learning*, pages 560–569. PMLR, 2018.
- [12] Leonard Berrada, Andrew Zisserman, and M Pawan Kumar. Training neural networks for and by interpolation. In *International conference on machine learning*, pages 799–809. PMLR, 2020.
- [13] Yonatan Bisk, Rowan Zellers, Ronan Le Bras, Jianfeng Gao, and Yejin Choi. PIQA: Reasoning about physical commonsense in natural language. In *Proceedings of the AAAI Conference on Artificial Intelligence*, volume 34, pages 7432–7439, 2020. doi: 10.1609/aaai.v34i05.6239.
- [14] Andy Brock, Soham De, Samuel L Smith, and Karen Simonyan. High-performance large-scale image recognition without normalization. In *International conference on machine learning*, pages 1059–1071. PMLR, 2021.
- [15] Yang Cao, Xiaoyu Li, and Zhao Song. Grams: Gradient descent with adaptive momentum scaling. *arXiv preprint arXiv:2412.17107*, 2024.
- [16] Da Chang and Ganzhao Yuan. Mgup: A momentum-gradient alignment update policy for stochastic optimization. *Advances in Neural Information Processing Systems*, 38:20488–20537, 2026.
- [17] Jinghui Chen, Dongruo Zhou, Yiqi Tang, Ziyan Yang, Yuan Cao, and Quanquan Gu. Closing the generalization gap of adaptive gradient methods in training deep neural networks. *arXiv preprint arXiv:1806.06763*, 2018.
- [18] Xi Chen, Kaituo Feng, Changsheng Li, Xunhao Lai, Xiangyu Yue, Ye Yuan, and Guoren Wang. Fira: Can we achieve full-rank training of llms under low-rank constraint? *Advances in Neural Information Processing Systems*, 38:120680–120712, 2026.
- [19] Xiangning Chen, Chen Liang, Da Huang, Esteban Real, Kaiyuan Wang, Hieu Pham, Xuanyi Dong, Thang Luong, Cho-Jui Hsieh, Yifeng Lu, et al. Symbolic discovery of optimization algorithms. *Advances in neural information processing systems*, 36:49205–49233, 2023.

- [20] Christopher Clark, Kenton Lee, Ming-Wei Chang, Tom Kwiatkowski, Michael Collins, and Kristina Toutanova. BoolQ: Exploring the surprising difficulty of natural yes/no questions. In *Proceedings of the 2019 Conference of the North American Chapter of the Association for Computational Linguistics: Human Language Technologies*, pages 2924–2936. Association for Computational Linguistics, 2019. doi: 10.18653/v1/N19-1300.
- [21] Peter Clark, Isaac Cowhey, Oren Etzioni, Tushar Khot, Ashish Sabharwal, Carissa Schoenick, and Oyvind Tafjord. Think you have solved question answering? try arc, the ai2 reasoning challenge. *arXiv preprint arXiv:1803.05457*, 2018.
- [22] Aaron Defazio. Why gradients rapidly increase near the end of training. *arXiv preprint arXiv:2506.02285*, 2025.
- [23] Aaron Defazio and Samy Jelassi. A momentumized, adaptive, dual averaged gradient method. *Journal of Machine Learning Research*, 23(144):1–34, 2022.
- [24] Aaron Defazio and Konstantin Mishchenko. Learning-rate-free learning by d-adaptation. In *International conference on machine learning*, pages 7449–7479. PMLR, 2023.
- [25] Aaron Defazio, Xingyu Yang, Harsh Mehta, Konstantin Mishchenko, Ahmed Khaled, and Ashok Cutkosky. The road less scheduled. *Advances in Neural Information Processing Systems*, 37:9974–10007, 2024.
- [26] Shenyang Deng, Zhuoli Ouyang, Tianyu Pang, Zihang Liu, Ruochen Jin, Shuhua Yu, and Yaoqing Yang. Rmnp: Row-momentum normalized preconditioning for scalable matrix-based optimization. *arXiv preprint arXiv:2603.20527*, 2026.
- [27] Tim Dettmers, Mike Lewis, Sam Shleifer, and Luke Zettlemoyer. 8-bit optimizers via block-wise quantization. *arXiv preprint arXiv:2110.02861*, 2021.
- [28] Jianbang Ding, Xuancheng Ren, Ruixuan Luo, and Xu Sun. An adaptive and momental bound method for stochastic learning. *arXiv preprint arXiv:1910.12249*, 2019.
- [29] Timothy Dozat. Incorporating nesterov momentum into adam, 2016.
- [30] Shiv Ram Dubey, Soumendu Chakraborty, Swalpa Kumar Roy, Snehasis Mukherjee, Satish Kumar Singh, and Bidyut Baran Chaudhuri. diffgrad: an optimization method for convolutional neural networks. *IEEE transactions on neural networks and learning systems*, 31(11):4500–4511, 2019.
- [31] John Duchi, Elad Hazan, and Yoram Singer. Adaptive subgradient methods for online learning and stochastic optimization. *Journal of machine learning research*, 12(7), 2011.
- [32] Pierre Foret, Ariel Kleiner, Hossein Mobahi, and Behnam Neyshabur. Sharpness-aware minimization for efficiently improving generalization. *arXiv preprint arXiv:2010.01412*, 2020.
- [33] Kevin Frans, Sergey Levine, and Pieter Abbeel. A stable whitening optimizer for efficient neural network training. *Advances in Neural Information Processing Systems*, 38:174086–174110, 2026.
- [34] Leo Gao, Jonathan Tow, Baber Abbasi, Stella Biderman, Sid Black, Anthony DiPofi, Charles Foster, Laurence Golding, Jeffrey Hsu, Alain Le Noac’h, Haonan Li, Kyle McDonell, Niklas Muennighoff, Chris Ociepa, Jason Phang, Laria Reynolds, Hailey Schoelkopf, Aviya Skowron, Lintang Sutawika, Eric Tang, Anish Thite, Ben Wang, Kevin Wang, and Andy Zou. The language model evaluation harness, 07 2024. URL <https://zenodo.org/records/12608602>.
- [35] Boris Ginsburg, Patrice Castonguay, Oleksii Hrinchuk, Oleksii Kuchaiev, Vitaly Lavrukhin, Ryan Leary, Jason Li, Huyen Nguyen, Yang Zhang, and Jonathan M Cohen. Stochastic gradient methods with layer-wise adaptive moments for training of deep networks. *arXiv preprint arXiv:1905.11286*, 2019.
- [36] Athanasios Glentis, Jiayang Li, Qiulin Shang, Andi Han, Ioannis Tsaknakis, Quan Wei, and Mingyi Hong. Scalable parameter and memory efficient pretraining for llm: Recent algorithmic advances and benchmarking. *arXiv preprint arXiv:2505.22922*, 2025.
- [37] Wenbo Gong, Meyer Scetbon, Chao Ma, and Edward Meeds. Towards efficient optimizer design for llm via structured fisher approximation with a low-rank extension. *arXiv preprint arXiv:2502.07752*, 2025.
- [38] Vineet Gupta, Tomer Koren, and Yoram Singer. Shampoo: Preconditioned stochastic tensor optimization. In *International Conference on Machine Learning*, pages 1842–1850. PMLR, 2018.

- [39] Mohamed Hassan, Aleksandar Vakanski, Boyu Zhang, and Min Xian. Gcsam: Gradient centralized sharpness aware minimization. *IEEE Access*, 2025.
- [40] Kaiming He, Xiangyu Zhang, Shaoqing Ren, and Jian Sun. Deep residual learning for image recognition. In *Proceedings of the IEEE conference on computer vision and pattern recognition*, pages 770–778, 2016.
- [41] C Evans Hedges. Orthograd improves neural calibration. *arXiv preprint arXiv:2506.04487*, 2025.
- [42] Byeongho Heo, Sanghyuk Chun, Seong Joon Oh, Dongyoon Han, Sangdoon Yun, Gyuwan Kim, Youngjung Uh, and Jung-Woo Ha. Adamp: Slowing down the slowdown for momentum optimizers on scale-invariant weights. *arXiv preprint arXiv:2006.08217*, 2020.
- [43] Tianjin Huang, Zhangyang Wang, Haotian Hu, Zhenyu Zhang, Gaojie Jin, Xiang Li, Li Shen, Jiaying Shang, Tianlong Chen, Ke Li, et al. Gradientstabilizer: Fix the norm, not the gradient.
- [44] Tianjin Huang, Ziquan Zhu, Gaojie Jin, Lu Liu, Zhangyang Wang, and Shiwei Liu. Spam: Spike-aware adam with momentum reset for stable llm training. *arXiv preprint arXiv:2501.06842*, 2025.
- [45] Maor Ivgi, Oliver Hinder, and Yair Carmon. Dog is sgd’s best friend: A parameter-free dynamic step size schedule, 2023.
- [46] John St John. Adamd: Improved bias-correction in adam. *arXiv preprint arXiv:2110.10828*, 2021.
- [47] Taejong Joo, Wenhan Xia, Cheolmin Kim, Ming Zhang, and Eugene Je. On surprising effectiveness of masking updates in adaptive optimizers. *arXiv preprint arXiv:2602.15322*, 2026.
- [48] Keller Jordan, Yuchen Jin, Vlado Boza, Jiacheng You, Franz Cesista, Laker Newhouse, and Jeremy Bernstein. Muon: An optimizer for hidden layers in neural networks. <https://kellerjordan.github.io/posts/muon/>, 2024.
- [49] Andrej Karpathy. Fineweb-edu-100b-shuffle. <https://huggingface.co/datasets/karpathy/fineweb-edu-100b-shuffle>, 2024.
- [50] Adrien Kegreisz. Ano: Faster is better in noisy landscape. *arXiv preprint arXiv:2508.18258*, 2025.
- [51] Nitish Shirish Keskar and Richard Socher. Improving generalization performance by switching from adam to sgd. *arXiv preprint arXiv:1712.07628*, 2017.
- [52] Ahmed Khaled, Konstantin Mishchenko, and Chi Jin. Dowg unleashed: An efficient universal parameter-free gradient descent method. *Advances in Neural Information Processing Systems*, 36:6748–6769, 2023.
- [53] Rahul Kidambi, Praneeth Netrapalli, Prateek Jain, and Sham Kakade. On the insufficiency of existing momentum schemes for stochastic optimization, 2018.
- [54] Diederik P Kingma and Jimmy Ba. Adam: A method for stochastic optimization. *arXiv preprint arXiv:1412.6980*, 2014.
- [55] Alex Krizhevsky, Geoffrey Hinton, et al. Learning multiple layers of features from tiny images, 2009.
- [56] Abhay Kumar, Louis Owen, Nilabhra Roy Chowdhury, and Fabian Gra. Zclip: Adaptive spike mitigation for llm pre-training. *arXiv preprint arXiv:2504.02507*, 2025.
- [57] Jungmin Kwon, Jeongseop Kim, Hyunseo Park, and In Kwon Choi. Asam: Adaptive sharpness-aware minimization for scale-invariant learning of deep neural networks. In *International conference on machine learning*, pages 5905–5914. PMLR, 2021.
- [58] Siyuan Li, Juanxi Tian, Zedong Wang, Luyuan Zhang, Zicheng Liu, Weiyang Jin, Yang Liu, Baigui Sun, and Stan Z Li. Unveiling the backbone-optimizer coupling bias in visual representation learning. *arXiv preprint arXiv:2410.06373*, 2024.
- [59] Siyuan Li, Juanxi Tian, Zedong Wang, Xin Jin, Zicheng Liu, Wentao Zhang, and Dan Xu. Taming llms by scaling learning rates with gradient grouping. *arXiv preprint arXiv:2506.01049*, 2025.
- [60] Siyuan Li, Juanxi Tian, Zedong Wang, Anna Wang, Xin Jin, Chang Yu, Ruoyu Sun, and Cheng Tan. SAC: Adaptive learning rate scaling with architectural constraints, 2026. URL <https://openreview.net/forum?id=EB92tITeNq>.

- [61] Tao Li, Pan Zhou, Zhengbao He, Xinwen Cheng, and Xiaolin Huang. Friendly sharpness-aware minimization. In *Proceedings of the IEEE/CVF conference on computer vision and pattern recognition*, pages 5631–5640, 2024.
- [62] Xi-Lin Li. Preconditioned stochastic gradient descent. *IEEE transactions on neural networks and learning systems*, 29(5):1454–1466, 2017.
- [63] Xilin Li. Black box lie group preconditioners for sgd. *arXiv preprint arXiv:2211.04422*, 2022.
- [64] Kaizhao Liang, Lizhang Chen, Bo Liu, and Qiang Liu. Cautious optimizers: Improving training with one line of code. *arXiv preprint arXiv:2411.16085*, 2024.
- [65] Hong Liu, Zhiyuan Li, David Hall, Percy Liang, and Tengyu Ma. Sophia: A scalable stochastic second-order optimizer for language model pre-training. In *International Conference on Learning Representations*, volume 2024, pages 1621–1650, 2024.
- [66] Liming Liu, Zhenghao Xu, Zixuan Zhang, Hao Kang, Zichong Li, Chen Liang, Weizhu Chen, and Tuo Zhao. Cosmos: A hybrid adaptive optimizer for memory-efficient training of llms. *arXiv preprint arXiv:2502.17410*, 2025.
- [67] Liyuan Liu, Haoming Jiang, Pengcheng He, Weizhu Chen, Xiaodong Liu, Jianfeng Gao, and Jiawei Han. On the variance of the adaptive learning rate and beyond. *arXiv preprint arXiv:1908.03265*, 2019.
- [68] Yizhou Liu, Ziming Liu, and Jeff Gore. Focus: First order concentrated updating scheme. *arXiv preprint arXiv:2501.12243*, 2025.
- [69] Yong Liu, Siqi Mai, Xiangning Chen, Cho-Jui Hsieh, and Yang You. Towards efficient and scalable sharpness-aware minimization. In *Proceedings of the IEEE/CVF Conference on Computer Vision and Pattern Recognition*, pages 12360–12370, 2022.
- [70] Ilya Loshchilov and Frank Hutter. Decoupled weight decay regularization. *arXiv preprint arXiv:1711.05101*, 2017.
- [71] Jun Lu. Adasmooth: an adaptive learning rate method based on effective ratio. In *Sentiment Analysis and Deep Learning: Proceedings of ICSADL 2022*, pages 273–293. Springer, 2023.
- [72] James Lucas, Shengyang Sun, Richard Zemel, and Roger Grosse. Aggregated momentum: Stability through passive damping. *arXiv preprint arXiv:1804.00325*, 2018.
- [73] Liangchen Luo, Yuanhao Xiong, Yan Liu, and Xu Sun. Adaptive gradient methods with dynamic bound of learning rate. *arXiv preprint arXiv:1902.09843*, 2019.
- [74] Yang Luo, Xiaozhe Ren, Zangwei Zheng, Zhuo Jiang, Xin Jiang, and Yang You. Came: Confidence-guided adaptive memory efficient optimization. In *Proceedings of the 61st Annual Meeting of the Association for Computational Linguistics (Volume 1: Long Papers)*, pages 4442–4453, 2023.
- [75] Kai Lv, Hang Yan, Qipeng Guo, Haijun Lv, and Xipeng Qiu. Adalomo: Low-memory optimization with adaptive learning rate. In *Findings of the Association for Computational Linguistics: ACL 2024*, pages 12486–12502, 2024.
- [76] Kai Lv, Yuqing Yang, Tengxiao Liu, Qipeng Guo, and Xipeng Qiu. Full parameter fine-tuning for large language models with limited resources. In *Proceedings of the 62nd Annual Meeting of the Association for Computational Linguistics (Volume 1: Long Papers)*, pages 8187–8198, 2024.
- [77] Jerry Ma and Denis Yarats. Quasi-hyperbolic momentum and adam for deep learning. *arXiv preprint arXiv:1810.06801*, 2018.
- [78] Pranshu Malviya, Goncalo Mordido, Aristide Baratin, Reza Babanezhad Harikandeh, Gintare Karolina Dziugaite, Razvan Pascanu, and Sarath Chandar. Torque-aware momentum. *arXiv preprint arXiv:2412.18790*, 2024.
- [79] Stephen Merity, Caiming Xiong, James Bradbury, and Richard Socher. Pointer sentinel mixture models. *arXiv preprint arXiv:1609.07843*, 2016.

- [80] Todor Mihaylov, Peter Clark, Tushar Khot, and Ashish Sabharwal. Can a suit of armor conduct electricity? a new dataset for open book question answering. In *Proceedings of the 2018 conference on empirical methods in natural language processing*, pages 2381–2391, 2018.
- [81] Konstantin Mishchenko and Aaron Defazio. Prodigy: An expeditiously adaptive parameter-free learner. *arXiv preprint arXiv:2306.06101*, 2023.
- [82] Thomas Möllenhoff and Mohammad Emtiyaz Khan. Sam as an optimal relaxation of bayes. *arXiv preprint arXiv:2210.01620*, 2022.
- [83] Depen Morwani, Nikhil Vyas, Hanlin Zhang, and Sham Kakade. Connections between schedule-free optimizers, ademamix, and accelerated sgd variants. *arXiv preprint arXiv:2502.02431*, 2025.
- [84] Matteo Pagliardini, Pierre Ablin, and David Grangier. The ademamix optimizer: Better, faster, older, 2025.
- [85] Denis Paperno, Germán Kruszewski, Angeliki Lazaridou, Ngoc Quan Pham, Raffaella Bernardi, Sandro Pezzelle, Marco Baroni, Gemma Boleda, and Raquel Fernandez. The LAMBADA dataset: Word prediction requiring a broad discourse context. In *Proceedings of the 54th Annual Meeting of the Association for Computational Linguistics (Volume 1: Long Papers)*, pages 1525–1534, Berlin, Germany, August 2016. Association for Computational Linguistics. URL <http://www.aclweb.org/anthology/P16-1144>.
- [86] Guilherme Penedo, Hynek Kydlíček, Loubna Ben allal, Anton Lozhkov, Margaret Mitchell, Colin Raffel, Leandro Von Werra, and Thomas Wolf. The fineweb datasets: Decanting the web for the finest text data at scale, 2024. URL <https://arxiv.org/abs/2406.17557>.
- [87] Thomas Pethick, Wanyun Xie, Kimon Antonakopoulos, Zhenyu Zhu, Antonio Silveti-Falls, and Volkan Cevher. Training deep learning models with norm-constrained lmos. *arXiv preprint arXiv:2502.07529*, 2025.
- [88] Boris T Polyak. Some methods of speeding up the convergence of iteration methods. *Ussr computational mathematics and mathematical physics*, 4(5):1–17, 1964.
- [89] Xingyu Qu, Peigeng Huang, and Samuel Horvath. Can muon fine-tune adam-pretrained models? *arXiv preprint arXiv:2605.10468*, 2026.
- [90] Colin Raffel, Noam Shazeer, Adam Roberts, Katherine Lee, Sharan Narang, Michael Matena, Yanqi Zhou, Wei Li, and Peter J Liu. Exploring the limits of transfer learning with a unified text-to-text transformer. *Journal of machine learning research*, 21(140):1–67, 2020.
- [91] Aditya Ranganath. Navigating llm valley: From adamw to memory-efficient and matrix-based optimizers. *arXiv preprint arXiv:2605.09176*, 2026.
- [92] Melissa Roemmele, Cosmin Adrian Bejan, and Andrew S Gordon. Choice of plausible alternatives: An evaluation of commonsense causal reasoning. In *2011 AAAI Spring Symposium Series*, 2011. URL <https://people.ict.usc.edu/~gordon/publications/AAAI-SPRING11A.PDF>.
- [93] Jian Rong, ChenHao Ma, QingHui Zhang, and Yong Cao. Rlion: A refined lion optimizer for deep learning, 2024.
- [94] Keisuke Sakaguchi, Ronan Le Bras, Chandra Bhagavatula, and Yejin Choi. Winogrande: An adversarial winograd schema challenge at scale. *Communications of the ACM*, 64(9):99–106, 2021.
- [95] Tom Schaul, Sixin Zhang, and Yann LeCun. No more pesky learning rates. In *International conference on machine learning*, pages 343–351. PMLR, 2013.
- [96] Joel Schlotthauer, Christian Kroos, Chris Hinze, Viktor Hangya, Luzian Hahn, and Fabian Küch. Pre-training llms on a budget: A comparison of three optimizers. *arXiv preprint arXiv:2507.08472*, 2025.
- [97] Andrei Semenov, Matteo Pagliardini, and Martin Jaggi. Benchmarking optimizers for large language model pretraining. *arXiv preprint arXiv:2509.01440*, 2025.
- [98] Maria-Eleni Sfyraiki and Jun-Kun Wang. Lions and muons: Optimization via stochastic frank-wolfe. *arXiv preprint arXiv:2506.04192*, 2025.
- [99] Noam Shazeer and Mitchell Stern. Adafactor: Adaptive learning rates with sublinear memory cost. In *International conference on machine learning*, pages 4596–4604. PMLR, 2018.

- [100] Zakhar Shumaylov, Nathaël Da Costa, Peter Zaika, Bálint Mucsányi, Alex Massucco, Yoav Gelberg, Carola-Bibiane Schönlieb, Yarin Gal, and Philipp Hennig. Muon is not that special: Random or inverted spectra work just as well. *arXiv preprint arXiv:2605.11181*, 2026.
- [101] Chongjie Si, Debing Zhang, and Wei Shen. Adamuon: Adaptive muon optimizer. *arXiv preprint arXiv:2507.11005*, 2025.
- [102] Minhak Song, Beomhan Baek, Kwangjun Ahn, and Chulhee Yun. Through the river: Understanding the benefit of schedule-free methods for language model training. *Advances in Neural Information Processing Systems*, 38:127524–127555, 2026.
- [103] Ilya Sutskever, James Martens, George Dahl, and Geoffrey Hinton. On the importance of initialization and momentum in deep learning. In *International conference on machine learning*, pages 1139–1147. pmlr, 2013.
- [104] Shohei Taniguchi, Keno Harada, Gouki Minegishi, Yuta Oshima, Seong Cheol Jeong, Go Nagahara, Tomoshi Iiyama, Masahiro Suzuki, Yusuke Iwasawa, and Yutaka Matsuo. ADOPT: Modified Adam can converge with any β_2 with the optimal rate. *Advances in Neural Information Processing Systems*, 37:72438–72474, 2024.
- [105] Tijmen Tieleman and Geoffrey Hinton. Divide the gradient by a running average of its recent magnitude. coursera: Neural networks for machine learning. In *Technical report*. University of Toronto, 2017.
- [106] Hugo Touvron, Matthieu Cord, Matthijs Douze, Francisco Massa, Alexandre Sablayrolles, and Hervé Jégou. Training data-efficient image transformers & distillation through attention. In *International conference on machine learning*, pages 10347–10357. PMLR, 2021.
- [107] Ashish Vaswani, Noam Shazeer, Niki Parmar, Jakob Uszkoreit, Llion Jones, Aidan N Gomez, Łukasz Kaiser, and Illia Polosukhin. Attention is all you need. *Advances in neural information processing systems*, 30, 2017.
- [108] Nikhil Vyas, Depen Morwani, Rosie Zhao, Itai Shapira, David Brandfonbrener, Lucas Janson, and Sham Kakade. Soap: Improving and stabilizing shampoo using adam for language modeling. In *International Conference on Learning Representations*, volume 2025, pages 93423–93444, 2025.
- [109] Guoxia Wang, Shuai Li, Congliang Chen, Jinle Zeng, Jiabin Yang, Dianhai Yu, Yanjun Ma, and Li Shen. Adagc: Improving training stability for large language model pretraining. *arXiv preprint arXiv:2502.11034*, 2025.
- [110] Jinbo Wang, Mingze Wang, Zhanpeng Zhou, Junchi Yan, Lei Wu, et al. The sharpness disparity principle in transformers for accelerating language model pre-training. In *International Conference on Machine Learning*, pages 64859–64879. PMLR, 2025.
- [111] Junjie Wang, Pan Zhou, Yiming Dong, Huan Li, Jia Li, Xun Zhou, Qicheng Lao, Cong Fang, and Zhouchen Lin. Conda: Column-normalized adam for training large language models faster. *arXiv preprint arXiv:2509.24218*, 2025.
- [112] Johannes Welbl, Nelson F Liu, and Matt Gardner. Crowdsourcing multiple choice science questions. In *Proceedings of the 3rd Workshop on Noisy User-generated Text*, pages 94–106, 2017.
- [113] Kaiyue Wen, David Hall, Tengyu Ma, and Percy Liang. Fantastic pretraining optimizers and where to find them. *arXiv preprint arXiv:2509.02046*, 2025.
- [114] Mitchell Wortsman, Tim Dettmers, Luke Zettlemoyer, Ari Morcos, Ali Farhadi, and Ludwig Schmidt. Stable and low-precision training for large-scale vision-language models. *Advances in Neural Information Processing Systems*, 36:10271–10298, 2023.
- [115] Less Wright and Nestor Demeure. Ranger21: a synergistic deep learning optimizer. *arXiv preprint arXiv:2106.13731*, 2021.
- [116] Tian Xie, Haoming Luo, Haoyu Tang, Yiwen Hu, Jason Klein Liu, Qingnan Ren, Yang Wang, Wayne Xin Zhao, Rui Yan, Bing Su, et al. Controlled llm training on spectral sphere. *arXiv preprint arXiv:2601.08393*, 2026.
- [117] Xingyu Xie, Pan Zhou, Huan Li, Zhouchen Lin, and Shuicheng Yan. Adan: Adaptive nesterov momentum algorithm for faster optimizing deep models. *IEEE Transactions on Pattern Analysis and Machine Intelligence*, 46(12):9508–9520, 2024.

- [118] Minghao Xu, Lichuan Xiang, Xu Cai, and Hongkai Wen. No more adam: Learning rate scaling at initialization is all you need. *arXiv preprint arXiv:2412.11768*, 2024.
- [119] Ruihan Xu, Jiajin Li, and Yiping Lu. On the width scaling of neural optimizers under matrix operator norms i: Row/column normalization and hyperparameter transfer. *arXiv preprint arXiv:2603.09952*, 2026.
- [120] Songlin Yang, Bailin Wang, Yikang Shen, Rameswar Panda, and Yoon Kim. Gated linear attention transformers with hardware-efficient training. *arXiv preprint arXiv:2312.06635*, 2023.
- [121] Songlin Yang, Bailin Wang, Yu Zhang, Yikang Shen, and Yoon Kim. Parallelizing linear transformers with the delta rule over sequence length. *Advances in neural information processing systems*, 37:115491–115522, 2024.
- [122] Songlin Yang, Jan Kautz, and Ali Hatamizadeh. Gated delta networks: Improving mamba2 with delta rule. In *International Conference on Learning Representations*, volume 2025, pages 29687–29707, 2025.
- [123] Zhewei Yao, Amir Gholami, Sheng Shen, Mustafa Mustafa, Kurt Keutzer, and Michael Mahoney. Adahessian: An adaptive second order optimizer for machine learning. In *proceedings of the AAAI conference on artificial intelligence*, volume 35, pages 10665–10673, 2021.
- [124] Hongwei Yong, Jianqiang Huang, Xiansheng Hua, and Lei Zhang. Gradient centralization: A new optimization technique for deep neural networks. In *European Conference on Computer Vision*, pages 635–652. Springer, 2020.
- [125] Yang You, Jing Li, Sashank Reddi, Jonathan Hseu, Sanjiv Kumar, Srinadh Bhojanapalli, Xiaodan Song, James Demmel, Kurt Keutzer, and Cho-Jui Hsieh. Large batch optimization for deep learning: Training bert in 76 minutes. *arXiv preprint arXiv:1904.00962*, 2019.
- [126] Weihao Yu, Mi Luo, Pan Zhou, Chenyang Si, Yichen Zhou, Xinchao Wang, Jiashi Feng, and Shuicheng Yan. Metaformer is actually what you need for vision. In *Proceedings of the IEEE/CVF conference on computer vision and pattern recognition*, pages 10819–10829, 2022.
- [127] Weihao Yu, Chenyang Si, Pan Zhou, Mi Luo, Yichen Zhou, Jiashi Feng, Shuicheng Yan, and Xinchao Wang. Metaformer baselines for vision. *IEEE Transactions on Pattern Analysis and Machine Intelligence*, 46(2):896–912, 2023.
- [128] Huizhuo Yuan, Yifeng Liu, Shuang Wu, Xun Zhou, and Quanquan Gu. Mars: Unleashing the power of variance reduction for training large models. *arXiv preprint arXiv:2411.10438*, 2024.
- [129] Yun Yue, Jiadi Jiang, Zhiling Ye, Ning Gao, Yongchao Liu, and Ke Zhang. Sharpness-aware minimization revisited: Weighted sharpness as a regularization term. In *Proceedings of the 29th ACM SIGKDD Conference on Knowledge Discovery and Data Mining*, pages 3185–3194, 2023.
- [130] Matthew D Zeiler. Adadelata: an adaptive learning rate method. *arXiv preprint arXiv:1212.5701*, 2012.
- [131] Rowan Zellers, Ari Holtzman, Yonatan Bisk, Ali Farhadi, and Yejin Choi. HellaSwag: Can a machine really finish your sentence? In *Proceedings of the 57th Annual Meeting of the Association for Computational Linguistics*, pages 4791–4800. Association for Computational Linguistics, 2019. doi: 10.18653/v1/P19-1472.
- [132] Michael Zhang, James Lucas, Jimmy Ba, and Geoffrey E Hinton. Lookahead optimizer: k steps forward, 1 step back. *Advances in neural information processing systems*, 32, 2019.
- [133] Minxin Zhang, Yuxuan Liu, and Hayden Schaeffer. Adagrad meets muon: Adaptive stepsizes for orthogonal updates. *arXiv preprint arXiv:2509.02981*, 2025.
- [134] Tong Zhang, Jiangning Zhang, Zhucun Xue, Juntao Jiang, Yicheng Xu, Chengming Xu, Teng Hu, Xingyu Xie, Xiaobin Hu, Yabiao Wang, et al. Evolution of optimization methods: Algorithms, scenarios, and evaluations. *arXiv preprint arXiv:2604.12968*, 2026.
- [135] Yihua Zhang, Pingzhi Li, Junyuan Hong, Jiayang Li, Yimeng Zhang, Wenqing Zheng, Pin-Yu Chen, Jason D Lee, Wotao Yin, Mingyi Hong, et al. Revisiting zeroth-order optimization for memory-efficient llm fine-tuning: A benchmark. *arXiv preprint arXiv:2402.11592*, 2024.

- [136] Yushun Zhang, Congliang Chen, Ziniu Li, Tian Ding, Chenwei Wu, Diederik Durk Kingma, Yinyu Ye, Zhi-Quan Luo, and Ruoyu Sun. Adam-mini: Use fewer learning rates to gain more. In *International Conference on Learning Representations*, volume 2025, pages 28033–28063, 2025.
- [137] Zhenyu Zhang, Ajay Jaiswal, Lu Yin, Shiwei Liu, Jiawei Zhao, Yuandong Tian, and Zhangyang Wang. Q-galore: Quantized galore with int4 projection and layer-adaptive low-rank gradients. *arXiv preprint arXiv:2407.08296*, 2024.
- [138] Jiawei Zhao, Zhenyu Zhang, Beidi Chen, Zhangyang Wang, Anima Anandkumar, and Yuandong Tian. Galore: Memory-efficient llm training by gradient low-rank projection. *arXiv preprint arXiv:2403.03507*, 2024.
- [139] Rosie Zhao, Depen Morwani, David Brandfonbrener, Nikhil Vyas, and Sham Kakade. Deconstructing what makes a good optimizer for language models, 2025. URL <https://arxiv.org/abs/2407.07972>.
- [140] Hanqing Zhu, Zhenyu Zhang, Wenyan Cong, Xi Liu, Sem Park, Vikas Chandra, Bo Long, David Z Pan, Zhangyang Wang, and Jinwon Lee. Apollo: Sgd-like memory, adamw-level performance. *Proceedings of Machine Learning and Systems*, 7, 2025.
- [141] Juntang Zhuang, Tommy Tang, Yifan Ding, Sekhar C Tatikonda, Nicha Dvornek, Xenophon Papademetris, and James Duncan. Adabelief optimizer: Adapting stepsizes by the belief in observed gradients. *Advances in neural information processing systems*, 33:18795–18806, 2020.
- [142] Juntang Zhuang, Boqing Gong, Liangzhe Yuan, Yin Cui, Hartwig Adam, Nicha Dvornek, Sekhar Tatikonda, James Duncan, and Ting Liu. Surrogate gap minimization improves sharpness-aware training. *arXiv preprint arXiv:2203.08065*, 2022.

Appendix

A Additional Experimental Hyperparameter Configurations

To improve the reproducibility of the benchmark results, this appendix reports the main optimizer hyperparameters used in the experiments. The main text reports the resulting perplexity, downstream performance, per-step optimizer runtime, and optimizer-state memory. In contrast, this appendix focuses on the training configurations, including learning rates, momentum coefficients, numerical stability constants, and method-specific auxiliary parameters.

A.1 Stage-1 C4-LLaMA Short-Context Screening

Table 19 summarizes the tuned hyperparameter configurations used in the Stage-1 C4-LLaMA short-context screening experiments. For each optimizer, we report the momentum coefficients, numerical stability constant, and the selected learning rate at each model scale. Method-specific auxiliary settings, such as projection rank and projection interval, are summarized in the table note.

A.2 Stage-2 FineWeb-Edu 32k Long-Context Experiments

Tables 20 report the best-run hyperparameter configurations for the Stage-2 FineWeb-Edu 32k experiments at 340M and 1B, respectively. The tables list the learning rate, momentum coefficients, numerical stability constant, and optimizer-specific auxiliary parameters encoded in the log filenames.

B Detailed Stage-2 Commonsense Reasoning Results

Tables 21–28 further report the detailed per-task Commonsense Reasoning results for each architecture and model scale. CS Avg. is the average over ARC-Easy, ARC-Challenge, HellaSwag, WinoGrande, PIQA, OpenBookQA, BoolQ, COPA [92], LAMBADA-OpenAI [85], and SciQ [112].

Table 19: Hyperparameter configurations for the C4-LLaMA short-context Stage-1 screening experiments.

Optimizer	β_1	β_2	β_3	ϵ	60M lr	130M lr	350M lr	1B lr
<i>T1: Element-wise adaptive moment and scalar control</i>								
Adan	0.9	0.92	0.99	1×10^{-8}	0.003	0.003	0.003	0.001
RAdam	0.9	0.99	–	1×10^{-8}	0.003	0.001	0.001	0.0005
AdamW	0.9	0.99	–	1×10^{-8}	0.003	0.001	0.001	0.0005
NAdam	0.9	0.99	–	1×10^{-8}	0.001	0.001	0.001	0.0005
MARS-AdamW	0.95	0.99	–	1×10^{-8}	0.005	0.005	0.005	0.001
Prodigy	0.9	0.95	–	1×10^{-8}	0.5	1	2	2
AdaBelief	0.9	0.999	–	$1 \times 10^{-16}/10^{-12}$	0.003	0.001	0.001	0.001
<i>T2: Matrix-level structural methods</i>								
MARS-Shampoo	0.95	0.99	–	1×10^{-8}	0.05	0.03	0.02	0.01
Muon	0.9	0.95	–	1×10^{-8}	0.02	0.01	0.006	0.006
RMNP	0.9/0.95	0.95	–	1×10^{-8}	0.01	0.01	0.01	0.01
SOAP	0.9	0.95	–	1×10^{-8}	0.003	0.002	0.001	0.0005
GaLore	0.9	0.98	–	1×10^{-6}	0.03	0.03	0.01	0.01
Shampoo	0.9	0.999	–	1×10^{-8}	0.05	0.05	0.02	0.01
<i>T3: Discretization and directional quantization</i>								
MARS-Lion	0.9	0.98	–	1×10^{-8}	0.0005	0.0002	0.0002	0.0002
Lion	0.9	0.98	–	–	0.0002	0.0002	0.0002	0.0001
<i>T4: State compression and structural aggregation</i>								
APOLLO	0.9	0.99	–	1×10^{-6}	0.02	0.01	0.01	0.01
Conda	0.9	0.99	–	1×10^{-8}	0.01	0.01	0.01	0.0005
8-bit Adam	0.9	0.99	–	1×10^{-8}	0.003	0.001	0.0005	0.0005
CAME	0.9	0.999	–	1×10^{-6}	0.001	0.0005	0.0005	0.0003
AdaFactor	0.9	–	–	–	0.002	0.002	0.001	0.0005
Adam-mini	0.9	0.99	–	1×10^{-8}	0.003	0.001	0.0005	0.0003
<i>T5: Curvature-aware and geometric regularization</i>								
AdamP	0.9	0.98	–	1×10^{-8}	0.005	0.001	0.001	0.0005
LAMB	0.9	0.99	–	1×10^{-6}	0.005	0.003	0.001	0.001
Sophia	0.9	0.99	–	1×10^{-8}	0.0002	0.0002	0.0002	0.0001

Note: – indicates that the corresponding hyperparameter is not used or that no explicit numerical stability constant is set. The learning rates are the final configurations used for each optimizer and model scale in the C4-LLaMA short-context Stage-1 screening experiments. AdaBelief uses $\epsilon = 1 \times 10^{-16}$ for 60M, 130M, and 350M, and $\epsilon = 1 \times 10^{-12}$ for 1B. RMNP uses $\beta_1 = \beta_2 = 0.95$ at 1B and applies an Adam-style auxiliary branch to non-matrix parameters. The projection ranks of APOLLO are 128/192/256/256, with projection interval 200. The ranks of Conda are 128/192/256/256, with projection intervals 2000/2000/2000/200. The ranks of GaLore are 128/256/256/1024, with projection intervals 200/500/500/200.

Table 20: Hyperparameter configurations for the FineWeb-Edu 32k Stage-2 experiments at model parameters of 340M and 1B.

Optimizer	340M					1B				
	lr	β_1	β_2	β_3	ϵ	lr	β_1	β_2	β_3	ϵ
<i>Transformer++</i>										
AdamW	1e-3	0.9	0.99	–	1e-15	1e-3	0.9	0.99	–	1e-15
AdamP	1e-3	0.9	0.98	–	1e-15	1e-3	0.9	0.98	–	1e-15
Adan	3e-3	0.9	0.92	0.99	1e-8	3e-3	0.9	0.92	0.99	1e-8
Lion	3e-4	0.9	0.99	–	–	3e-4	0.9	0.99	–	–
MARS-AdamW	3e-3	0.95	0.99	–	1e-8	3e-3	0.95	0.99	–	1e-8
MARS-Lion	2e-4	0.9	0.98	–	1e-12	1e-4	0.9	0.98	–	1e-12
MARS-Shampoo	1e-2	0.95	0.99	–	1e-12	5e-3	0.95	0.99	–	1e-12
Muon	5e-3	0.9	0.95	–	1e-15	3e-3	0.9	0.95	–	1e-15
RMNP	3e-3	0.9	0.99	–	1e-15	3e-3	0.9	0.99	–	1e-15
SOAP	3e-3	0.9	0.95	–	1e-15	3e-3	0.9	0.95	–	1e-15
APOLLO	3e-3	0.9	0.99	–	1e-12	3e-3	0.9	0.99	–	1e-12
Conda	1e-2	0.9	0.99	–	1e-12	5e-3	0.9	0.99	–	1e-12
<i>GLA</i>										
AdamW	1e-3	0.9	0.99	–	1e-15	1e-3	0.9	0.99	–	1e-15
AdamP	1e-3	0.9	0.98	–	1e-15	1e-3	0.9	0.98	–	1e-15
Adan	3e-3	0.9	0.92	0.99	1e-8	3e-3	0.9	0.92	0.99	1e-8
Lion	3e-4	0.9	0.99	–	–	3e-4	0.9	0.99	–	–
MARS-AdamW	3e-3	0.95	0.99	–	1e-8	3e-3	0.95	0.99	–	1e-8
MARS-Lion	2e-4	0.9	0.98	–	1e-12	1e-4	0.9	0.98	–	1e-12
MARS-Shampoo	1e-2	0.95	0.99	–	1e-12	5e-3	0.95	0.99	–	1e-12
Muon	5e-3	0.9	0.95	–	1e-15	3e-3	0.9	0.95	–	1e-15
RMNP	3e-3	0.9	0.99	–	1e-15	3e-3	0.9	0.99	–	1e-15
SOAP	3e-3	0.9	0.95	–	1e-15	3e-3	0.9	0.95	–	1e-15
APOLLO	3e-3	0.9	0.99	–	1e-12	3e-3	0.9	0.99	–	1e-12
Conda	1e-2	0.9	0.99	–	1e-12	5e-3	0.9	0.99	–	1e-12
<i>DeltaNet</i>										
AdamW	1e-3	0.9	0.99	–	1e-15	1e-3	0.9	0.99	–	1e-15
AdamP	1e-3	0.9	0.98	–	1e-15	1e-3	0.9	0.98	–	1e-15
Adan	3e-3	0.9	0.92	0.99	1e-8	3e-3	0.9	0.92	0.99	1e-8
Lion	3e-3	0.9	0.99	–	–	3e-3	0.9	0.99	–	–
MARS-AdamW	3e-3	0.95	0.99	–	1e-8	3e-3	0.95	0.99	–	1e-8
MARS-Lion	2e-4	0.9	0.98	–	1e-12	1e-4	0.9	0.98	–	1e-12
MARS-Shampoo	1e-2	0.95	0.99	–	1e-12	5e-3	0.95	0.99	–	1e-12
Muon	5e-3	0.9	0.95	–	1e-15	3e-3	0.9	0.95	–	1e-15
RMNP	3e-3	0.9	0.99	–	1e-15	3e-3	0.9	0.99	–	1e-15
SOAP	3e-3	0.9	0.95	–	1e-15	3e-3	0.9	0.95	–	1e-15
APOLLO	3e-3	0.9	0.99	–	1e-12	3e-3	0.9	0.99	–	1e-12
Conda	1e-2	0.9	0.99	–	1e-12	5e-3	0.9	0.99	–	1e-12
<i>Gated DeltaNet</i>										
AdamW	1e-3	0.9	0.99	–	1e-8	1e-3	0.9	0.99	–	1e-8
AdamP	1e-3	0.9	0.98	–	1e-15	1e-3	0.9	0.98	–	1e-15
Adan	3e-3	0.9	0.92	0.99	1e-8	3e-3	0.9	0.92	0.99	1e-8
Lion	1e-4	0.9	0.99	–	1e-8	1e-4	0.9	0.99	–	1e-8
MARS-AdamW	5e-3	0.95	0.99	–	1e-15	3e-3	0.95	0.99	–	1e-15
MARS-Lion	2e-4	0.9	0.98	–	1e-12	1e-4	0.9	0.98	–	1e-12
MARS-Shampoo	1e-2	0.95	0.99	–	1e-12	5e-3	0.95	0.99	–	1e-12
Muon	3e-3	0.9	0.99	–	1e-15	3e-3	0.9	0.99	–	1e-15
RMNP	3e-3	0.9	0.99	–	1e-15	3e-3	0.9	0.99	–	1e-15
SOAP	3e-3	0.9	0.95	–	1e-15	1e-3	0.9	0.95	–	1e-15
APOLLO	3e-3	0.9	0.99	–	1e-12	3e-3	0.9	0.99	–	1e-12
Conda	1e-2	0.9	0.99	–	1e-12	5e-3	0.9	0.99	–	1e-12

Table 21: Detailed Stage-2 Commonsense Reasoning results for Transformer++ at 340M.

Optimizer	PPL	CS Avg.	ARC-E	ARC-C	HellaSwag	WinoGrande	PIQA	OBQA	BoolQ	COPA	LAMBADA	SciQ
SOAP	23.90	53.75	54.92	31.31	44.42	54.30	67.79	36.80	61.28	71.00	38.56	77.10
RMNP	24.37	53.35	54.71	29.52	43.35	54.22	66.65	34.80	60.58	74.00	38.00	77.70
MARS-AdamW	24.57	52.50	51.89	28.50	42.97	51.85	66.65	34.40	60.61	73.00	36.87	78.30
AdamW	24.62	52.28	52.44	29.52	42.09	54.54	66.97	35.20	58.78	69.00	35.71	78.50
AdamP	24.68	51.69	50.80	30.12	42.65	53.04	66.65	32.80	59.48	70.00	35.92	75.40
Muon	25.05	53.25	53.20	29.95	42.84	55.64	66.21	35.60	61.50	72.00	36.19	79.40
Adan	25.55	52.48	51.39	29.52	42.30	53.12	66.27	31.60	60.61	75.00	37.88	77.10
Lion	26.02	51.07	51.43	28.07	40.09	51.54	65.45	33.60	60.86	69.00	34.47	76.20
MARS-Lion	26.20	51.61	50.93	27.30	40.27	51.07	65.94	35.60	60.89	72.00	34.23	77.90
MARS-Shampoo	26.43	51.96	52.10	28.67	42.95	54.06	66.21	32.00	61.77	69.00	36.46	76.40
Conda	28.30	51.61	52.65	28.41	39.77	54.54	65.51	35.20	60.58	67.00	33.44	79.00
APOLLO	34.08	48.19	47.52	26.96	37.52	51.14	64.47	31.60	60.03	67.00	24.02	71.60

Table 22: Detailed Stage-2 Commonsense Reasoning results for Transformer++ at 1B.

Optimizer	PPL	CS Avg.	ARC-E	ARC-C	HellaSwag	WinoGrande	PIQA	OBQA	BoolQ	COPA	LAMBADA	SciQ
SOAP	18.72	57.71	60.14	34.64	53.21	58.01	70.89	37.40	61.87	72.00	45.39	83.50
AdamW	18.90	56.55	59.85	34.64	51.21	55.33	70.35	36.00	61.83	69.00	44.05	83.20
MARS-AdamW	18.94	57.46	61.24	35.84	52.55	58.41	70.51	37.20	59.24	70.00	44.50	85.10
AdamP	19.04	56.82	60.77	35.41	51.26	55.01	70.78	38.40	59.60	70.00	42.71	84.20
RMNP	19.40	57.12	59.97	35.24	51.53	56.27	70.35	36.20	61.74	72.00	44.19	83.70
Adan	19.41	57.21	59.81	34.39	51.61	56.83	70.51	37.20	61.07	73.00	43.97	83.70
MARS-Shampoo	19.74	57.30	59.09	33.87	51.89	57.22	70.73	38.20	62.26	71.00	44.28	84.40
Conda	19.86	57.24	59.01	33.79	51.32	57.93	70.29	36.80	62.02	76.00	42.69	82.50
Muon	19.86	56.36	59.26	32.76	50.31	54.85	71.71	37.40	59.85	70.00	43.04	84.40
Lion	20.26	55.22	57.70	32.00	48.13	53.35	69.31	37.60	61.10	72.00	40.15	80.90
MARS-Lion	21.17	54.51	56.02	31.23	47.04	53.91	69.80	37.60	57.61	72.00	39.96	79.90
APOLLO	25.29	53.61	54.67	30.89	45.46	52.49	68.82	35.80	60.83	75.00	33.13	79.00

Table 23: Detailed Stage-2 Commonsense Reasoning results for GLA at 340M.

Optimizer	PPL	CS Avg.	ARC-E	ARC-C	HellaSwag	WinoGrande	PIQA	OBQA	BoolQ	COPA	LAMBADA	SciQ
SOAP	27.04	52.21	52.99	29.27	43.11	52.80	66.54	33.80	60.61	67.00	36.60	79.40
Muon	27.47	52.50	52.69	29.01	43.32	52.41	66.81	34.80	62.23	72.00	35.14	76.60
MARS-AdamW	28.28	51.24	53.37	28.41	41.55	50.59	66.92	34.00	60.12	66.00	34.89	76.50
RMNP	28.60	50.72	50.55	27.73	40.77	51.38	66.21	33.80	60.40	66.00	34.48	75.90
AdamP	28.66	51.14	52.53	27.82	40.81	50.12	67.41	33.60	60.83	70.00	34.04	74.30
AdamW	28.67	51.06	53.07	29.01	40.13	51.78	66.76	33.80	59.33	67.00	34.29	75.40
Adan	29.00	51.01	52.19	27.22	40.55	50.83	66.27	34.80	60.00	69.00	33.07	76.20
MARS-Shampoo	29.20	52.01	53.75	29.10	42.44	52.33	66.70	35.40	61.35	67.00	34.60	77.40
Lion	29.47	50.14	50.13	27.56	39.54	51.78	65.61	32.20	59.57	70.00	33.46	71.60
MARS-Lion	29.67	50.69	52.15	27.47	39.56	52.25	65.61	34.40	60.52	67.00	32.04	75.90
Conda	37.38	48.28	47.10	26.54	35.42	50.28	62.95	33.20	61.59	65.00	27.81	72.90
APOLLO	37.75	48.38	48.48	29.01	38.45	49.49	64.36	32.40	58.87	66.00	24.28	72.50

Table 24: Detailed Stage-2 Commonsense Reasoning results for GLA at 1B.

Optimizer	PPL	CS Avg.	ARC-E	ARC-C	HellaSwag	WinoGrande	PIQA	OBQA	BoolQ	COPA	LAMBADA	SciQ
SOAP	20.62	57.57	59.72	34.39	53.06	58.88	69.80	38.20	60.55	73.00	44.77	83.30
MARS-Shampoo	21.53	57.33	60.14	35.07	51.13	55.80	70.84	37.00	61.71	72.00	45.18	84.40
Muon	21.54	56.85	60.61	33.79	50.48	54.06	70.73	36.60	58.84	76.00	42.19	85.20
AdamP	21.86	55.31	60.02	32.94	49.19	54.70	69.21	38.40	59.51	69.00	39.96	80.20
MARS-AdamW	21.89	55.71	58.50	33.87	49.81	54.85	69.91	36.80	58.10	75.00	40.05	80.20
AdamW	22.06	56.69	61.15	33.11	48.47	54.54	69.59	39.80	61.90	76.00	40.54	81.80
RMNP	22.23	55.79	59.39	32.76	49.36	53.91	69.80	36.80	59.57	71.00	42.44	82.90
Lion	22.40	53.96	57.15	31.91	47.10	53.35	69.70	36.40	58.17	70.00	38.29	77.50
Adan	22.51	55.07	58.38	31.66	48.45	53.83	69.48	35.40	61.65	70.00	39.34	82.50
Conda	22.89	54.95	57.15	32.08	48.92	53.51	69.64	37.40	61.22	71.00	39.18	79.40
MARS-Lion	23.79	53.91	55.60	31.31	45.72	53.91	69.48	36.00	61.80	70.00	38.46	76.80
APOLLO	27.78	52.33	53.54	31.48	45.89	52.49	67.52	35.20	57.89	66.00	34.39	78.90

Table 25: Detailed Stage-2 Commonsense Reasoning results for DeltaNet at 340M.

Optimizer	PPL	CS Avg.	ARC-E	ARC-C	HellaSwag	WinoGrande	PIQA	OBQA	BoolQ	COPA	LAMBADA	SciQ
SOAP	26.02	52.60	54.55	28.58	42.70	52.80	67.19	36.80	59.60	69.00	36.50	78.30
AdamP	26.77	51.53	52.69	27.22	41.30	53.12	66.81	32.00	61.31	67.00	36.15	77.70
MARS-AdamW	26.79	51.69	53.75	28.41	41.72	52.64	67.52	33.00	59.66	67.00	35.11	78.10
RMNP	26.80	53.25	55.01	30.20	41.71	53.04	66.87	34.80	60.24	74.00	35.75	80.90
AdamW	27.16	51.74	51.60	29.18	40.66	52.57	66.43	34.80	62.14	70.00	33.92	76.10
Muon	27.18	52.00	55.22	29.27	42.25	52.41	66.87	33.40	61.13	67.00	33.77	78.70
Adan	27.28	51.78	52.31	29.78	41.39	52.88	67.41	34.60	57.55	70.00	33.53	78.30
Lion	28.20	49.96	49.83	26.28	39.13	52.01	65.94	32.40	59.69	66.00	32.29	76.00
MARS-Lion	28.25	50.94	50.42	28.92	39.87	52.09	64.64	32.80	61.71	67.00	34.17	77.80
MARS-Shampoo	28.26	51.43	52.31	28.67	41.19	52.72	66.38	33.80	58.93	70.00	32.25	78.00
Conda	29.09	51.46	53.03	28.41	40.89	54.30	64.80	34.00	59.24	70.00	32.49	77.40
APOLLO	34.73	49.04	50.55	27.65	39.02	50.36	64.47	32.20	58.84	70.00	24.24	73.10

Table 26: Detailed Stage-2 Commonsense Reasoning results for DeltaNet at 1B.

Optimizer	PPL	CS Avg.	ARC-E	ARC-C	HellaSwag	WinoGrande	PIQA	OBQA	BoolQ	COPA	LAMBADA	SciQ
SOAP	20.38	56.49	59.55	33.45	51.44	55.49	71.33	38.20	55.02	74.00	43.78	82.60
AdamW	20.66	55.56	59.51	33.62	49.71	52.72	70.62	36.60	59.33	69.00	41.94	82.60
MARS-AdamW	20.67	56.80	61.53	33.19	50.78	55.09	70.51	39.40	60.76	73.00	42.05	81.70
AdamP	20.68	56.73	61.41	34.56	49.74	53.51	71.16	38.40	60.49	73.00	42.98	82.00
Adan	20.88	56.50	58.75	33.70	50.72	54.85	70.19	36.60	61.50	73.00	41.35	84.30
RMNP	21.06	57.32	61.74	34.47	50.04	56.75	70.57	36.60	61.68	74.00	41.99	85.40
Muon	21.18	56.65	59.30	33.19	50.30	54.85	70.19	37.00	61.25	76.00	41.98	82.40
MARS-Shampoo	21.25	56.74	59.85	32.42	50.62	56.59	70.84	39.60	62.35	71.00	41.80	82.30
Lion	21.44	54.22	58.08	31.91	47.38	53.75	68.72	36.80	55.17	72.00	39.38	79.00
Conda	21.75	56.10	57.95	34.64	49.86	54.38	70.13	36.60	61.62	73.00	42.01	80.80
MARS-Lion	22.72	53.65	55.26	32.00	45.63	53.75	69.04	35.00	57.86	71.00	38.72	78.20
APOLLO	25.58	53.88	55.68	32.25	46.69	53.67	69.64	35.60	58.26	72.00	35.01	80.00

Table 27: Detailed Stage-2 Commonsense Reasoning results for Gated DeltaNet at 340M.

Optimizer	PPL	CS Avg.	ARC-E	ARC-C	HellaSwag	WinoGrande	PIQA	OBQA	BoolQ	COPA	LAMBADA	SciQ
SOAP	23.53	54.77	56.10	31.57	47.29	55.33	68.99	34.20	61.41	72.00	39.26	81.60
RMNP	23.65	54.45	55.56	30.89	46.28	52.88	68.82	36.80	60.80	72.00	40.27	80.20
MARS-AdamW	24.17	54.91	57.95	30.97	46.49	54.30	67.41	35.60	61.62	74.00	38.68	82.10
AdamP	24.32	53.82	54.08	30.46	45.10	54.38	68.01	37.40	58.81	73.00	37.94	79.00
Muon	24.34	54.45	55.01	33.02	45.60	53.99	67.08	34.40	61.77	73.00	38.58	82.00
AdamW	24.47	53.67	55.26	31.23	44.63	51.93	67.25	33.40	61.19	74.00	37.67	80.10
Lion	24.76	53.24	54.21	29.52	43.29	52.72	66.97	36.00	58.99	75.00	35.92	79.80
Adan	24.78	52.83	54.00	30.97	45.63	53.83	67.57	34.60	54.89	68.00	38.00	80.80
MARS-Lion	25.31	52.96	53.54	30.03	43.56	54.46	67.74	34.20	60.64	70.00	37.16	78.30
MARS-Shampoo	25.99	53.37	51.60	29.86	45.20	54.14	67.52	34.80	62.35	69.00	38.17	81.00
Conda	26.11	53.45	54.92	29.86	44.24	52.96	67.08	35.20	61.71	71.00	36.60	80.90
APOLLO	30.36	50.92	51.56	29.35	42.26	50.91	67.41	34.00	57.68	69.00	29.54	77.50

Table 28: Detailed Stage-2 Commonsense Reasoning results for Gated DeltaNet at 1B.

Optimizer	PPL	CS Avg.	ARC-E	ARC-C	HellaSwag	WinoGrande	PIQA	OBQA	BoolQ	COPA	LAMBADA	SciQ
SOAP	19.86	57.22	59.47	33.36	52.36	56.12	70.35	38.00	60.61	75.00	43.99	82.90
MARS-AdamW	20.04	58.18	64.44	35.24	52.80	58.09	70.67	37.80	62.57	72.00	44.05	84.10
RMNP	20.26	57.30	62.04	34.73	51.80	57.14	70.35	37.80	60.40	71.00	42.95	84.80
AdamP	20.29	57.07	60.65	35.24	50.87	55.49	69.75	38.00	61.65	73.00	43.59	82.50
Muon	20.32	57.20	58.54	33.87	51.40	57.06	70.89	38.20	59.48	74.00	43.70	84.80
AdamW	20.33	57.01	59.43	33.79	50.48	54.85	70.57	37.60	61.19	77.00	42.89	82.30
Lion	20.38	55.74	57.62	32.51	49.64	55.09	71.33	37.80	59.27	71.00	41.04	82.10
Adan	20.55	57.93	63.64	36.69	52.45	58.01	69.75	36.80	57.37	76.00	43.04	85.60
MARS-Shampoo	20.61	57.58	58.88	34.47	51.96	57.93	70.24	37.60	61.25	75.00	43.94	84.50
Conda	21.07	57.18	57.83	33.45	51.24	55.49	70.19	39.00	62.08	74.00	43.37	85.20
MARS-Lion	21.24	55.50	57.41	32.34	48.79	54.54	70.95	37.20	59.88	71.00	40.56	82.30
APOLLO	25.61	53.73	55.85	31.66	47.68	54.85	68.23	35.80	61.77	68.00	34.31	79.20

Table 29: Dimension-A methodological taxonomy of the surveyed optimizer set. SF-AdamW denotes Schedule-Free AdamW.

Core mechanism	Pipeline site	Four-axis summary	N	Example
T1: Element-wise adaptive moment and scalar control				
T1.1 Scalar bases and direct Adam variants				
Adam-style moments, bias correction, de-coupled decay, Nesterov, rectified, belief, and cross-moment variants	S3 + local S5	Full domain, moment state, diagonal adaptive geometry, LR/WD finalize	25	AdamW
T1.2 Multi-timescale, momentum correction, and variance reduction				
Fast/slow EMA fusion, alignment-aware momentum correction, or STORM-style recursive gradient correction	S3; Axis II	partly Full domain, temporal or VR state, diagonal geometry, LR/WD finalize	10	AdEMA-Mix
T1.3 Iterate averaging and automatic tuning				
Schedule-free averaging, distance-based learning-rate inference, optimizer switching, initialization-time LR scaling	S3 + S5	Full domain, scalar or iterate state, base geometry, global-step finalize	10	SF-AdamW
T2: Matrix-level structural methods				
T2.1 Spectral orthogonalization				
Orthogonalization of two-dimensional gradients or momentum	S1 + S2	Matrix domain, momentum state, polar operator, routed writeback	8	Muon
T2.2 Kronecker-factored preconditioning				
Row/column covariance, Fisher, or structured Fisher factors for matrix gradients	S1 + S2 + S3	Kronecker/eigen domain, factor state, metric geometry, damped writeback	8	SOAP
T2.3 Low-rank subspace projection				
Project gradients and states into a low-rank subspace, then reconstruct	S2 + S3 + S4	Projected subspace, projected state, adaptive geometry, projection-back	3	GaLore
T3: Discretization and directional quantization				
T3 Direction quantization				
Sign or related maps that preserve direction and coarsen magnitude	S2 + simplified S3	Full domain, raw or momentum state, sign geometry, LR/WD radius	7	Lion
T4: State compression and structural aggregation				
T4.1 Row-column factorization				
Approximate matrix second moments with row/column statistics	S3 + S4	Full domain, row/column state, adaptive geometry, broadcast denominator	2	CAME
T4.2 Low-bit quantization and error compensation				
Quantize optimizer state with dynamic scaling, stochastic rounding, or error control	S3 + S4	Full domain, low-bit state, base geometry, dequantized finalize	2	8-bit Adam
T4.3 Block/layer-level state sharing				
Share moment or curvature statistics over heads, blocks, or layers	S1 + S3 + S4	Block support, shared state, block-adaptive geometry, broadcast writeback	5	Adam-mini
T4.4 Fused backprop-update				
Update parameters during backpropagation and release gradients early	S3 + S5	Full support, streaming state, base geometry, immediate writeback	2	LOMO
T5: Curvature-aware and geometric regularization				
T5.1 Adversarial perturbation (SAM family)				
Re-evaluate gradients at a local perturbation point	S5 + extra gradient	Base domain, perturbed-gradient state, base geometry, sharpness wrapper	8	SAM
T5.2 Diagonal Hessian estimation				
Estimate Hessian/Gauss-Newton diagonals and apply clipped updates	S3 + S5	Full domain, HVP/Hessian state, clipped curvature geometry, LR/WD finalize	2	Sophia
T5.3 Update post-processing and selective filtering				
Centralize, project, normalize, mask, or sparsify computed updates	S2 or S5	Base domain, base state, base geometry, filter or mask	13	GC
T5.4 Layer-wise trust-region scaling				
Rescale layer-wise updates by parameter/update norm ratios	S1 + S5	Layer support, base state, base geometry, trust-ratio finalize	2	LAMB